الجمهورية الجزائرية الديموقراطية الشّعبية

République Algérienne Démocratique et populaire

وزارة التّعليم العالي والبحث العلمي

Ministère de l'Enseignement Supérieur et de la Recherche Scientifique

Université Mohamed El Bachir El Ibrahimi Bordj Bou Arreridj — **جامعة محمد البشير الإبراهيمي برج بوعريريج**

Faculté des sciences et de la technologie — **كلية العلوم والتكنولوجيا**

Département des sciences de la matière — **قسم علوم المادّة**

THESE

Soutenance de Thèse en vue de l'obtention du diplôme de **DOCTORAT LMD**

Spécialité : Sciences et Génie des Matériaux

Présenté par :

ZERROUG Meriem

Thème

Étude Et extraction Physico-Chimique Des Inhibiteurs De Corrosion Des Substances Naturelles.

Soutenue publiquement le : 09/10/2025

Devant le jury :

Mr HELLATI Abdelhak	Professeur université Bordj Bou Arreridj	Président
Mr BOUZID Abderrazak	Professeur université de Bordj Bou Arreridj	Directeur de thèse
Mme FERKOUS Hana	Maitre de conférences université de Skikda	Co-directeur
Mme HAMLA Meriem	Maitre de conférences université de B. B. Arreridj	Examinateur
Mme BERREDJEM Malika	Professeur université de Skikda	Examinateur
Mme DELIMI Amel	Maitre de conférences université de Skikda	Examinateur

2025/2026

الجمهورية الجزائرية الديموقراطية الشّعبية

People's Democratic Republic Of Algeria

وزارة التّعليم العالي والبحث العلمي

Ministry Of Higher Education And Scientific Research

Mohamed El Bachir El Ibrahimi Bordj Bou Arreridj University **جامعة محمد البشير الإبراهيمي برج بوعريريج**

Faculty Of Sciences And Technology **كلية العلوم والتكنولوجيا**

Departement of Material sciences **قسم علوم المادّة**

A DISSERTATION

Submitted in Partial Fulfillment of the Requirements for the Degree of **DOCTORATE LMD**

Field: Materials Science and Engineering

Presented by:

ZERROUG Meriem

Entitled

Physicochemical Study and Extraction of Corrosion Inhibitors from Natural Substances

Publicly defended on: 10/09/2025

Advisory Comitee :

Pr. HELLATI Abdelhak	University of Bordj Bou Arreridj	Chairman
Pr. BOUZID Abderrazak	University of Bordj Bou Arreridj	Thesis Director
Dr. FERKOUS Hana	University of Skikda	Co-director
Dr. HAMLA Meriem	University of Bordj Bou Arreridj	Examiner
Dr. BERREDJEM Malika	University of Skikda	Examiner
Dr. DELIMI Amel	University of Skikda	Examiner

2025/2026

Acknowledgements

First of all I would like to express my gratitude to God who gave me the strength and the ability to finish this humble work
Second, He who does not thank people does not thank God.
I would like to thank some of the people who helped me realize this work. And hope those who I did not mention or thank will forgive me.
I would like to express the deepest appreciation to my Advisor, Pr. Abderrazak BOUZID, who has supervised me throughout this research work. Without his guidance, patience, and persistent help this dissertation would not have possible. I would also like to extend my deepest gratitude to my co-advisor Dr. Hana FERKOUS who was keen on completing the thesis to the fullest through continuous guidance, urging research, generating ideas, and following up on the latest scientific works in the field.
gratefully acknowledge the scientific and technical help and training provided by Professor Hatem MAJDOUB from the university of Monastir and interfaces and advanced materials Laboratory in Tunisia . Thanks also go to the laboratory's staff's assistance and their contribution in accepting me among them and making the training run smoothly, particularly Dr. Zayneb JEBALI.
I would also like to express my thanks and gratitude to my committee members, Pr.HELLATI Abdelhak Dr. HAMLA Meriem, Pr. BERREDJEM Malika, and Dr.DELIMI Amel for their suggestions and revisions provided to my research work. I am grateful to all of those with whom I have had the pleasure to work during this and other related projects.

Dedication

No one has been more important to me in the pursuit of this project than the members of my family.

I would like to thank my parents whose love and guidance are with me in whatever I pursue.

My beloved brother: Omar El-Farouk

Most importantly, I would love to thank my loving and supportive husband, Sofiane, and my wonderful children, Mohamed Ali, Aliyaa Salma and Ibrahim Abdennour who provide unending inspiration.

To my family, my family in law and friends

Table of contents

Table of Contents

List of figures

List of figures

List of Tables

List of tables

Abbreviations & symbols

Abbreviations & symbols

AA : Ammophila Arenaria

AHA : Artemisia Herba Alba

C_{dl} : Double layer capacitance

CPE : Consant phase element

Ecorr : Corrosion potential

EIS: Electrochemical impedance spectroscopy

FTIR: Fourier transform infrared spectroscopy

HOMO: Highest Occupied Molecular Orbital

I_{corr}: Corrosion current density

LUMO: Lowest Unoccupied Molecular Orbital

MD: Molecular dynamics simulation

MEP : Molecular electrostatic potential

OCP : Open circuit potential

PDP: potentiodynamic polarization

R_p : Polarization resistance

βa : Tafel anodic slop

βc : Tafel cathodic slop

η: Inhibition efficiency

θ: Surface coverage

$\Sigma n_i \mu_i$: the sum of the chemical potentials of the i^{th} compound in its final and initial states

General Introduction

General Introduction

Corrosion is one of the problems that affect our daily life, due to the presence of metals mainly in various public and private installations. This can lead to the loss of natural resources, loss of time and money due to work stopping for replacing or maintaining the affected parts of equipment and last but not least harm the human safety and the environment [1, 2]. A recent study [3] gathered past studies determining the total corrosion costs of various industrial countries and percentages of avoidable costs:

The united kingdom ($ 3.2 billion, 1969 U.S dollars) with 23% of total costs being avoidable losses

German federal republic ($6 billion, 1969 dollars) with 25% of total costs being avoidable losses

Sweden ($ 58-77 million, 1964 dollars) with 25-35% of total costs being avoidable losses

Finland ($ 47-62 million, 1965 dollars)

Ruusia ($ 6.7 billion, 1969 U.S dollars)

Australia ($ 550 million, 1973 dollars)

india ($ 330 million, 1971 dollars)

Japan ($ 9.2 billion, 1974 dollars)

USA ($ 9.67 billion, 1975 dollars)

Thus, it is necessary to know the performance and the behavior of various metals during their exposure to the factors that cause this undesirable natural phenomenon. Some metals have a natural ability to resist rust known as noble metals. Other metals also resist by interacting with oxygen in the air and forming a thin oxide film that blocks the metal’s tendency to undergo further reaction by the phenomenon of passivation.

Since Iron is the second most abundant metal [4], it is widely used in many fields but it falls within the category of non-resistant metals, which has made it a subject of study in many researches related to corrosion resistance in various environments, as is the case with the current study.

Although the phenomenon of corrosion has been fought in many different ways, its occurrence is still spontaneous and inevitable.

The use of corrosion inhibitors is an effective way to reduce corrosion levels to a significant and satisfactory extent, taking into account the environmental and health international standards in most cases.

Green inhibitors (ecofriendly inhibitors) are considered to be a safe and an effective method that have been the subject of interest and research by many researchers and scholars in the field [5-8].

The study of the influence of the latter is the subject of the present thesis.

Electrochemical measurements are practical for predicting corrosion behavior. It offers a rapid method of estimating corrosion rates and to determine other types of corrosion behavior and evaluation of inhibitors of metal corrosion in aggressive media [9-12]. Computational modelings are considered as powerful tools for more understanding corrosion inhibitors action for various metals in numerous electrolytes. These tools can theoretically derive the effectiveness of compounds to be tested as inhibitors towards metallic corrosion and give information about the molecular sites responsible for interactions with metallic surface using quantum chemical calculations using density functional theory (DFT), explain the interaction between the metal and the surface in the form the energy of adsorption (Eads) by Monte Carlo (MC) and Molecular dynamics (MD) simulations. The MC and MD simulations also provide the information about how the inhibitor molecules are oriented on the metallic surface[13]

Thus, the main objectives of this study were to

(1) select and obtain extracts from local natural resources then characterize them by different techniques,

(2) screen the anti-inhibitory activity of the plants extracts by both experimental and theoretical methods and

(3) Perform metal surface experiments before and after the successful deposit of the inhibitor molecules.

The thesis manuscript is organized as follows; Chapter 1 provides some basic definitions and concepts of corrosion and an overview of the important thermodynamic parameters of relevance to corrosion electrochemistry. Chapter 2 presents the selected materials and both the experimental and theoretical procedures that have been applied to evaluate the inhibitory power as well as the surface characterization before and after adding the extracts. Chapter 3 focuses on the experimental results and a brief comparison between the two plants. The final chapter outlines the theoretical results.

The main results were finally exposed in a general conclusion.

Chapter I

Theoretical Basis

CHAPTER I. CORROSION THEORETICAL BASIS OVERWIEW

Introduction

Corrosion is a natural process that gradually degrades the properties of materials causing structural damage, financial cost, and safety risks. From industrial infrastructures to electronic devices, corrosion has an extensive and profound impact

The study of corrosion is important for a number of reasons. First, it can help to identify the factors that contribute to corrosion and develop methods to prevent or mitigate it. Second, it can help to develop new materials that are more resistant to corrosion. Third, it can help to improve the design and operation of structures and equipment to minimize the risk of corrosion damage. It is a multidisciplinary field that draws on the expertise of chemists, physicists, engineers, and materials scientists [14].

The unwanted impacts of metal corrosion can be significant, but it can be reduced by using corrosion-resistant materials, protecting metal surfaces, and using corrosion inhibitors. There is growing interest in the use of green inhibitors from plants as they contain a variety of naturally occurring substances that can inhibit corrosion [15].

I.1. Corrosion

I.1.1. Definition

Corrosion is a natural phenomenon that causes deterioration of metal, including its properties, and is also caused by a redox reaction [16]. It can be defined in several ways. Some definitions are very direct and focus on a specific form of corrosion, while others are more general and cover many forms of deterioration. It can be characterized as a chemical or electrochemical reaction between a material, usually metallic, and its environment.

These are some technical definitions:

NACE/ASTM G193

*“Corrosion is the deterioration of a material, usually a metal, that results from a chemical or electrochemical reaction with its environment.” [*17*]*

ISO 8044

*“Physicochemical interaction between a metal and its environment that results in changes in the properties of the metal, and which may lead to significant impairment of the function of the metal, the environment or the technical system, of which these form part.” [*18*]*

International Union of Pure and Applied Chemistry.

*"Corrosion is an irreversible interfacial reaction of a material (metal, ceramic, or polymer) with its environment which results in the consumption of the material or in dissolution into the material of a component of the environment." [*19*]*

From a thermodynamic point of view, the decrease in the energy level is the main cause of metal corrosion.

E. McCafferty

"Corrosion is the destructive attack of a ***metal*** *by its reaction with the environment." [*20*]*

I.1.2. Classification

The most common way to classify it is as follows:

- *According to the nature of the corrosive agent*; this latter determines whether the corrosion of metals is wet or dry.
- *According to the mechanism:* metal corrosion can be chemical or electrochemical. [21]

a. Chemical corrosion:

This corrosion mechanism is a heterogeneous reaction between a solid phase, the metal, exposed to high temperatures, in a dry atmosphere and in the presence of gases such as air, oxygen, ammonia, carbon dioxide, chlorine or combustion products, as well as in non-electrolyte liquid media such as oil, gasoline, hydrocarbons, various organic solvents, liquid bromine, etc.

Corrosion products are generally retained on the metal surface and the further development of the corrosion process depends on the structure, chemical composition and mechanical properties of the layer thus formed. This layer of corrosion products hinders the access of the oxidant to the metal surface, which delays the corrosion process due to the slower formation of the corrosion product layer.

b. Electrochemical corrosion:

It is a spontaneous process of metal destruction, due to its physicochemical interaction with an electrolyte-containing environment. As a result, it occurs in two acts: the oxidation of the metal, generating its ions, and the reduction of the oxidizing agent, which is part of the corrosive environment and whose speeds depend mainly on the potential of the metal which represents the Gibbs free energy and the concentration of the oxidant substance, respectively.

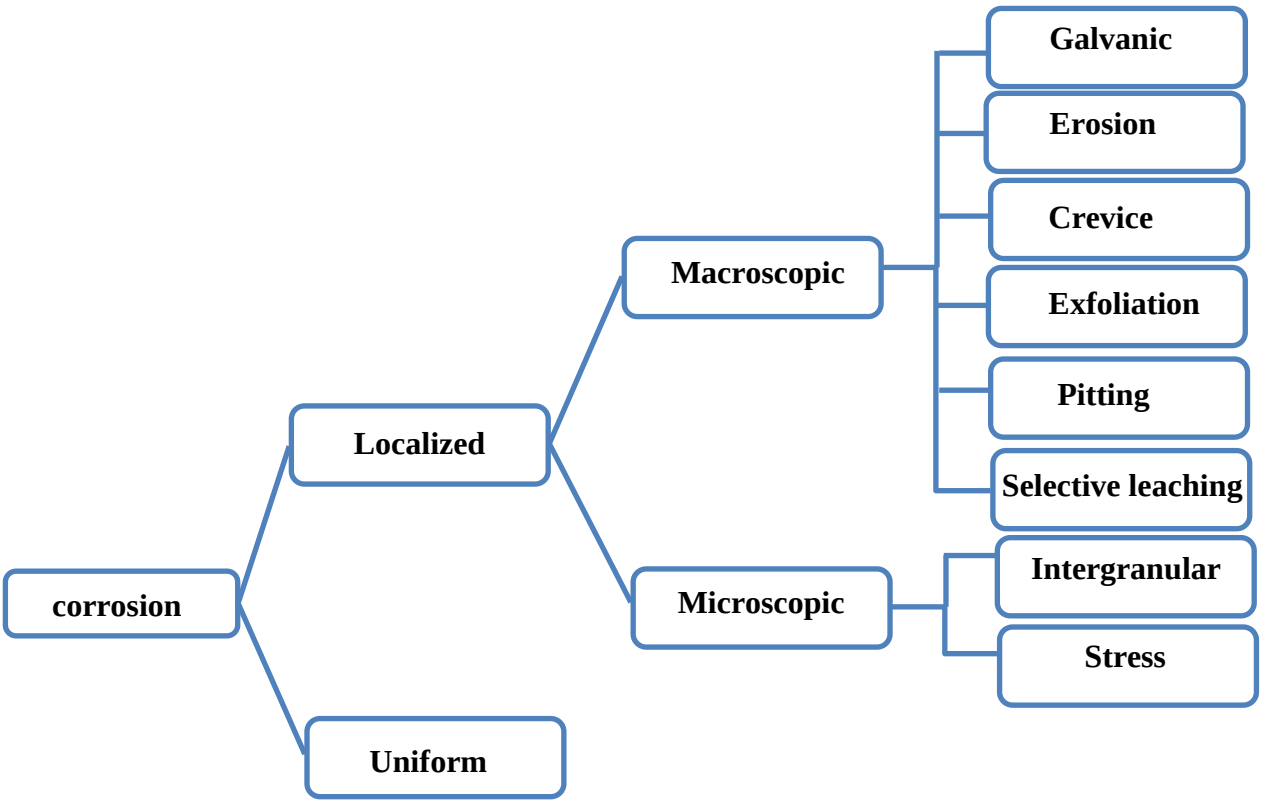

Figure I.1: Corrosion classification according to the appearance of the corroded metal

It is the most common type of corrosion in practice, as well as the most dangerous for metals. Electrochemical corrosion is the cause of the destruction of metals exposed to atmospheric conditions (atmospheric corrosion), soil, various aqueous electrolytes (seawater, fresh water, saline solutions, acids and bases) and non-aqueous (melted salts, organic electrolytes).

- *According to the appearance of the corroded metal:* Corrosion can be uniform, i.e. the metal corrodes at the same rate over its entire surface, or it can be localized, in which only small areas are affected. The classification by appearance, uniform or localized, is very useful for a preliminary discussion which, if necessary, requires establishing differences between macroscopic localized corrosion and microscopic local attack (**Figure I.1**).

Localized corrosion: When small areas of the metal are affected. Localized corrosion is divided into macroscopic and microscopic.

Galvanic corrosion: This form of corrosion is produced when two different metals in contact or connected by an electrical conductor are exposed to a conductive solution. In this case, there is an electrical potential difference between the different metals and induces and directs the passage of the electric current through the corrosive agent, so that the current flow corrodes one of the metals of the formed pair. The greater the potential difference between the metals, the greater the risk of galvanic corrosion. It is worth noting that this type of corrosion only causes the deterioration of one of the metals, while the other metal in the pair suffers hardly any damage. The metal that corrodes is called the active metal, while the one that does not suffer damage is called the noble metal. The area ratio between the two metals is very important, as a very large surface of noble metal compared to the active metal will accelerate corrosion and, on the contrary, a larger surface of the active metal compared to the noble metal decreases the attack.

Erosion corrosion: This is an attack accelerated by the high flow velocity, i.e. the destruction of a metal by the action of abrasion or friction caused by a flow, liquid or gas, (with or without suspended matter) [22]. Some methods used to prevent erosion attacks are the use of harder materials, or the change of the speed or environment.

Crevice corrosion: The environmental conditions in a crevice can eventually become very different from those of a clean and open surface, so that a very aggressive environment can develop and cause corrosion in the crevices. These are usually found in gaskets, overlaps, screws, etc.

Pitting corrosion: Pitting corrosion is characterized by the formation of small holes in the metal surface. It results from the existence of different electrochemical potentials due to a difference in oxygen concentration. The parts with a lack of oxygen act as an anode and the parts with an excess of oxygen, as a cathode. Pitting corrosion is a slow process that can take months or years to become visible, but it naturally causes unexpected failures. The small size of the pit and the tiny amounts of metal that dissolve, once formed, make its detection very difficult at the beginning [23].

Exfoliation corrosion: Exfoliation corrosion is a type of corrosion that occurs beneath the surface of a material. It starts on a clean surface, but spreads beneath it. It is distinguished from pitting corrosion by the fact that the attack has a laminated appearance, all layers of the

material are corroded and the attack is generally effective. This mechanism is known in aluminium alloys and is prevented by the use of alloys or heat treatments [23].

Selective leaching corrosion: This corrosive phenomenon produces a porous metal with very poor mechanical properties. It is produced by the removal of one of the elements of an alloy, the most important example being dezincification or the removal of zinc in copper-zinc alloys. In this case, the remedy is to use alloys that are not sensitive to this process [23].

Intergranular corrosion: The solidification of a molten metal begins with the formation of nuclei, each of which follows a regular atomic arrangement to form what are called grains or crystals. However, due to random nucleation, the planes of atoms located near the grains do not fit perfectly and the space between them is called the grain boundary. Grain boundaries are preferentially attacked by a corrosive agent and the attack is related to the segregation of specific elements or the formation of a compound at the boundary [23].

Stress-corrosion cracking: Also known as stress corrosion cracking, it occurs when a metal is simultaneously exposed to a corrosive environment and tensile mechanical stresses. Cracks form that can be transgranular or intergranular. The latter propagate through the metal until the stresses are released or the metal fractures [24].

a. **Uniform corrosion:** When a metal corrodes at the same rate over its entire surface. It is carried out on large parts of the surface of a metal. This can be developed in a wet or dry environment and can be caused chemically or electrochemically [25]. This type of corrosion is the most common and easiest to predict.

I.2. Corrosion control methods

Currently, there are several methods for controlling, reducing and preventing metal corrosion. However, these attempts to interfere with the corrosion mechanism are not able to completely prevent it. There are five main methods of corrosion control [26] :

I.2.1. Material selection

Each metal and alloy has a unique and inherent corrosion behavior that is reflected in its position in the electrochemical series or galvanic series. This can range from the high-

resistance range of noble or passive metals such as gold and platinum to the low-resistance range of active metals such as sodium and magnesium.

I.2.2. Coatings

Corrosion-resistant coatings can be divided into two main groups: metallic and non-metallic (organic and inorganic). The objective is the same regardless of the type of coating: to isolate the metal surface from the corrosive environment. The concept of applying a coating with a more noble metal on an active metal is based on the advantage of a greater corrosion resistance of the noble metal. Alternatively, a more active metal can be applied and, in this case, the coating corrodes or sacrifices instead of the substrate.

Non-metallic coatings can be organic and inorganic. The organic coating may contain corrosion inhibitors.

Non-metallic inorganic coatings include porcelain, cement, and silicate-based inks, glass coatings, and other corrosion-resistant ceramics. Like organic coatings, inorganic coatings are used for corrosion applications as barrier coatings to isolate the metal from the corrosive environment.

I.2.3. Cathodic protection

In practice, this method consists in modifying the potential of the metal to be protected by using an anode in the electrolyte. This can be applied by two systems: a forced current system and a sacrificial anode system.

- ✓ Forced current system

In this system, an external power supply is used to create a current that flows from the anode to the cathode. This current causes the cathode to become more negative, which prevents it from corroding.

- ✓ Sacrificial anode system

In this system, a sacrificial anode is used to corrode in place of the protected metal. The sacrificial anode is made of a more active metal than the protected metal, so it corrodes more

easily. As the sacrificial anode corrodes, it releases electrons that flow to the protected metal, preventing it from corroding.

I.2.4. Design

The design principle can eliminate many corrosion problems and reduce the time and costs associated with maintenance and repairs. Corrosion frequently occurs in small spaces or cracks where the corrosive environment begins to be more aggressive. These areas can be eliminated or reduced at least in the design process. When stress corrosion is possible, components can be designed to operate at stress levels below those that are likely to collapse.

I.2.5. Corrosion inhibitors

One of the most modern methods of corrosion control is the use of corrosion inhibitors, which is the subject of this thesis. Therefore, this section will be more detailed than the previous ones. These substances act as negative catalysts for the corrosion reaction and, in general, they must be compatible with the system to be protected, thermally stable under operating conditions, easy to handle and store, economical and do not modify the process of the system to be protected [27].

I.2.5.1. Definition

A corrosion inhibitor is a chemical that, when added to a corrosive environment, reduces the rate of corrosion to acceptable levels [27, 28].

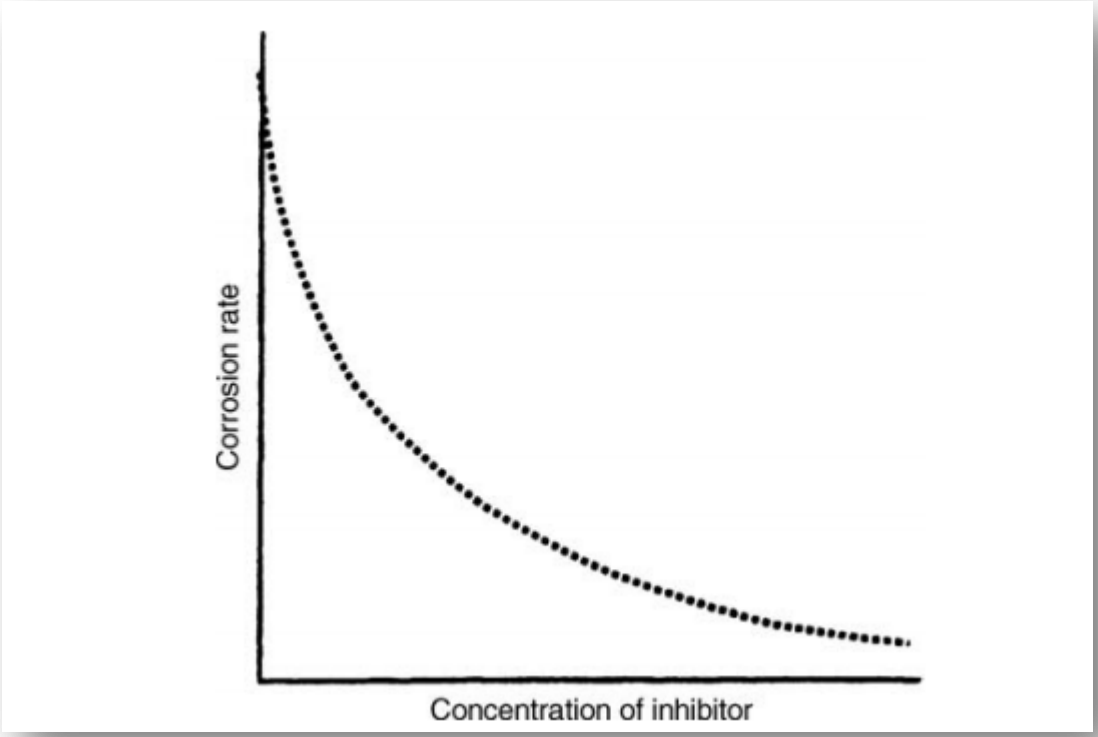

Figure I.2: Relationship between inhibitor concentration and corrosion rate [29].

The correlation between inhibitor concentration and corrosion rate is illustrated in **Figure I.2**, while the correlation between inhibitor concentration and degree of inhibition is shown in **Figure I.3**. It is common practice to apply corrosion inhibitors at low doses. To be effective, a corrosion inhibitor must to be both compatible with the fluid and capable of reducing corrosion. The inhibition efficacy of the corrosion inhibitor is generally assessed and is defined as follows:

$$IE\% = \left(\frac{W_{corr} - W'_{corr}}{W_{corr}}\right) * 100 \qquad (I.1)$$

Where: W_{corr} is the corrosion rate in the absence of inhibitor and W'_{corr} is in the presence of inhibitor.

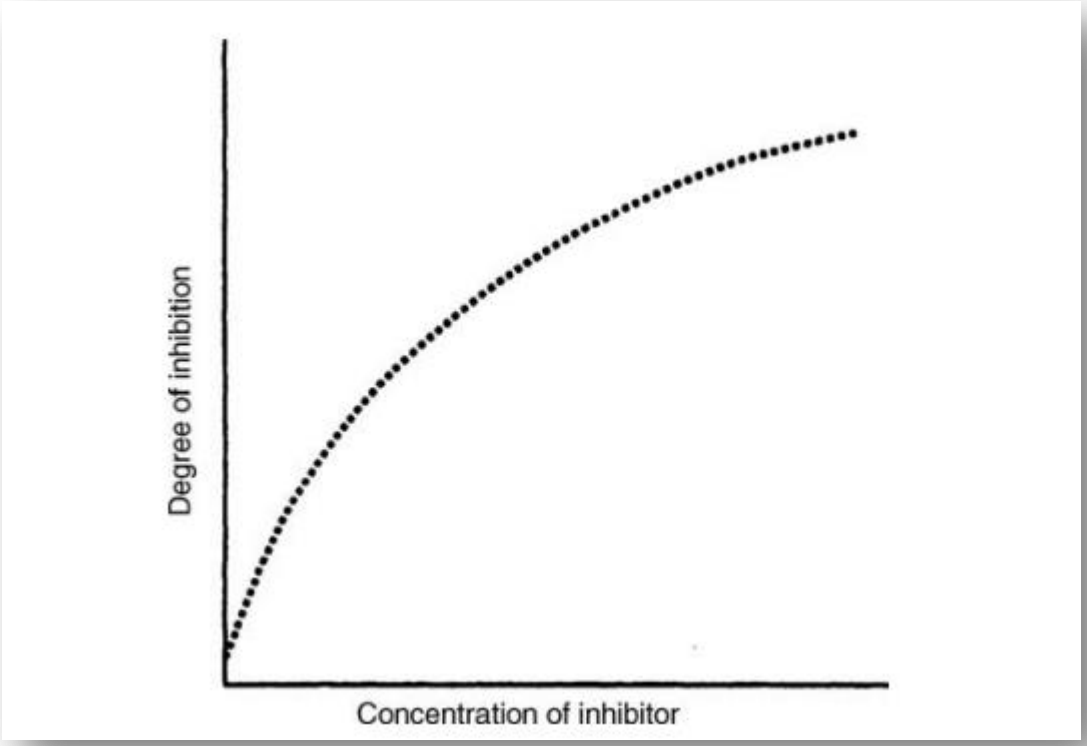

Figure I.3: Relationship between degree of inhibition and inhibitor concentration [29].

There are two methods in which a corrosion inhibitor might reduce corrosion. Through its interactions with corrosive species, it has the ability to transform corrosive media into an environment that is less or non-corrosive. In other instances, it prevents corrosion by interacting with the surface of the metal.

The occurrence of adsorption can be influenced by various circumstances, including but not limited to inhibitor compositions, electrolyte types, temperature, and so on. Coordinate covalent bonds may develop during the chemical adsorption process.

It is common practice to do green corrosion inhibition at room temperature, and the effectiveness of the inhibition is typically found to be inversely proportional to temperature [30].

The effect of green corrosion inhibitors is also regulated by the structure of the components, such as [31]:

- The inhibitors are generally in onium ions form, i.e cations that would result from the substitution of hydrogen atoms in those ions by other groups, which are adsorbed on the metal surface having active cathodic sites

- The plant extracts contain compounds that has O- and N- atoms carrying free electrons which facilitate to form bonds with the electrons that are freely available on the metal surfaces

I.2.5.2. Classification of corrosion inhibitors

Based on their mode of interaction, there are two main classes of inhibitors [29, 32]:

- Environment modifiers
- Adsorbent inhibitors

The inhibitory mechanism of environmental modifiers interacts with corrosive species in order to prevent metal degradation. The effectiveness of deoxygenants, including hydrazine or sodium sulfite combined with cobalt nitrate and biocides, in preventing microbial corrosion can be proved. In neutral and alkaline solutions, the reduction of oxygen serves as a cathodic process that can be alleviated by deoxygenants, thus preventing corrosion.

Cathodic reaction: $O_2 + 2H_2O + 4e^- \longrightarrow 4OH^-$

Oxygen elimination: $2SO_3^{2-} + O_2 \longrightarrow 2SO_4^{2-}$

In the case of adsorbent inhibitors, the inhibition mechanism consists of a chemical reaction between the inhibitor and the metal surface, forming a protective film that prevents the metal from reacting with corrosive species. This type of inhibitor is often used in the protection of steel and other metals in aqueous environments by two steps:

1. Transport of the inhibitor to the metal surface. The inhibitor must be able to reach the metal surface in order to be effective. This can be done by diffusion, convection, or advection.
2. Metal-inhibitor interactions. Once the inhibitor reaches the metal surface, it must interact with the metal in order to prevent corrosion.

The effectiveness of a corrosion inhibitor depends on a number of factors, including the type of corrosive environment, the type of metal, and the concentration of the inhibitor.

Based on whether the corrosion inhibitor suppresses the cathodic or anodic reaction, inhibitors are categorized into three different types [29]:

- Cathodic inhibitors: These inhibitors suppress the cathodic reaction, which is the reduction of oxygen.
- Anodic inhibitors: These inhibitors suppress the anodic reaction, which is the oxidation of the metal.
- Mixed inhibitors: These inhibitors suppress both the cathodic and anodic reactions.

Cathodic inhibitors interfere with hydrogen evolution in acidic solutions and oxygen reduction in alkaline or neutral solutions. As shown in **Figure I.4**, it has also been noted that the cathodic branch of the polarization curve changes with introduction of a cathodic inhibitor.

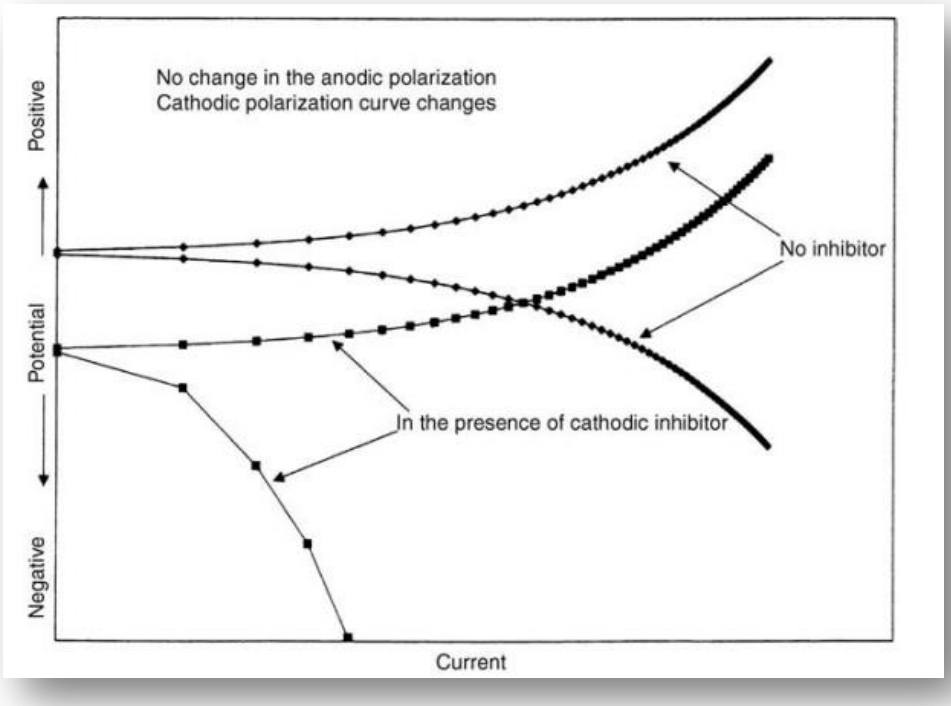

Figure I.4: Polarization Curve with the Addition of a Cathodic Inhibitor [29].

Many differences are observed in the cathodic branch of uninhibited or inhibited systems.

Substances that exhibit a high hydrogen potential in acidic solutions, as well as those that become insoluble in alkaline solutions, are typically effective as cathodic inhibitors. Inorganic inhibitors like phosphates, silicates, and borates in alkaline solutions, which impede oxygen reduction at cathodic sites. Calcium and magnesium carbonates, among other substances, obstruct cathodic sites because of their low solubility.

Anodic inhibitors typically demonstrate effectiveness at pH levels ranging from 6.5 to 10.5, which is considered near-neutral to basic. Oxy-anions like chromates, molybdates, tungstates, and sodium nitrites serve as highly effective anodic inhibitors. These oxy-anions are believed to play a crucial role in the repair of defects in the passive iron oxide film on the surface of iron. The concentration of the inhibitor is crucial in the case of chromate or dichromate. At times, dichromate is regarded as a "dangerous inhibitor" when the concentration of the inhibitor is inadequate. In the same vein, the harmful effects and environmental contamination do not support the utilization of chromates.

Mixed-type inhibitors act on both branches of the polarization curve, namely cathodic and anodic.

Organic inhibitors adsorb onto the metal surface, forming a barrier to anode dissolution and oxygen reduction at cathodic sites. The protective functional groups in mixed-type organic inhibitors can be amino, carboxy, or phosphonates, among others.

I.2.5.3. Adsorption of inhibitors on metal surface.

Generally, the adsorption of inhibitor molecules on the metal-solution interface inhibits corrosion by altering potential between the electrode and the solution, which is caused by an uneven distribution of electric charges at the interface [29]. The electrolyte-metal interface is characterized by the presence of an electric double layer, and occasionally a triple layer. **Figure I.5** illustrates a schematic representation of the electric double layer.

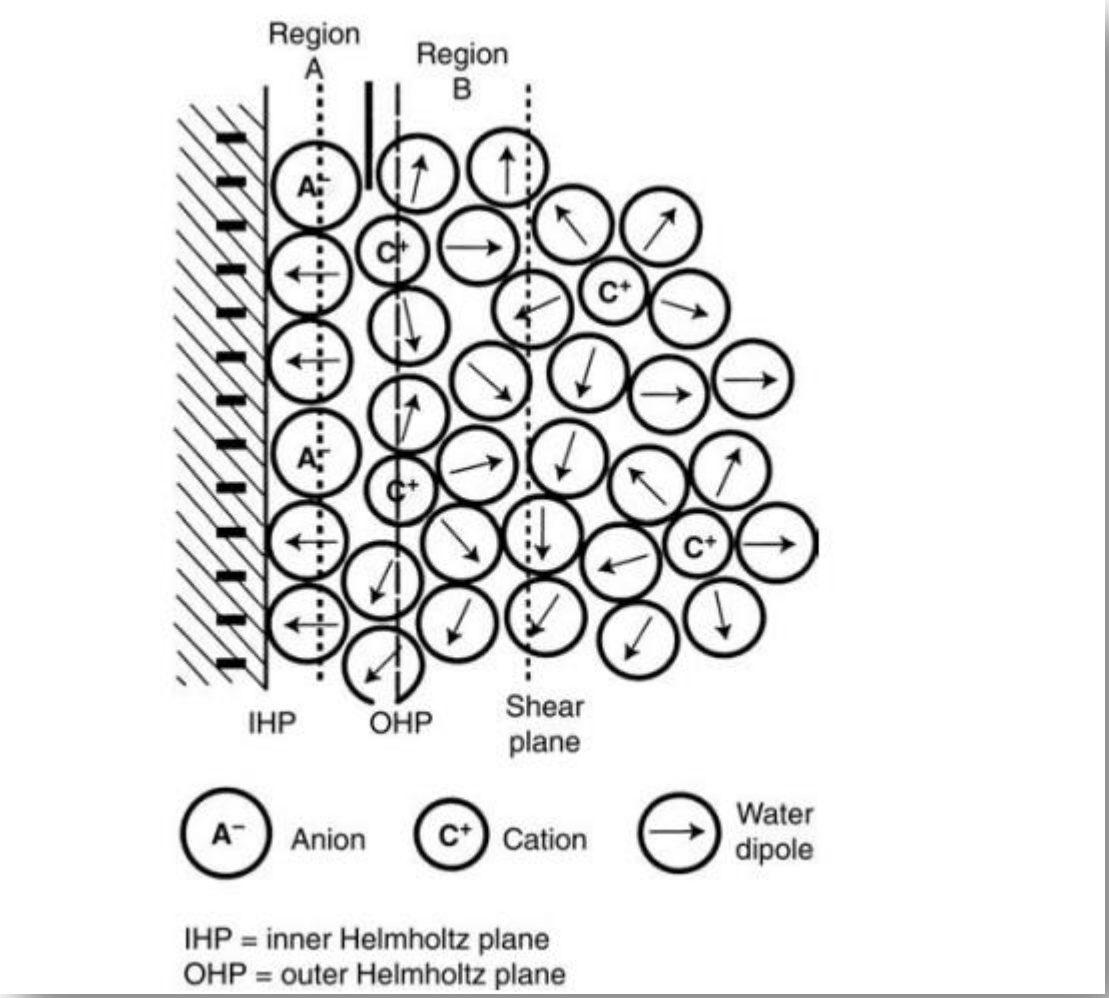

Figure I.5: Schematic illustration of the electrical double layer [29]**.**

The first layer consists of a film of charges on the surface of the metal resulting from either a deficit or an excess of electrons. The second layer (region A) is formed on one side of the interface solution, in particular by adsorbed ions. The centers of these charges form the inner Helmholtz plane of the double layer. These anions lose their coordinated water molecules, displacing the adsorbed water molecules on the metal surface, and then in turn adsorb in portions on the pure metal surface. These ions are known as potential determining ions. The charges are partly counterbalanced by hydrated ions of the opposite charge in the external Helmholtz plane in the B region called counter-ions. On the outer face of this zone (region C) in the **Figure I.6**, it is called the diffuse Gouy-Chapman layer, where the concentration of contractions decreases towards the electrolyte and balances the net charge near the metal surface.

The ions formed in the double layer are distributed not only by the kinetic motion and the electric field of the surface, but also by the specific chemical interaction between the ions and the interface, i.e. where region A has been reached by the ions. These interactions are distance dependent and include hydrogen and covalent bonds and π bonds or hydrophobic interactions that do not occur in the outer region.

The potential variation that occurs with the interface distance is illustrated in **Figure I.6**. Considering regions A and B as a parallel capacitor, the potential falls linearly from P_a to P_b, and this potential, referred to the Stern potential, cannot be measured directly, but is assessed relative to the hydrogen electrode. The electrochemical standards potential can be measured. The incorporation of a corrosion inhibitor to the electric double layer changes its composition and structure. Therefore, the measurement of the electric double layer capacity prior and after the addition of the corrosion inhibitor can be used to monitor the adsorption of the inhibitor.

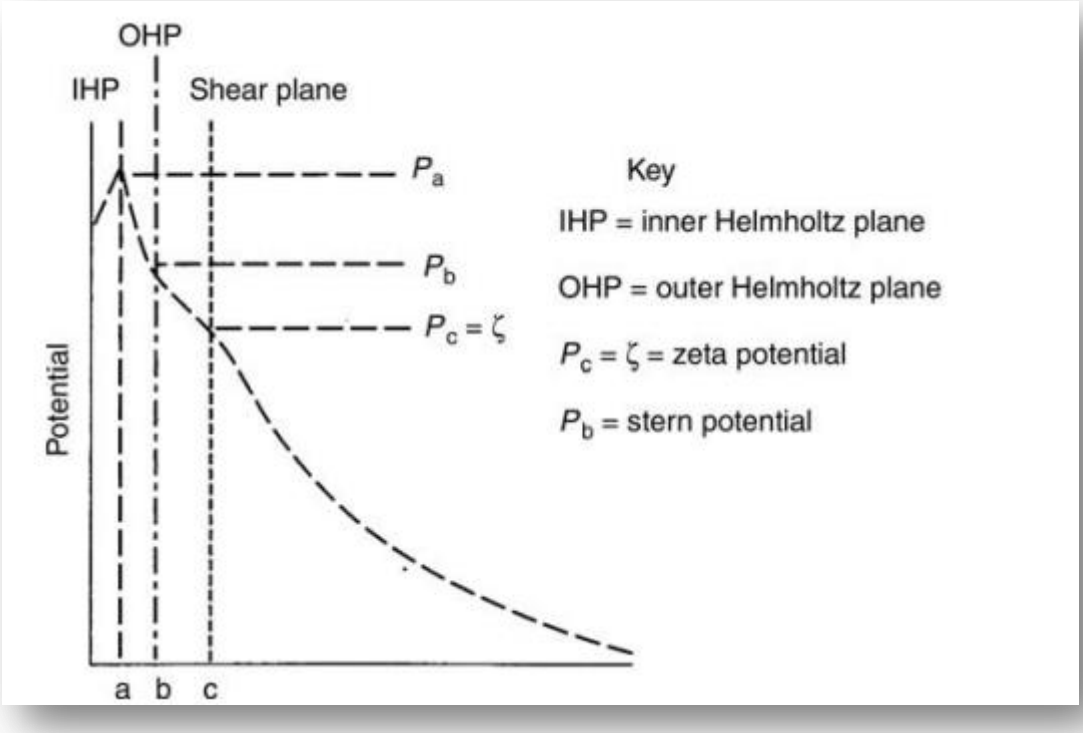

Figure I.6: Potential variation in the double layer [29].

It is also possible to identify changes in the zeta potential by monitoring the adsorption of inhibitors. Just beyond the outer Helmholtz plane lays the zeta potential, which is necessary to initiate electrokinetic activity with the electrolyte. The total potential drop does not change

when a supporting electrolyte is added. However, the thickness of the double layer decreases as the same number of charges of the opposite sign is still required to balance the potential-determining ions. Consequently, there is a decrease in the zeta potential and a modification to the potential distribution. Electric double layers alter the structure and characteristics of polar neutral ions and molecules when they contact with them. When an inhibitor ***I*** approaches and adsorbs on the metal-solution interface, this can be written as follows:

$$M(nH_2O)_{ads} + I_{(sol)} \longrightarrow MI_{ads} + nH_2O_{(sol)} \qquad I.2$$

It is the inhibitor that is responsible for the displacement of the water molecules that were first adsorbed on the metal during the process of inhibitor adsorption. The adsorption of an inhibitor onto a metal takes place due to the fact that the energy of interaction between the metal and the inhibitor is more favorable than the energy of interaction between the water molecules and the metal [29].

The dielectric characteristics of water are influenced by the adsorption of an inhibitor onto the metal. In the large volume of water, water molecules are randomly oriented and the dielectric constant is equal to 80. In the electric double layer, the orientation of water molecule dipoles results in a reduction of the dielectric constant. The values of the dielectric constants of water have been estimated to be 6 and 40, respectively, in the inner and outer Helmholtz planes. Ions or molecules possessing a significant dipole moment, upon adsorption onto the metal surface, influence the electric double layer, resulting in alterations to the dielectric characteristics of water molecules within the Helmholtz double layer [29].

I.2.5.4. Methods for the study of inhibitors

The study of inhibition can have essentially two different objectives:

- The knowledge of the protective efficiency of the added inhibitor and

- The understanding of its mechanism of action [33].

While the methods used for the study of the mechanisms can be very varied and have different functions, the methods used to verify the effectiveness of inhibitors are often the

same usual methods for evaluating corrosion phenomena, based on the expression (I.1) or other similar expressions.

The properties of a corrosion inhibitor are not the only factor in determining its effectiveness, but there are other factors related to the metal to be protected, such as the condition of its surface, purity or hydrogen permeability, as well as those depending on the environment, such as its pH, dissolved oxygen concentration, aggressive ions or interfering species. Normally, inhibitors quickly lose their effectiveness by raising the temperature of the environment, its dissolved oxygen content and salt concentration; while an increase in pH generally strengthens it.

The gravimetric test is a very reliable and accurate technique. To determine the corrosion rate by this method, the material to be studied must be subjected to an attack by the corrosive agent for a fairly long period of time, which makes it a long and tedious test. Once the attack is complete, the change in weight that the material undergoes is determined in order to obtain the corrosion rate in milligrams of material lost per day and a surface in dm^2 of exposed material.

The development of instrumental electrochemical techniques has greatly facilitated the experimental determination of the effectiveness of inhibitors and has largely contributed to the progress of research in the field of inhibition, to the point that electrochemical methods are currently the most widely used in the study of the behavior of inhibitors.

I.2.5.5. Green Corrosion Inhibitors: Some previous studies

Currently several investigations have been carried out using different plant sources as corrosion inhibitors. Many extracts and oils extracted from different parts of various plants have been used for this purpose. Many active groups contained in these extracts, are considered as the key factors inhibiting corrosion, are very fruitful for preventing different forms of corrosion. Some interesting works are mentioned in **Table I.1**.

Table I.1: Different natural products and their anti-corrosive properties.

	Inhibitor	Metal	Corrosive medium	Observations	Ref
1	*Citrus* peel	Aluminium	0.5 to 2M HCl	At 10°C the IE was 91%.	[13]
2	*Henna* leaves	Mild Steel	1M HCl	At C=1.2 g/L the IE was 92.06%	[14]
3	Cladodes of *opuntia ficus indica*	Steel	1M HCl	The IE was 94%	[15]
4	*Green Tea*	Carbon Steel	1M HCl	At C=0.08 g/L the IE was 78%	[16]
5	*Cytisus multiflorus* flowers	Carbon Steel	1 M H_2SO_4	At C=0.5 g/L the IE was 95.91%	[17]
6	*Rosmarinus officinalis* plant	XC48 Steel	1M HCl	At C= 0.4 g/L the IE was 91%	[18]
7	*Moringa oleifera* leaves	Copper	1 M (HNO_3+H_3PO_4)	At C= 0.3 g/L the IE was 89.30%	[19]
8	*Cryptostegia grandiflora* Leaves	Mild Steel	1 M H_2SO_4	At C= 0.5 g/L the IE was 83.54%	[20]
9	*Diospyros kaki* leaves	St 37 Steel	1M HCl	At C= 0.225 g/L the IE was 91.00%	[21]
10	Grains of *peganum harmala*	6063 Al alloy	1M HCl	At C= 0.025 g/L the IE was 91.78%	[22]
11	*Geissosper mum* leave	C38 Steel	1M HCl	The IE was 90% at 20°C	[23]
12	*glycine max* leaves	Mild steel	0.5 M HCl	At C= 0.5 g/L the IE was 84.50%	[24]
13	*Lanneacoromandelica* leaves	Mild steel	1 M H_2SO_4	At C= 250 mg/L the IE was 88.50%	[25]

I.3. Thermodynamics of corrosion

The corrosion process is directly related to Gibbs' free energy. Higher the Gibbs' free energy higher will be the corrosion. Green corrosion inhibitors can be utilized to reduce free energy. Inhibitors accumulate on the active site surfaces of corroded metals, creating a barrier that reduces the corrosion rate.

This can be summarized in the three following cases [34].

1. The change in free energy (ΔG) is positive. The metal is active and corrosion can occur. This is the most common case among commonly used metals.
2. However, it may happen that even when ΔG is greater than zero, instead of showing corrosion, the metal remains apparently unaffected. It is said that the metal is passivated.
3. On the other hand, if $\Delta G \leq 0$, the metal is indifferent to the usual aggressive agents and no corrosion reaction is possible. This is the case of noble metals.

If one wants to know the possibility that a corrosion reaction will occur spontaneously in certain real circumstances, one must know the energy changes associated with the reaction.

The change in free energy is given by:

$$\Delta G = \sum n_i \mu_i \, (final\ stage) - \sum n_i \mu_i \, (initial\ stage) \qquad I.3$$

Where $\Sigma n_i \mu_i$ is the sum of the chemical potentials of the i^{th} compound in its final and initial states. The greater the change in energy, the more likely the process is to occur [35].

If the sign of the balance is negative, it means that it is passing from a state of higher energy to a state of lower energy. This type of process is spontaneous and occurs in nature by releasing energy. If the change in free energy in a reaction is equal to the total reversible work that can be done, then:

$$-\Delta G = \Delta W \qquad I.4$$

Where $-\Delta G$ is the change in free energy of a spontaneous reaction, ΔW denotes any type of work (electrical, expansion, gravitational, etc.).

I.3.1. Thermodynamic parameters of adsorption isotherms.

Thermodynamic parameters of adsorption isotherms include standard Gibbs free energy (ΔG), standard enthalpy (ΔH) and standard entropy (ΔS) [36, 37]. Analysis of these parameters allows to determine the feasibility of the adsorption process, as well as the effect of temperature on them. These parameters can be calculated from the estimated values of the equilibrium constant, K, from adsorption isotherms at different temperatures, as follows:

$$K = \frac{1}{C_{H_2O}} \exp\left(\frac{\Delta G_{ads}}{RT}\right) \qquad I.5$$

Where: C_{H_2O} is the concentration of water molecules (in mL L^{-1}) at the metal/solution interface.

The obtained values of ΔG_{ads} are plotted against temperature according to the following equation: [38]

$$\Delta G_{ads} = \Delta H_{ads} - T\Delta S_{ads} \qquad I.6$$

The intercept of the line represents the values of ΔH_{ads}. By entering the values in the previous equation, the values of ΔS_{ads} are calculated for all the temperatures studied.

This equation is used primarily at the level of perfect gas systems, but its use can be extended to adsorption at very dilute solid-liquid interfaces, as it implies that the intermolecular distance is large enough to ensure ideal gas-like behavior.

Gibbs free energy (ΔG_{ads}): It can be used to determine if a process is spontaneous or not. Negative values of ΔG_{ads} imply a spontaneous process, while positive values mean that energy must be supplied to the system because it cannot evolve on its own.

Enthalpy of adsorption (ΔH_{ads}): provides information on the exothermic or endothermic nature of the process, the activation energy can also be estimated and also allows

to differentiate if it is a process that occurs by physical adsorption (low values) or chemical adsorption (high values).

Entropy of adsorption (ΔS_{ads}): It allows to predict the extent of changes at the surface of the adsorbent, because if the changes are very deep in the same thing, reversibility is affected by what would give a negative value of the adsorption entropy, otherwise, it indicates a great possibility of reversibility.

I.3.2. Adsorption isotherms

Adsorption differs from absorption in that the latter implies the accumulation of the absorbed substance throughout the volume of the absorbent, and not only at its surface. Two limiting adsorption behaviors can be distinguished, physisorption and chemisorption, although it is common to observe intermediate behaviors.

- Physical adsorption or physisorption: Gas molecules remain bound to the surface of the solid by Van der Waals forces (dipole-dipole interactions, dispersion, and/or induction). This fact defines all the characteristics of physisorption (**Table I.2**).
- Chemical adsorption or chemisorption: It was proposed by Langmuir in 1916. In this case, gas or solute molecules remain attached to the surface by forming a strong chemical bond. This fact defines the characteristics of chemisorption (**Table I.2**).

Table I.2: Characteristics of physical adsorption and chemical adsorption [20]**.**

Physical adsorption or physisorption	Chemical adsorption or chimisorption
✓ It is a weak interaction. ✓ It is an exothermic process in which the released heats, the ΔH_{ads} (about 20-40 kJ/mol) are similar to the condensation enthalpies of the adsorbed substance. ✓ The released energy is adsorbed in the form of vibration by the solid network and the ΔH_{ads} can be measured by increasing the sample temperature. ✓ The physioadsorbed molecule retains its identity because the energy is insufficient to break the bond, although its geometry may be distorted. ✓ Physical adsorption is a non-specific process because the forces present are not and there is no marked selectivity between adsorbate and adsorbent. ✓ Physical adsorption occurs in multilayers. Another layer can be adsorbed on a layer of dispersed gas. The ΔH_{ads} for the first layer are determined by the forces between the adsorbent (M) and the adsorbate (A), while the ΔH_{ads} for the following layers depend on the A-A interactions and are therefore similar to the condensation enthalpy.	✓ It is a stronger interaction. ✓ The enthalpies of chemisorption are typically in the range of -100 to -500 kJ/mol, which is similar to the energy released when chemical bonds are formed. However, chemisorption can also result in the breaking of bonds, in which case the enthalpy of chemisorption could be positive or negative. In general, chemisorption is exothermic, meaning that it releases heat. This is because a spontaneous process requires the free energy (ΔG) to be negative. The translational freedom of the adsorbate is reduced during chemisorption, which decreases the entropy (ΔS). As a result, the enthalpy (ΔH) must be negative in order for ΔG to be negative. There are some exceptions to this rule, such as when the adsorbate dissociates or exhibits high surface mobility. ✓ Chemisorption is specific. For example, N_2 is chemically absorbed at room temperature on Fe, W, Ca and Ti, but not on Ni, Zn, Ag, Cu or Pb. ✓ As it involves the formation of a bond between the adsorbent and the adsorbate, the process stops after the formation of a monolayer on the surface. Although only one layer can be chemisorbed, physical adsorption of new layers of adsorbate can occur on the first. ✓ In general, chemisorption involves the breaking and formation of bonds, so the chemisorbed molecule does not retain the same electronic structure (bonds) as in the gas phase.

The amount of material adsorbed in a system depends on the temperature and the pressure or concentration of the adsorbate. If the temperature is kept constant during the experiment, the degree of adsorption can be studied as a function of the pressure or concentration and thus generate what is called the adsorption isotherm.

I.3.3. Types of adsorption isotherms

Experimental isotherms can be classified into five types, according to S. Brunauer [39].

Type I: called the Langmuir isotherm, corresponds to a monolayer adsorption. The amount adsorbed increases with pressure or concentration until it reaches a limiting value corresponding to the surface coating by a monolayer. This is the isotherm characteristic of a chemisorption process only.

Type II: indicates physical adsorption in multiple layers. The initial rapid rise corresponds to the formation of the first layer, which in this case has a higher formation constant than the rest of the layers (the enthalpy of formation of the first layer is more negative than that of the rest of the layers). As the pressure or concentration continues to increase, the second layer of adsorbed molecules is formed, followed by others.

Type III: also corresponds to physical adsorption in multiple layers but where the equilibrium formation constant of the first layer is the same as for the following ones (no difference is observed between the filling of the first layer and the rest).

Types IV and V: correspond to multilayer adsorption on porous materials.

They differ from types II and III due to the presence of a horizontal branch (saturation) and a hysteresis loop (the adsorption and desorption curves differ).

I.4. Mild Steel Corrosion

Mild steel is a popular choice for a variety of applications because it is relatively inexpensive, easy to work with, and has good strength and ductility. However, it is also susceptible to corrosion, which can be a major problem in some applications.

There are a number of factors that can contribute to the corrosion of mild steel, including the type of environment it is exposed to, the presence of moisture and oxygen, and the presence of other corrosive substances. The type of corrosion that occurs can also vary depending on the environmental conditions.

I.4.1. Corrosion of carbon steel in hydrochloric acid

Carbon steel is widely used, but its major drawback is its vulnerability to corrosion, especially when it is in contact with an aggressive environment such as hydrochloric acid. In an aqueous environment, the electrochemical corrosion process of steel can be simplified by two simultaneous elementary electrochemical reactions. For example, in the anodic zone:

$$Fe \rightarrow Fe^{2+} + 2e^{-} \quad I.7$$

The ferrous ions Fe^{2+} pass into the solution and can be subsequently oxidized to ferric ions Fe^{3+}. In the cathodic zone, the electrons produced are consumed in order to maintain the electronic balance. The corresponding cathodic reactions are the reduction of dissolved oxygen in water (I.8) or the reduction of the proton with hydrogen evolution (I.9) [40]:

$$O_2 + 2H_2O + 4e^{-} \rightarrow 4OH^{-} \quad I.8$$

$$2H^{+} + 2e^{-} \rightarrow H_2 \quad I.9$$

The hydroxide ions OH^- formed in the solution can then combine with the ferrous ions Fe^{2+} and precipitate as iron hydroxide on the surface of the steel, when the concentrations of ferrous and hydroxide ions allow :

$$Fe^{2+} + 2OH^{-} \rightarrow Fe(OH)_2 \quad I.10$$

In general, in hydrochloric acid medium, the Cl^- anions can accelerate corrosion by probably promoting anodic dissolution. The mechanism can be expressed as follows [41]:

$$Fe = 2Cl^{-} \rightarrow FeCl_2 + 2e^{-} \quad I.11$$

$FeCl_2$ is an unstable product, it will be oxidized to FeOOH, and Cl^- will be released again, to restart a new cycle [41].

FeOOH can be transformed into Fe2O3 (hematite), in the presence of oxygen and into Fe_3O_4 (magnetite) if oxygen is insufficient [42]. These compounds, by covering the metal surface, form a passivation layer which can be protective depending on its tightness. In fact, the porosity of this layer will control the corrosion rates.

In general, in an acidic medium, steel undergoes generalized corrosion induced by solvated protons H^+ and a layer of corrosion product composed mainly of Fe_2O_3 is formed [42].

I.4.2. Pourbaix diagrams of iron in aqueous medium

Pourbaix had the idea to draw these diagrams for each metal, from the Nernst law giving the expression of the equilibrium potential [43]. Pourbaix diagrams represent electrochemical equilibrium diagrams that indicate the potentials as a function of pH.

Figure I. 7 shows an example of an E-pH diagram for iron in aqueous medium under standard temperature and pressure conditions (T = 25 °C, P = 1 atm). In this example, only hematite (Fe_2O_3) and magnetite (Fe_3O_4) are considered. The concentration of dissolved ferrous and ferric ions is 10^{-6} mol/L. This diagram highlights several domains:

- ✓ corrosion of the metal: areas where the iron is soluble in the form of ions (Fe^{2+} and Fe^{3+});
- ✓ immunity of the metal: zone where the metal does not react, domain of stability of iron (Fe);
- ✓ passivation of the metal: zones of stability of metallic oxides that protect iron (Fe_2O_3, Fe_3O_4);
- ✓ thermodynamic stability of water at atmospheric pressure: region delimited by parallel lines, in dotted lines (a) and (b).

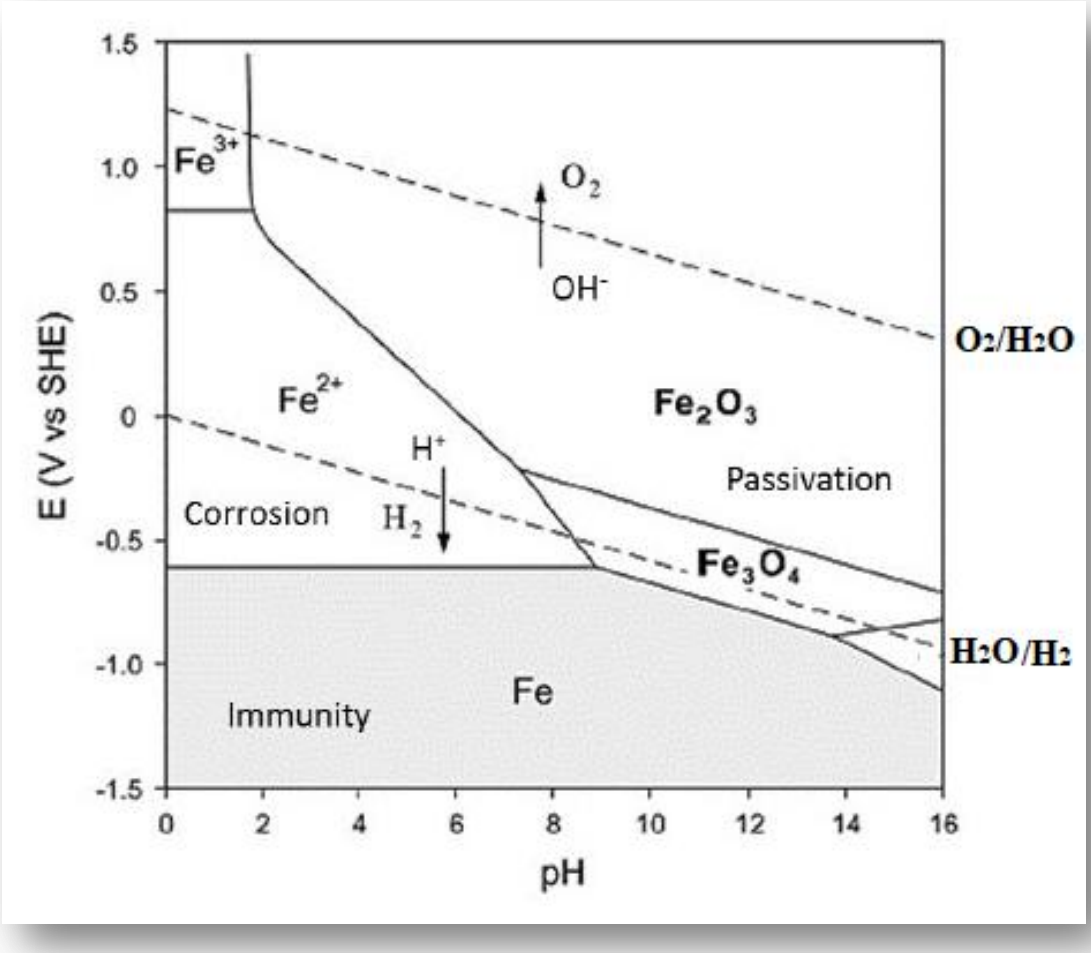

Figure I.7: Simplified Pourbaix diagram of the iron/water system at $\mathbf{25°C}$ and $\mathbf{1}\boldsymbol{atm}$ (for $[\boldsymbol{Fe^{2+}}] = [\boldsymbol{Fe^{3+}}] = \mathbf{10^{-6}}\ \boldsymbol{mol/L}$) [44].

In this case, the diagram shows the different oxidation states of iron as a function of pH and potential in an aqueous environment. The diagram shows that iron is stable at a neutral pH and a positive potential. However, iron is prone to corrosion in an acidic or basic pH.

Chapter II

Material, Methods, Extraction

And Modelling

CHAPTER II. MATERIAL, METHODS, EXTRACTION AND MODELLING

Introduction

The first step in this work is a screening step that will allow us to select plants based on several criteria:

Chemical criteria: The first selection criterion for plants from the North African flora is the presence and abundance of polyphenols and polysaccharides in the selected species, an important criterion for having a significant yield.

Polyphenols and polysaccharides can inhibit corrosion by forming a protective layer on the surface of the metal. This layer can prevent direct contact of the metal with oxygen and water, which are the main agents of corrosion. They can also act by modifying the pH of the solution. A low pH (acidic) can promote corrosion, while a high pH (alkaline) can inhibit it. Polyphenols and polysaccharides can increase the pH of the solution, which can help to inhibit corrosion.

Polyphenols and polysaccharides are effective and environmentally friendly corrosion inhibitors. They are non-toxic and do not produce hazardous waste. They are therefore an attractive alternative to traditional corrosion inhibitors, which are often toxic and/or polluting.

Polyphenols and polysaccharides can be used to inhibit the corrosion of different types of metals, such as steel, aluminum, and copper. They can also be used to inhibit the corrosion in different environments, such as water, air, and aqueous solutions.

Among botanical families that are rich in polyphenols in the North African flora, for example: Asteraceae, Rosaceae, and Lamiaceae. Likewise, among those that are rich in polysaccharides, the following families can be cited as examples: Poaceae, Fabaceae, Cactaceae.

Bibliographical criteria: The second criterion is the knowledge on the chosen species. A bibliographical search was undertaken on the botanical species correctly identified during the preliminary screening phase. This revealed the almost absence of chemical or electrochemical publications.

Supply criteria: The availability and ease of harvesting in the natural environment of the plant naturally eliminates rare or very small plants.

Based on the results of this screening, *Artemisia Herba Alba* and *Ammophila Arenaria* were selected for the current study

Many studies have focused on the Artemisia L. genus because of the many therapeutic chemicals it contains. Artemisia oil is an effective corrosion inhibitor due o its high concentration of bioactive compounds [45]. Some of the examined species are : Artemisia vulgaris L. oil [46], Artemisia Herba Alba essential oil [47], Artemisia Mesatlantica essential oil [48], and Artemisia Herba Alba methanolic extract [49].

Ammophila arenaria is widely known and exploited but unlike the Artemisia L. genus, the literature on its aqueous extract has not yet been cited as a corrosion inhibitor.

However, the extraction methods and the experiences used to evaluate the inhibition effectiveness of the two plant extracts on steel in HCl solution were detailed in this chapter. Additionally, we conducted some analysis for the extracts and the morphological properties of the steel surface for further deeper understanding of the inhibitors behavior.

The experimental findings were validated by integrating various theoretical models, along with other computational methods to further enhance our understanding the experimental results.

Part one: *Artemisia Herba Alba*

II.1.1. Wormwood (*Artemisia Herba Alba*)

II.1.1.1. Botanical description of *Artemisia Herba Alba* (AHA)

Artemisia is the genus name for wormwoods, it comes from the name of the Greek goddess of the hunt Artemis; herba-alba means white herb [50]. Its scientific name is Artemisia herba-alba asso or Artemisia incultadel; in French Armoise blanche and in Arabic شيح (**Figure II.1**). It is native to the various habitats of the Mediterranean region, where it occurs as a shrub growing up to 1 m in height. This plant is also considerable as a fodder for sheep and for livestock in Algeria where it grows abundantly [51]. It has the following systematic position:

Kingdom: Plantae

Subkingdom: Tracheobionta

Division: Magnoliopsida

Class: Mangnoliphyta

Subclass: Asteridae

Order: Asterales

Family: Asteraceae

Genus: Artemisia

Species*: Artemisia Herba-Alba*

Figure II.1: Wormwood Artemisia Herba-Alba

II.1.1.2. General Morphology

Artemisia Herba Alba (AHA) is a monthly plant that is very common in arid to semi-arid zones. It is a species described as an herb 30cm to 50cm tall with a flowering and slender

stem, slightly hairy and its leaves are oblong, cut into segments of dark green on the face and white cottony on their lower part, it also has small yellow tubular flowers (fidure I.8); it gives off a very strong smell, sometimes unpleasant [52].

II.1.1.3. Interest of the plant

The aerial part of *Artemisia herba alba* (AHA) has significant antioxidant activities. Indeed, this part of the plant is rich in compounds with antioxidant activity such as flavonoids, polyphenols and tannins. In addition, several scientific studies have also proven the effectiveness of white wormwood as an antidiabetic, antiparasitic, antibacterial, antiviral, antioxidant, antimalarial, antipyretic, antispasmodic and antihemorrhagic [53]. In traditional medicine, wormwood is very used in case of gastric disorder such as diarrhea and abdominal pain. It is also used as a remedy for inflammation of the gastrointestinal tract [54]. By far the most frequently cited remedy in the literature is the use of *Artemisia herba alba* in the treatment of diabetes mellitus [55].

II.1.2. Plant Extraction and characterization

The aerial components of the plant were harvested in autumn in northeastern Algeria. After cleaning the leaves using distilled water, leaving them to dry in a shaded area, the dried material was ground to a fine powder. The extraction of the dried powder obtained was done with an adequate volume (1/10ml) of mixed proportion (20/80 v/v) of water/methanol at room temperature by stirring for 24 h in the dark. The extract was filtered, dried and then stored at 4 °C until use.

The structural properties of the crude extract were examined by the infrared spectroscopy analysis (FTIR) using a “Shimadzu FTIR-8400S (Japan)” in the frequency range of $4000 – 400\ cm^{-1}$.

To determine the principal chemical elements in the leaves’ extracts, the “Liquid Chromatographic/Electrospray Ionization Mass Spectroscopy” ($LC/ESI-MS$) methodology HPLC-Triple quadrupole was performed on the crude extract using a mass spectrometer system “Agilent 6400 series”. For the separation of the samples an “Agilent Poroshell 120EC-C18 column” was used with a Formic acid solution “phase A” and an Acetonitrile solution “phase B” at room temperature and a volumetric flow rate of $0.5\ mL\ min^{-1}$. With the mass spectrometer (MS), nitrogen as the drying gas ($7\ mL\ min^{-1}, 300°C$) for an electrospray

ionization system, a $20\ psi$ nebulizer pressure, and a $4000\ V$ capillary voltage were used. In negative-ion mode, the MS was scanned at $1\ spectrum\ m\ s^{-1}$.

II.1.3. Metal and corrosive solution

Steel sheets used for the tests contains over 99.5% iron. The other chemical components are listed in **Table II.1** with their weight fractions. The specimens used in the weight loss study and the surface analyses have the following dimensions $2 \times 0.5 \times 0.2\ cm^3$. While the samples used for the electrochemical tests were cylindrical in shape with an exposed surface section of $0.27\ cm^2$. Samples were first polished using wet SiC paper ($grade$ 220– 2000), washed using distilled water, then degreased with acetone, and finally dried before each test.

The 1 M HCl solution was prepared using Hydrochloric acid (37%).

Table II.1: Mild steel chemical composition

$Element$	C	S	Mn	Si	Al	P
$Percentage\ (wt\%)$	0.21	*0.05*	*0.05*	*0.38*	*0.01*	*0.09*

II.1.4. Gravimetric study

In a $1\ M\ HCl$ solution containing different inhibitor concentrations varying from 0 to 1000 ppm, we performed gravimetric measurements on samples after being polished, cleaned, degreased and dried in order to determine the corrosion rate ($mg\ cm^{-2}\ h^{-1}$). Next, Samples were weighed and soaked in the prepared solutions as mentioned previously for 5 hours at ambient temperature then reweighed.

The inhibition efficiency determined by this method (IE_{wl}) can thus be defined based on the next formula [56]:

$$IE_{wl} = \frac{W_{corr} - W_{corr}'}{W_{corr}} \times 100 \qquad (II.1)$$

Where W_{corr}: the corrosion rate in $1\ M\ HCl$ an

W_{corr} ′: the corrosion rate in $1\ M\ HCl$ with various inhibitor doses.

II.1.5. Electrochemical measurements

The $EC-LAB\ V\ 10.33$ software was used for the investigation of potentiodynamic polarization (PDP) and electrochemical impedance spectroscopy (EIS) in a typical three-electrode cell (the counter electrode is platinum, the reference electrode is saturated calomel (SCE) and mild steel as the working electrode). The polarization curves were registered at a rate of 0.5 mV/s from an open circuit potential (OCP) of $-200\ mV\ to\ +200\ mV$. For the frequency range of $50\ kHz\ to\ 10\ mHz$, EIS quantifications were done using signal amplitude of $10\ mV$ peak-to-peak at the OCP.

The current densities, i_{corr} and i'_{corr} ($A\ cm^{-2}$), of mild steel corrosion in $1M\ HCl$ solution without and with the inhibitor, respectively, defined the inhibition efficiency from potentiodynamic polarization measurements (IE_{pdp}) using the next formula [57]:

$$IE_{pdp} = \frac{i_{corr} - {i_{corr}}'}{i_{corr}} \times 100 \qquad (II.2)$$

(CPE): constant phase element used to characterize the interfacial behaviors instead of using an ideal capacitor. The impedance of the CPE is estimated using the following equation [58]:

$$Z_{CPE} = \frac{1}{Q(jw)^a} \qquad (II.3)$$

Q is the CPE magnitude,

w is the angular frequency,

j is the imaginary unit,

And *a* is the CPE exponent ($0 < a < 1$).

The CPE is considered as an ideal capacitor.

The inhibition efficiency defined by electrochemical impedance spectroscopy (IE_{EIS}) is given as follows [59]:

$$IE_{EIS} = \frac{R_{ct} - {R_{ct}}'}{R_{ct}} \times 100 \qquad (II.4)$$

R_{ct}*:* the charge transfer resistance in the inhibited solution and

R'_{ct}*:* the charge transfer resistance in the uninhibited solutions.

$$C_{dl} = \frac{\varepsilon \varepsilon_0 A}{d} \qquad (II.5)$$

C_{dl}: is the double-layer capacitance (μ$F\ cm^{-2}$);

A: the projected surface area,

ε : the medium's dielectric constant and ε_0 : the permittivity of free space ($8854 \times 10^{-14}\ F\ cm^{-1}$) [60].

II.1.6. Surface characterization

The morphological examination of the steel surface after immersion in the aggressive solution that contains $900\ ppm$ of the inhibitor was performed using "an Asylum Research MFP-3D (Oxford Instruments company)" for the atomics force microscopy (AFM) and with "a TESCAN VEGA-3 micrograph" at $20.0\ kV$ for scanning electron microscopy (SEM).

X-ray diffraction (XRD) and X-ray Photoelectron Spectroscopy (XPS) were used to investigate the metal surface structure. XRD analysis was conducted using $CuK\alpha 1$ radiation on "a Siemens D5000 diffractometer" in "a Bragg Brentano setup" (tension $V = 45\ kV$, current $I = 30\ A$). Simultaneously, XPS measurements were conducted using "a Kratos Axis Ultra" with $AlK\alpha$ ($1486.6\ eV$) radiation, employing a carbon $C\ 1s$ line of $284.4\ eV$ as a reference to adjust the binding energies for the charge energy shift. As a result, utilizing a pass energy of $20\ eV$, high-resolution spectra were obtained with an energy resolution of $0.9\ eV$.

II.1.7. Molecular modeling

Theoretical computations were conducted to enhance the comprehension of the experimental corrosion data. The $DMol3$ module [61] incorporated in "Material Studio 2017^{TM} Software" was utilized for this purpose. The generalized gradient approximation $GGA - BP86$ with double numerical basis (DNP) [62, 63] was utilized to optimize the geometry of the primary components present in the *Artemisia* extract, dicaffeolyquinic acids. The inhibitors' molecular reactivity with steel was investigated using (μ), (η), (ω) [64].

Chemical potential $$\mu = -\chi = \frac{E_{HOMO} + E_{LUMO}}{2} \qquad (II.6)$$

Global hardness $$\eta = (-E_{HOMO} + E_{LUMO})/2 \qquad (II.7)$$

Electrophilicity index $\omega = \mu^2/2\eta$ $(II.8)$

$$\Delta N = \frac{\chi_{Fe}-\chi_{inh}}{2(\eta_{Fe}+\eta_{inh})} \quad (II.9)$$

ΔN : The amount of electrons transferred from the inhibitor to the steel surface,

E_{HOMO} is the energy of the highest-occupied molecular-orbitals,

E_{LUMO} is the energy of the lowest unoccupied molecular-orbitals,

χ is the electronegativity with $\chi_{Fe} = 4.82\ eV$, and $\eta_{Fe} = 0$ [64].

The Fukui indices (f_k^- and f_k^+) were calculated to determine the local reactivity,:

$$f_k^- = \rho_N - \rho_{N-1}\ (electrophilic\ attack) \quad (II.10)$$

$$f_k^+ = \rho_{N+1} - \rho_N\ (nucleophilic\ attack) \quad (II.11)$$

The electronic densities are ρ_N (atom), ρ_{N+1} (anion) and ρ_{N-1}(cation).

The adsorption energy is given as:

$$E_{ads} = E_{inh-steel} - (E_{inh} + E_{steel}) \quad (II.12)$$

The solubilization process of the inhibitors' aqueous phase was investigated using the "COnductor-like Screening Model" for "Real Solvents" ($COSMO - RS$) [65]. "Metropolis Monte Carlo simulations" (MCS) [66, 67] and the Adsorption module [68] were used to model the inhibition in "Materials Studio 2017TM". The MCS method can determine the adsorbate/adsorbent configuration with the lowest overall energy. The simulation of the Dicaffeoylquinic acid isomers adsorption on steel surface was done. For this purpose, a variety of boxes were constructed and sized according to the kind and number of molecules. To determine the interaction forces throughout the simulation phase the force fIeld "Dreiding" [69] was used.

Part two: Ammophila Arenaria

II.1.1. Sand sedge (Ammophila Arenaria)

II.1.1.1. Botanical description of *Ammophila Arenaria*

Ammophila arenaria group occupies mobile sands. It is a powerful species that allows the formation and fixation of a larger sand surface. This grouping represents 25-50% of ground cover and dominant vegetation cover in the coastal part of the dune cord in eastern Algeria [70].

The species *Ammophila arenaria (AA)* or (قصب الرمال) is described as a "grass" of a bright green color, more or less glaucous (see figure II.2) [71-74]. The genus Ammophila belongs to the family Poaceae and the tribe Agrostideae [75]. Etymologically, the name of this genus translates the strict affinity of these plants for the sands (**Figure II.2**). It presents the following systematic position:

Kingdom: *Plantae*

Subkingdom: *Tracheobionta*

Division: *Mayroliophyta*

Class: Liliopsidaa

Subclass: *Commelinidae*

Order: Cyperales

Family: *Poaceae*

Genus: *Ammophila*

Species: *Ammophila Arenaria*

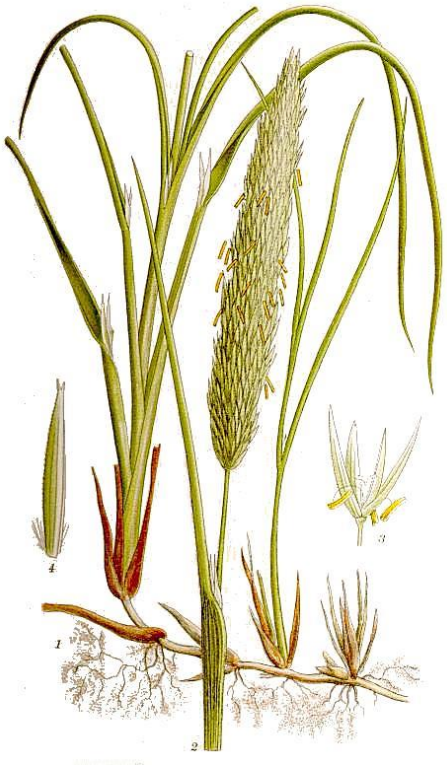

Figure II.2: Sand Sedge Ammophila Arenaria

The species *Ammophila arenaria (AA)* are classified as perennials, which means they can grow and produce an inflorescence from the same root over several years. Perennials can

die out of season and regrow even larger and stronger after this cycle [76]. Specifically for *Ammophila*, growth is slower in winter, while the leaves start to grow vigorously in spring and summer, dying in autumn [77].

II.1.1.2. General Morphology

Ammophila is a robust, erect, perennial, rhizomatous grass, reaching 120 cm in height. Rhizomes spreading horizontally and vertically; the youngest parts of the rhizome with white coherent pith and bearing overlapping yellowish-white scales; the oldest parts yellowish-brown and hollow-based, the scale leaves mostly perishing. Roots white and fleshy when young, becoming brownish and nerved with age, up to four per node. Aerial shoots are formed mainly along the vertical rhizomes, forming dense tufts; the stems of the aerial shoots form elongated internodes when buried, thus becoming vertical rhizomes. Leaves up to 6 mm wide and 60 cm long, but sometimes up to 90 cm long, pointed, usually tightly rolled up, except in humid conditions.

II.1.1.3. Interest of the plant

Ammophila is a robust, erect, perennial, rhizomatous grass, reaching 120 cm in height. Rhizomes spreading horizontally and vertically; the youngest parts of the rhizome with white coherent pith and bearing overlapping yellowish-white scales; the oldest parts yellowish-brown and hollow-based, the scale leaves mostly perishing. Roots white and fleshy when young, becoming brownish and nerved with age, up to four per node. Aerial shoots are formed mainly along the vertical rhizomes, forming dense tufts; the stems of the aerial shoots form elongated internodes when buried, thus becoming vertical rhizomes. Leaves up to 6 mm wide and 60 cm long, but sometimes up to 90 cm long, pointed, usually tightly rolled up, except in humid conditions.

II.1.2. Extraction and characterization of *AA*

During the flowering period of *Ammophila arenaria* in the Gafsa region (Tunisia); the stems were collected from marram grass. The final humidity level achievd after two months of air-drying the stems is $8-10\%$.The dried stems were stored under controlled conditions (average relative humidity: 50%; average temperature: approximately $25°C$) [78].

To extract the polysaccharides, the dried stems were ground using a cutting mill "Cutting Mill SM 100 from Retsch" until they passed through a $2\ mm$ aperture screen. With a solid–liquid ratio of $1:30\ (w/v)$, 50g of the plant powder was extracted with water for $2\ hours$ at $300\ rpm$ at $60°C$ with mechanical stirring. The resulting mixtures was filtered through a $G0$ sintered glass funnel "SCHOTT DURAN, Mainz, Germany". Afterwards, the centrifugation of the filtrates were operated for $20\ minutes$ at $3500\ rpm$, followed by precipitation using 80% ethanol and additional filtration on a $G2$ funnel to purify the extracted products. To further purify the precipitate from salts and low molecular weight molecules, it was dialyzed over deionized water utilizing dialysis tubing with a $30\ kDa$ molecular weight cutoff until the dialysate conductivity equaled that of deionized water. The pure product was obtained by freeze-drying the dialysate [79]. The process described from collection to obtaining the extract is schematized in **Figure II.3**.

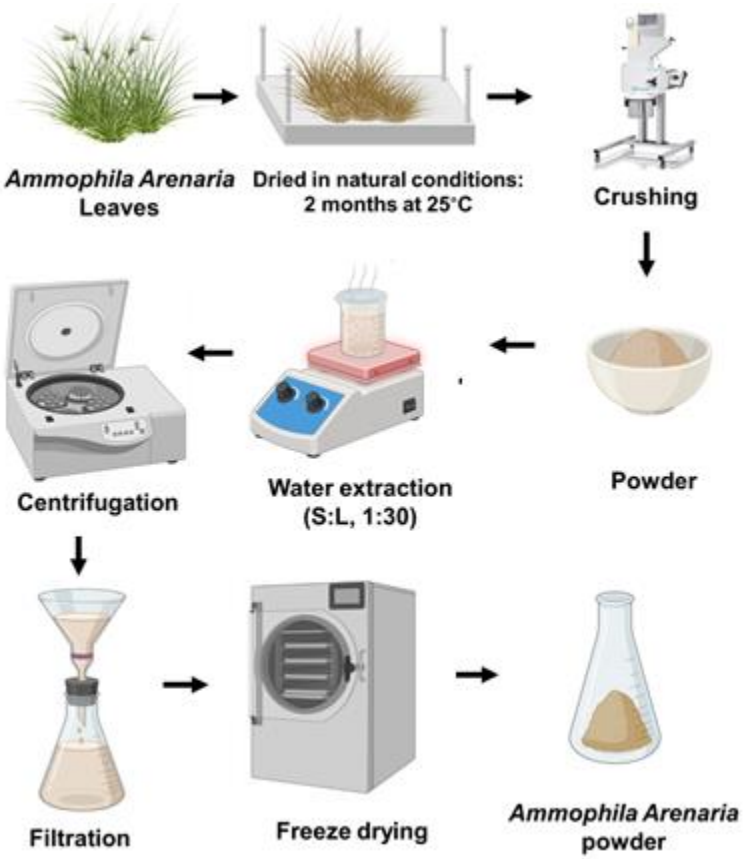

Figure II.3: Preparation procedure of ***Ammophila Arenaria*** leaves

The infrared spectroscopy "PERKIN ELMER spectrum two ATR-FTIR" was used to obtain the FTIR spectrum of *Ammophila Arenaria* extract in the frequency range of $4000–600\ cm^{-1}$.

II.1.3. Metal and corrosive solution

The chemical composition of mild steel specimens in weight percent is as follows ($wt\%$): $0.35\ C, 0.01\ Si, 0.5\ Mg, 0.035\ P, 0.035\%\ S$, with Fe the remaining. The mild steel was used as the working electrode for the electrochemical measurements: (OCP) Open Circuit Potential, (PDP) PotentioDynamic Polarization, and (EIS) Electrochemical Impedance. Carefully polishing and abrading the exposed surface of the samples with emery sheets of varying grades, then using double-distilled water for cleaning, the absolute ethanol for degreasing and rinsing with acetone to dry. In the studies, 2% dimethylsulfoxide (DMSO) was used to dissolve the extract first. Then it was introduced in a $1\ M\ HCl$ solution without and with different concentrations of *Ammophila Arenaria* extract ranging from $25\ to\ 700\ ppm$. The acidic solution was acquired from the chemical supplier "Merck".

II.1.4. Electrochemical measurements

The electrochemical measurements were performed using "EC-Lab.V.10.33 software", with a typical three-electrode cell where the working electrode was a mild steel rod, the counter electrode is a platinum sheet with a surface area of $1\ cm^2$, the reference electrode was an $Ag/AgCl$. PDP curves were registered within a potential range of $200\ mV$ from the (OCP) Open Circuit Potential at a rate of $0.5\ mV\ s^{-1}$. The corrosion current densities (I_{corr}) were determined by extrapolating the linear Tafel segments, from both anodic and cathodic curves, to the corrosion potential and the inhibition efficiency (IE_{pdp}) was evaluated using the previous relationship (II.2).

EIS investigations were carried out at the equilibrium potential following $1\ hour$ of immersion, utilizinging a signal amplitude of $10\ mV$ for the frequency range of $50\ kHz\ to\ 10\ Hz$ to determine the electrochemical parameters, such as (R_{ct}) the charge transfer resistance and (C_{dl}) the capacity of the double layer. Then the inhibitory efficiency was estimated based on (I_{corr}) the obtained current densities through the established formula (II.4).

II.1.5. Surface characterization

To examine the influence of inhibitor on the mild steel surface, the samples were immersed in HCl solution with and without inhibitor, using the optimal concentration, for 12 hours. After removing the samples carefully from the solutions and drying them thoroughly,

"Scanning Electron Microscopy" (SEM) and "Atomic Force Microscopy" (AFM) were used to characterize the surface films created on the metal specimens.

II.1.6. Theoretical calculations

Quantum chemistry calculations were done for understanding molecular structure, electron distribution, and reaction activity [80-83]. For this purpose, the commercial "Turbomole 7.4 program" was utilized to optimize the geometric parameters of the studied inhibitors, cellulose, hemicellulose, and lignin, as well as the $Fe60$ cluster [84-86]. Calculations in quantum chemistry were done using the "def2-TZVP basis set" and the "B3LYPDFT" [87-89]. Several chemical descriptors were calculated and analyzed, including (E_{HOMO}) the highest occupied molecular orbital energy, (E_{LUMO}) the lowest unoccupied molecular orbital energy, (E_g) the energy gap, hardness (η), softness (σ), electronegativity (χ); dipole moments (μ) and electrophilicity index (ω) and the following formulas are the equations associated with the chemical descriptors:

$$E_g = E_{LUMO} - E_{HOMO} \qquad (II.13)$$

$$\eta = \frac{E_{LUMO} - E_{HOMO}}{2} \qquad (II.7)$$

$$\sigma = \frac{1}{\eta} \qquad (II.14)$$

$$\chi = \frac{I + A}{2} \qquad (II.15)$$

$$\mu = \frac{E_{LUMO} + E_{HOMO}}{2} \qquad (II.6)$$

$$\omega = \frac{\mu^2}{4\eta} \qquad (II.8)$$

To investigate and analyze weak interactions occurring in three dimensions, an insightful approach involves exploring non-covalent interactions (NCI) [90, 91]. Many theoretical models were employed in this study, including (RDG) the Reduced Density

Gradient, (QTAIM) the Reduced Density Gradient, Quantum Theory of Atoms-in-Molecules and (IGM) the Independent Gradient Model. The RDG analysis relies on electron densities (ρ) and reduced density gradients (RDGs), described by the following mathematic formula:

$$s = \frac{1}{2(3\pi^2)^{1/3}} \frac{|\nabla\rho|}{\rho^{4/3}} \qquad (II.16)$$

Here, ρ represents the electron density and

$\nabla\rho$ represents its initial derivative.

This approach is particularly effective for identifying van der Waals interactions and weak non-covalent interactions, including hydrogen bonding and steric repulsions, which are significant at specific distances and can substantially influence the overall system [92]. On the other hand, the IGM provides insights into covalent and non-covalent interactions within both intra- and intermolecular regions. The description is as follows:

$$\delta g^{IGM} = \delta g^{intra} + \delta g^{inter} \qquad (II.17)$$

$$\delta g^{inter} = \left|\nabla\rho^{IGM,inter}\right| - |\nabla\rho| \qquad (II.18)$$

The term δg^{inter} defines the interactions between the host and guest (II.18) and it is dependent on ($\nabla\rho^{IGM,inter}$) which is the norm of the electron density gradient determined using the IGM mode.

Based on the RDG and IGM, NCI analyses were investigated and weak interactions were identified within the analyzed system employing the computational tool Multiwfn [93]. Geometries, "Frontier Molecular Orbital" (FMO), "Molecular Electrostatic Potential" (MEP), and RDG plots were retrieved and visualized using the "Visual Molecular Dynamics" (VMD) interface [94]. Furthermore, color scatter plots of the components were generated utilizing gnuplot [95]. The advanced computational techniques facilitated a comprehensive analysis of the weak interactions present within the system being examined.

Chapter III

EXPERIMENTAL STUDY

CHAPTER III. Experimental Study

Part One: Inhibition Effect Of *Artemisia Herba Alba* Extract

III.1.1. Characterization of the plant extract

Figure III.1 presents the infrared (FTIR) spectrum of the plant extract, revealing secondary metabolites in the $400 - 4000\ cm^{-1}$ range. The peak at 3300 cm^{-1} corresponds to $O-H$ stretching vibration. The peak at 2925 cm^{-1} is caused by $C-H$ stretching vibration. At $1605\ cm^{-1}$ The stretching vibrations of $C=O$ and $C=N$ create a band .The band created at $1393\ cm^{-1}$ is attributed to the $C-H$ bending in CH_3 [96]. The absorption bands at 1519 and $1252\ cm^{-1}$ are related to the $C=C$ vibration of aromatic rings. On the other hand, the stretching vibrations of $C-O$ or $C-N$ are responsible for the adsorption bands at $1162\ cm^{-1}$ and $1062\ cm^{-1}$. The adsorption bands below $1000\ cm^{-1}$ can be attributed to $C-H$ bending.

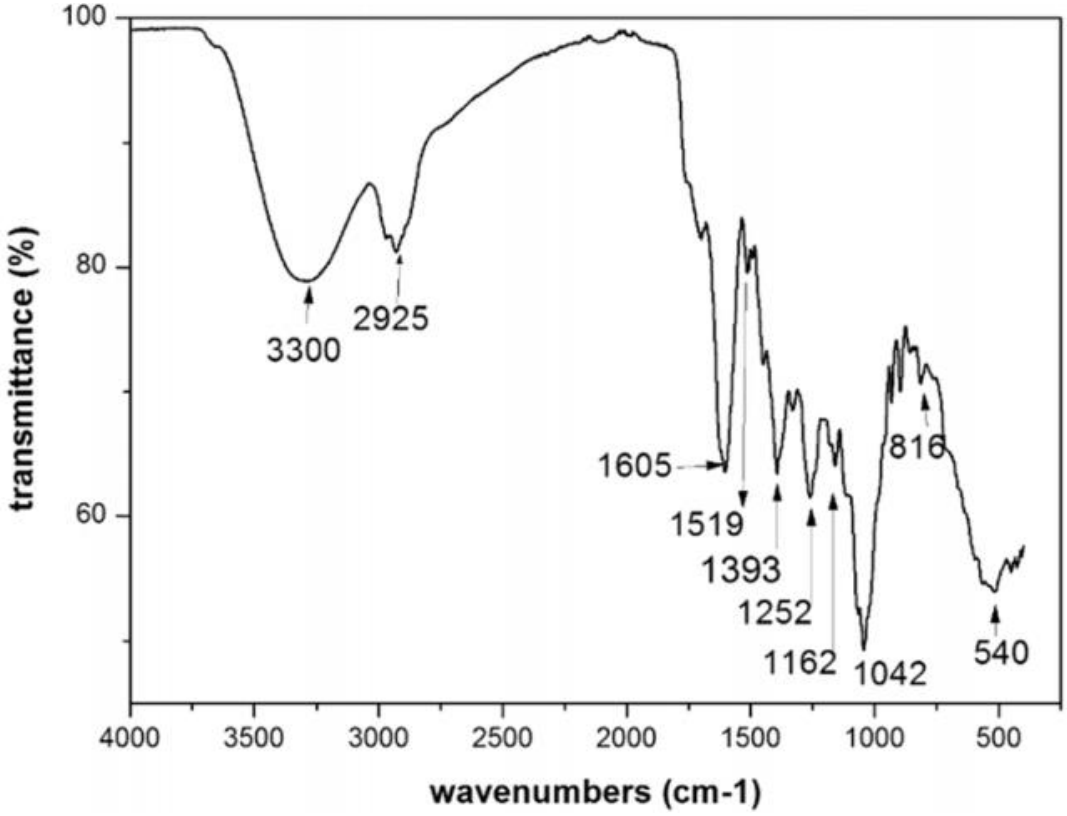

Figure III.1: FTIR spectrum of the inhibitor: AHA crude extract.

Like many plant extracts, the presence of chemical compounds with functional groups and aromatic rings in this inhibitor can assure reactions with iron cations contained in the solution producing organometallic complexes that provide a protection to the metal [97].

Furthermore, the LC-MS has analyzed the hydroalcoholic extract of AHA extract as a result many phenolic compounds were highlighted. The identification of the secondary metabolites structures was based on comparing the λ max and MS spectra of each compound with literature data on phenolic constituents of the *Artemisia* genus [98, 99]. In (**Table III.1**) a list of the main compounds along with their retention times and m/z ratios is reported.

Table III.1: The detected constituents in the *AHA* crude extract by $\boldsymbol{LC/MS}$

ID	T_r (min)	Identification	m/z *[M-H]-*
1	*0,65–0,91*	Dicaffeoylquinic acid	*515*
2	*1,77–2,37*	Feruloylquinic acid	*367*
3	*3,86–5,83*	Dicaffeoylquinic acid	*515*
4	*6,25–6,71*	Dicaffeoylquinic acid	*515*
5	*7,91–8,2*	Tricaffeoylquinic acid	*677*
6	*8,78–9,00*	Tectorigenin	*299*
7	*9,01–9361*	Cirsiliol	*329*
8	*9,78–10,06*	Iristectorigenin	*329*
9	*10,78–11,02*	Vitexin	*431*

The FTIR analysis detected the functional groups for like aromatic rings, $C-O$ bonds, $O–H$ bonds, $C=O$ bonds, and $C=C$ bonds in all of these compounds. These reactive linkages can form a protective layer, potentially enhancing the adsorption of *AHA* crude extract constituents on the steel surface, which may improve corrosion inhibition.

Furthermore, according to the delineated areas of the peaks, the primary organic constituents in the *AHA* extract are primarily "Dicaffeoylquinic acids" ($DCQA$), which manifest at various retention times..

In **Table III.2** the 6 isomers of phenolic acid along with their associated molecular structures are listed.

Table III.2: Chemical structures of "Dicaffeoylquinic acid" isomers.

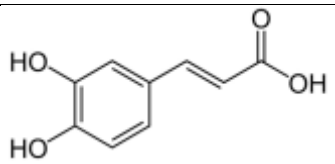			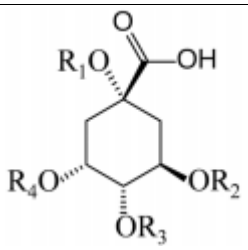		
Caffeic acid			*Quinic acid*		
1,3-DCQA	*1,4-DCQA*	*1,5-DCQA*	*3,4-DCQA*	*3,5-DCQA*	*4,5-DCQA*
R1 *C*	*C*	*C*	*H*	*H*	*H*
R2 *C*	*H*	*H*	*C*	*C*	*H*
R3 *H*	*C*	*H*	*C*	*H*	*C*
R4 *H*	*H*	*C*	*H*	*C*	*C*

III.1.2. Weight loss measurements

The gravimetric measurements of mild steel immersed in $1M\ HCl$ in the presence and the absence of different concentrations of the inhibitor is presented in **Table III.3**. the corrosion rate decreases by increasing the concentration of the inhibitor which can be explained by the decrease in the phenomenon of dissolution of the metal due to the deposition of the inhibitor on the surface of the metal [100].

Table III.3: Impact of AHA concentration on the corrosion parameters of mild steel in an acidic environment

$Concentration\ (mg/L)$	$W_{corr}\ (10^{-5} g\ h^{-1}\ cm^{-2})$	$IE_{wl}(\%)$
Blank	*92.63*	-
25	*45.306*	*51.07*
100	*20.4808*	*77.89*
400	*10.221*	*88.96*
600	*8.9994*	*90.28*
900	*4.6818*	*94.94*
1000	*5.5485*	*94.01*

The corrosion rates continue to decline, attaining a minimum at an extract concentration of $900\ mg/L$ in the acidic solution, which corresponds to a maximum inhibition efficiency of 94.94%; thereafter, the value stabilizes. Even At the minimal applied concentration of $25\ mg/L$, the steel exhibits effective corrosion protection with an inhibition efficiency IE_{wl} exceeding 50%.

These results indicate that the inhibitor is effective for mild steel.

III.1.3. Electrochemical characterization

III.1.3.1. Polarization Curves

Figure III.2 shows the polarization plots of mild steel in a 1 $M\ HCl$ solution, derived from the electrochemical analysis conducted both in the presence and absence of Artemisia extract. Concurrently, **Table III.4** delineates the relevant electrochemical parameters.

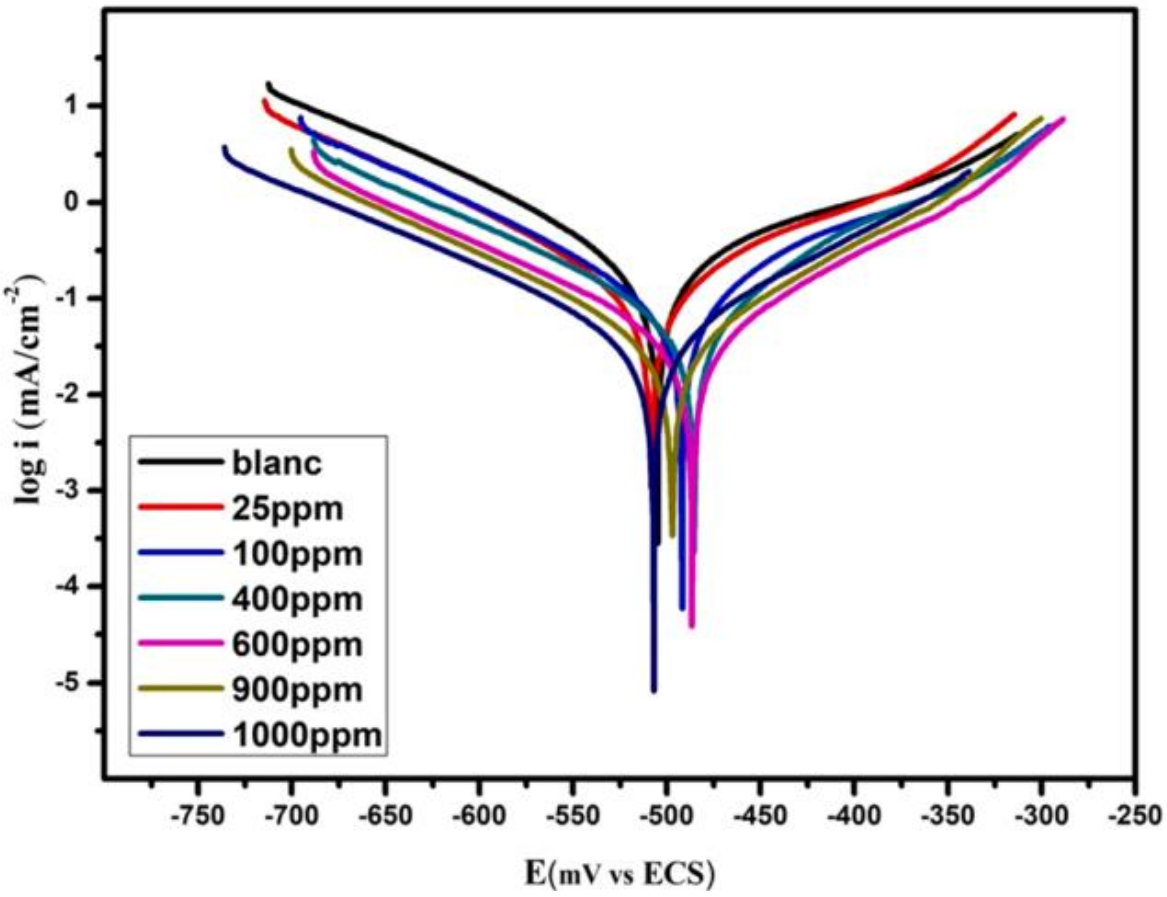

Figure III.2: Influence of inhibitor concentration on mild steel polarization curves in **1 *M HCl***.

The electrochemical polarization studies indicate that the incorporation of Artemisia extract at varying concentrations into the aggressive solution reduces the current density values. This outcome indicates that the degradation of steel in 1M HCl is significantly inhibited by the *Artemisia* extract based on the proportional relation between the current density values and the extent of steel degradation. Particularly for the inhibited solution with 900 mg/L of the extract, current density decreases to 59 $\mu A\ cm^{-2}$, approximately an order of magnitude lower than the current density recorded without the inhibitor (517 $\mu A\ cm^{-2}$). This low I_{corr}value also correlates to a very high $IE_{pdp}$of 88.5%.

The *Artemisia* extract inhibits both cathodic reduction and anodic dissolution reactions in steel, resulting in a little shift of E_{corr} towards more noble values (less than 85 mV), indicating that the inhibitor functions as a mixed-type inhibitor.[101, 102].

The anodic and cathodic Tafel slopes (βa and βc) are altered in the presence of the extract, as indicated in **Table IIIIII.4**, demonstrating that the mechanism of this process is affected by this inhibitor [103].

Table III.4: The influence of inhibition dosage on the electrochemical parameters assessed for Mild Steel in $\mathbf{1}\boldsymbol{M\ HCl.}$

$C(mg/L)$	$E_{corr}(mV\ SCE^{-1})$	$I_{corr}(\mu A\ cm^{-2})$	$\beta_a(mV\ dec^{-1})$	$\beta_b(mV\ dec^{-1})$	IE_{pdp} (%)	$R_p(\Omega\ cm^2)$
$Blank$	-504.886	516.62	335.2	235.6	–	220
25	-508.369	257.256	239.4	219	50.2	364
100	-491.791	200.66	235	226.6	61.1	488
400	-485.442	136.662	199	242	73.5	768
600	-486.544	62.76	173.4	211.2	87.8	1120
900	-497.027	59.304	168.8	207.8	88.5	1162
1000	-506.885	78.136	198.8	246.6	84.8	1164

The inhibitory efficiency increased with the increasing of the concentration of additives. This increase suggests that the surface of the steel sample is more covered when the inhibitor molecules is more present in the solution, this is the case when the concentration of the inhibitor is higher. As a result, the adsorption of the inhibitor molecules on the metal surface can be assumed, shielding it from corrosion.

III.1.3.2. Electrochemical impedance spectroscopy

The Nyquist impedance curves for steel in $1\ M\ HCl$ solution with different concentrations of *Artemisia* extract exhibited a singular capacitive loop, indicating that a charge transfer process governs the corrosion of steel in $1\ M\ HCl$. Moreover, inhibitor adsorption on the metal surface may be the origin of low-frequency inductive loops [104]. Another possible explanation for this phenomenon is that it is due to the relaxation process that occurs in the conjugated system as a result of species adsorption [105, 106]. The passivated surface redissolving phenomenon may be the cause of the observed loop at either frequency [107]. Stated differently, the development of the inductive loop at low frequencies may be caused by corrosion products adsorbing on the electrode surface[108].

Figure III.3 illustrates the Nyquist plots of the imaginary component ($-Im(z)$) of the impedance Z in relation to its real component ($Re(z)$). The schematic in **Figure III.3** indicates that enlarging the semicircles while maintaining their characteristics leads to an increased R_{ct} and hence a reduced corrosion rate [109]. An increase in the number of inhibitor molecules that are adsorbed onto the surface of the metal is responsible for this impact. This increase is proportional to the concentration of the inhibitor molecules in solution.

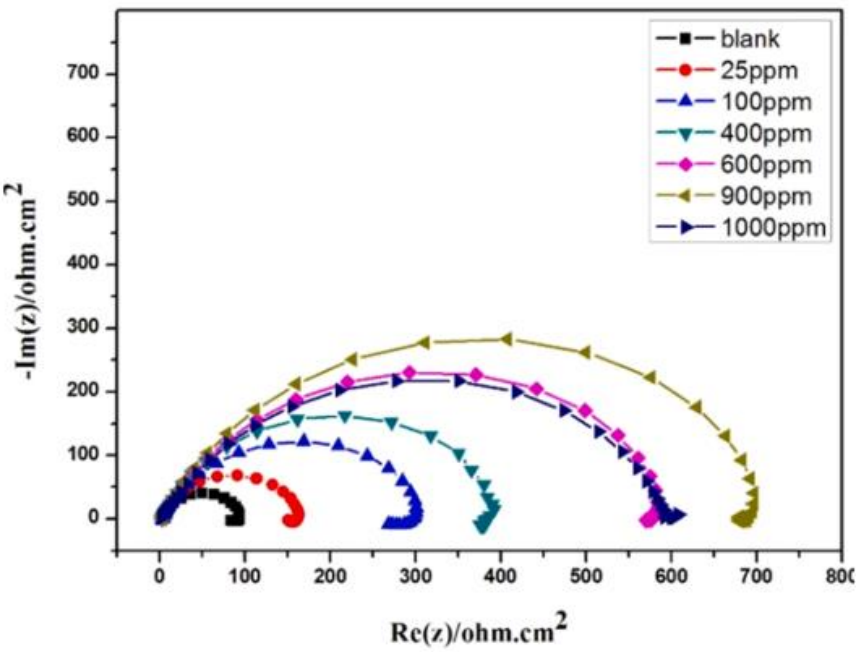

Figure III.3: The influence of inhibitor concentration on the Nyquist curves regarding mild steel immersed in $\mathbf{1}\boldsymbol{M\ HCl}$.

The observed loops deviate from perfect semicircles, likely attributable to the heterogeneity of the electrochemical system, which may be influenced by contaminants or the formation of porous layers [110].

The circuit depicted in **Figure III. 4** aligns with the experimental results obtained.

R_s represents the resistance of the test solution, while R_{ct} denotes the charge transfer resistance.

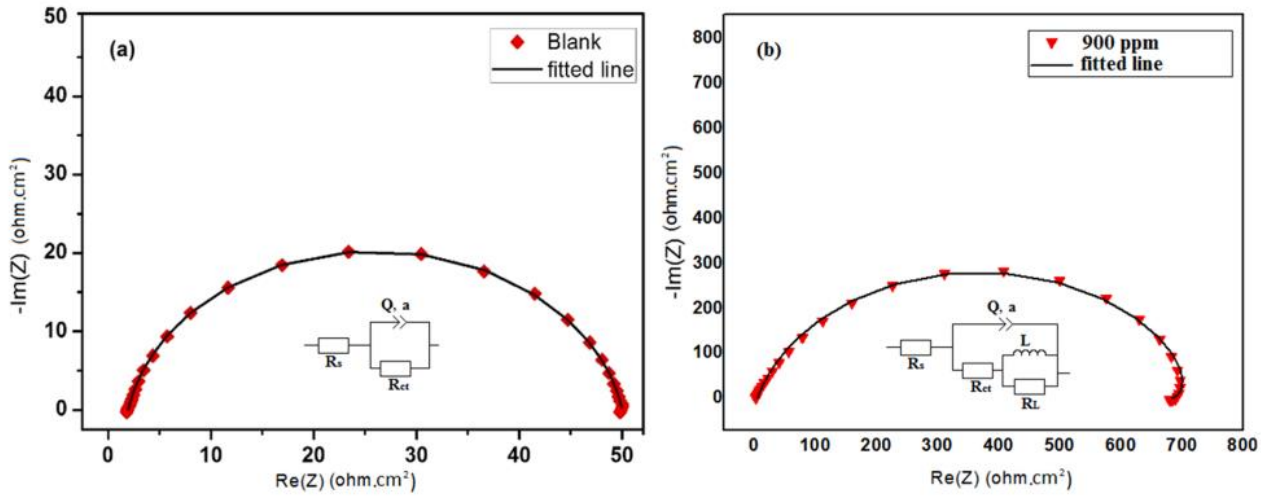

Figure III.4: Curves fitted for: (a) the blank solution (b) the $\mathbf{900}\ \boldsymbol{ppm}$ concentration of the inhibitor under investigation.

Table III.5 is a listing of the significant impedance parameters that were derived from the examination of the Nyquist diagram. As a result of the EIS experiments, in the presence of Artemisia the resistance R_{ct} increases while the double layer capacity C_{dl} decreases. The adsorption of inhibitor molecules on the metal surface causes a change in the double layer that exists between the solution and the charged metal surface, which is used as an electric capacitor, resulting in a decrease in its electrical capacity. This adsorption provides an explanation for both the observed decrease in C_{dl} as well as the various inhibitor doses. According to the equation (II.5), it is possible that this decrease might be attributed to a decrease in the dielectric constant of the medium(ε) and/or an increase in the thickness of the double layer (d). At the point where the metal and solution come into contact with one another, the adsorption of the inhibitor molecules decreases the rate of corrosion and limits the active surface area.

The next equation was used to determine the surface coverage in **Table III.5** [111]:

$$\theta = \frac{C_{dl} - C'_{dl}}{C_{dl}}$$

Whith $C_{dl}$is the inhibited double-layer adsorption capacity,

C'_{dl} is the uninhibited double-layer adsorption capacity.

Table III.5:: The influence of inhibitor dosage on the impedance parameters obtained from electrochemical impedance spectroscopy tests conducted on mild steel in a 1 M hydrochloric acid solution.

$Conc.$	R_s	R_{ct}	R_L	Q	A	C_{dl}	L	θ	$IE_{EIS}(\%)$
(ppm)	Ωcm^2			$10^{-3}(F\ s^a cm^{-2})$		$(\mu\mathrm{F}\ cm^2)$	$(H\ cm^2)$		
$Blank$	1.97	48.06	-	0.4	0.89	245.44	-	-	-
25	3.17	148.7	13.5	0.189	0.89	121.54	40.01	0.633	67
100	4.66	270.1	34.26	0.115	0.85	62.31	75.2	0.809	82.2
400	4.34	376.3	25.6	0.088	0.86	50.53	14.21	0.85	87.22
600	3.99	573	44.9	0.08	0.81	38.82	22.02	0.886	91.61
900	5.33	679.4	49.05	0.05	0.83	25	24.18	0.923	92.92
1000	3.66	593	32.45	0.073	0.77	28.57	3.69	0.913	91.89

(A) values range from 0.77 to 0.89. The inhibition efficacy (IE_{EIS}) increases with the rising concentration of the inhibitor in the solution, demonstrating that corrosion control is contingent upon on the concentration of inhibitor, as shown in **Figure III.4**,. This result corresponds to the same behavior observed as in polarization measurements.

III.1.3.3. Impact of Temperature

The influence of temperature within the range of $298-323\,K$ on the corrosion inhibition of mild steel in $1\,M\ HCl$, both in the absence and presence of $900\,ppm$ of Artemisia inhibitor, was examined by potentiodynamic polarization analysis. The polarization curves and corresponding data are presented in **Figure III. 5** and **Table III.6,** respectively.

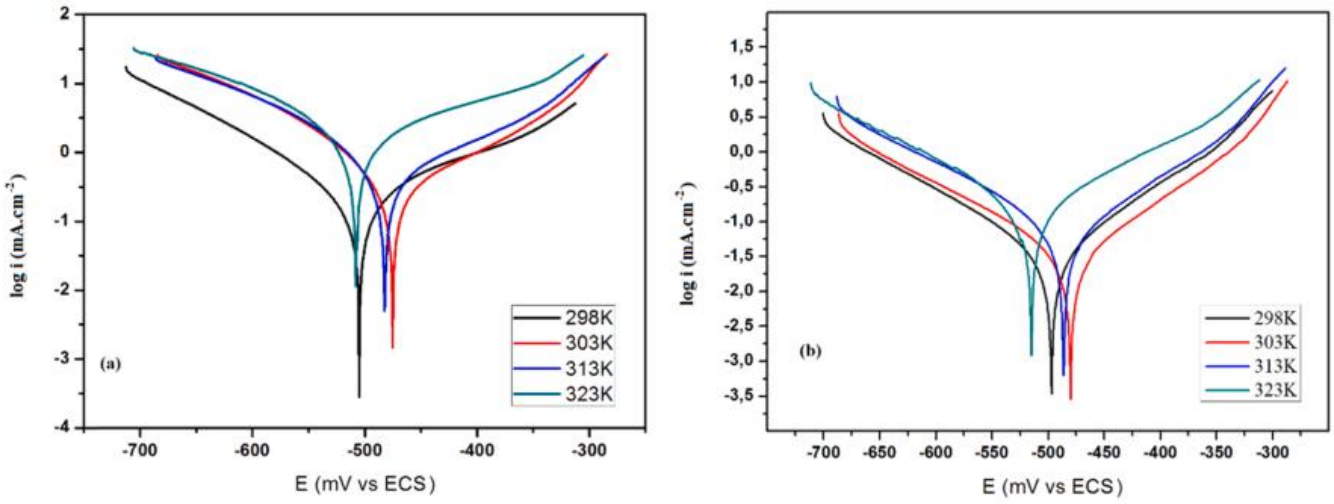

Figure III.5: The influence of temperature on the polarization curves of mild steel in $\mathbf{1}\boldsymbol{M\ HCl}$ (a) blank (b) $\mathbf{900}\ \boldsymbol{ppm}$ of inhibitor.

The current density increases when Artemisia is present, and the E_{corr} readings exhibit a modest degree of variation when the temperature is raised. In addition, it is important to emphasize that the efficiency of inhibition is practically constant, which suggests that Artemisia possesses an inhibition effect that is not reliant on temperature.

Table III.6: The influence of temperature on the electrochemical parameters of mild steel in $\mathbf{1}\boldsymbol{M\ HCl}$.

$Concentration$	T (K)	E_{corr}(mV) Vs ECS	$I_{corr}(\mu A\ cm^{-2})$	$E_{pdp}(\%)$
$Blank$	298	-504.886	516.63	-
	303	-475.088	826.886	-
	313	-482.086	1312.758	-
	323	-508.01	5747.42	-
900 ppm	298	-497.027	59.304	88.5
	303	-479.975	44.102	94.6
	313	-486.169	93.996	92.8
	323	-514.86	305.696	94.6

III.1.4. Adsorption isotherm study

The adsorption onto the metal surface is in general the spontaneous behavior of organic inhibitors in aggressive media. While two types of adsorption are known:

physisorption and chemisorption, the interactions between the metal, electrolyte, and inhibitor (three components of the system) are responsible on determining which form of adsorption happens [112].

After fitting various isotherms to the experimental data to investigate the adsorption mechanism of the inhibitor, the optimal fit corresponded to Langmuir's isotherm.

In **Figure III. 6** illustrates a straight line with a correlation coefficient of $R^2 = 0.999$ and a slope of 1.07 , depicting the ratio $C/\theta\ vs. C$. The equation for the Langmuir isotherm is as follows [113]:

$$\frac{C}{\theta} = \frac{1}{K} + C$$

With $K = \frac{1}{999} \exp\left(-\frac{\Delta G_{ads}}{RT}\right)$

K: the equilibrium constant of the adsorption reaction, was determined to be 0.0569 L/mg;

999: represents the water concentration in the solution (g/L);

C: denotes the extract concentration in the solution (mg/L);

R: the universal gas constant and

T: the thermodynamic temperature [114].

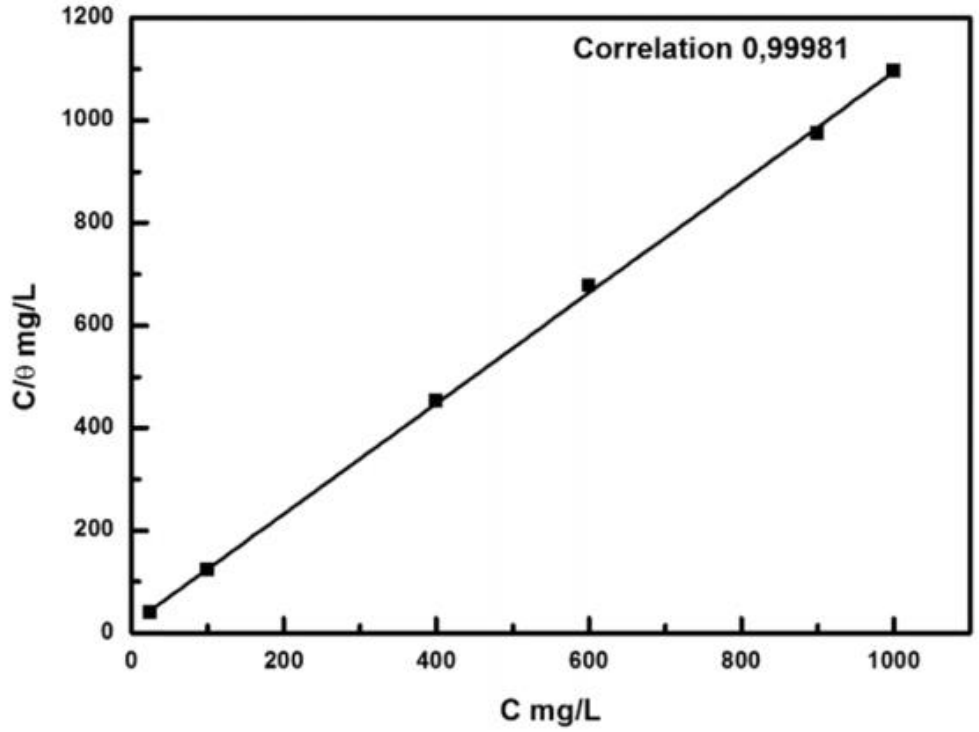

Figure III.6: The ***L***angmuir adsorption isotherm for polyphenols from ***Artemisia Herba Alba*** on steel at $\mathbf{298}\ \boldsymbol{K}$.

Finally, the computed value of the free energy of adsorption $\Delta G_{ads} = -27.01\ kJ/mol$ is negative indicating that the inhibitor's adsorption on the metal surface occurs spontaneously and that the adsorbed layer is stable. Physisorption, as is well known, happens when the inhibitor-free energy of adsorption is around $-20\ kJ/mol$, while chemisorption happens when it is around $-40\ kJ/mol$. Both chemisorption and physisorption may be implicated in our study, considering the estimated free energy adsorption of *AHA*, as documented in other publications [115-118]. Although such free energy values of adsorption are assigned to physisorption, certain authors suggest that chemisorption can also occur [117].

The thermodynamic parameters are estimated to precise the adsorption characteristics.

III.1.4.1. Thermodynamic parameters

The Arrhenius equation offers a more accurate estimation of the temperature dependence of the corrosion rate [117]. **Figure III.7** illustrates the logarithm of the corrosion current density ($\ln I_{corr}$) in relation to the inverse of the absolute temperature ($1/T$). **Table III.7** presents the activation energies calculated from the slopes utilizing the Arrhenius equation. [119] :

$$i_{corr} = k \exp(-\frac{E_a}{RT})$$

With: k represents the Arrhenius preexponential factor ($\mu A\ cm^{-2}$),

E_a represents the apparent activation energy (kJ/mol) and

R represents the universal gas constant.

Enthalpy and entropy were calculated using the alternate formulation of the Arrhenius equation [60] :

$$i_{corr} = \frac{RT}{Nh} \exp\left(\frac{\Delta S_a^0}{R}\right) exp(-\frac{\Delta H_a^0}{RT})$$

With: h represents the Planck constant,

N represents the Avogadro number,

ΔS_a^0 represents the activation entropy and

ΔH_a^0 represents the activation enthalpy.

The reorganization of this equation provides [120] :

$$\ln\left(\frac{i_{corr}}{T}\right) = \ln\left(\frac{R}{Nh}\right) + \left(\frac{\Delta S_a^0}{R}\right) - \left(\frac{\Delta H_a^0}{RT}\right)$$

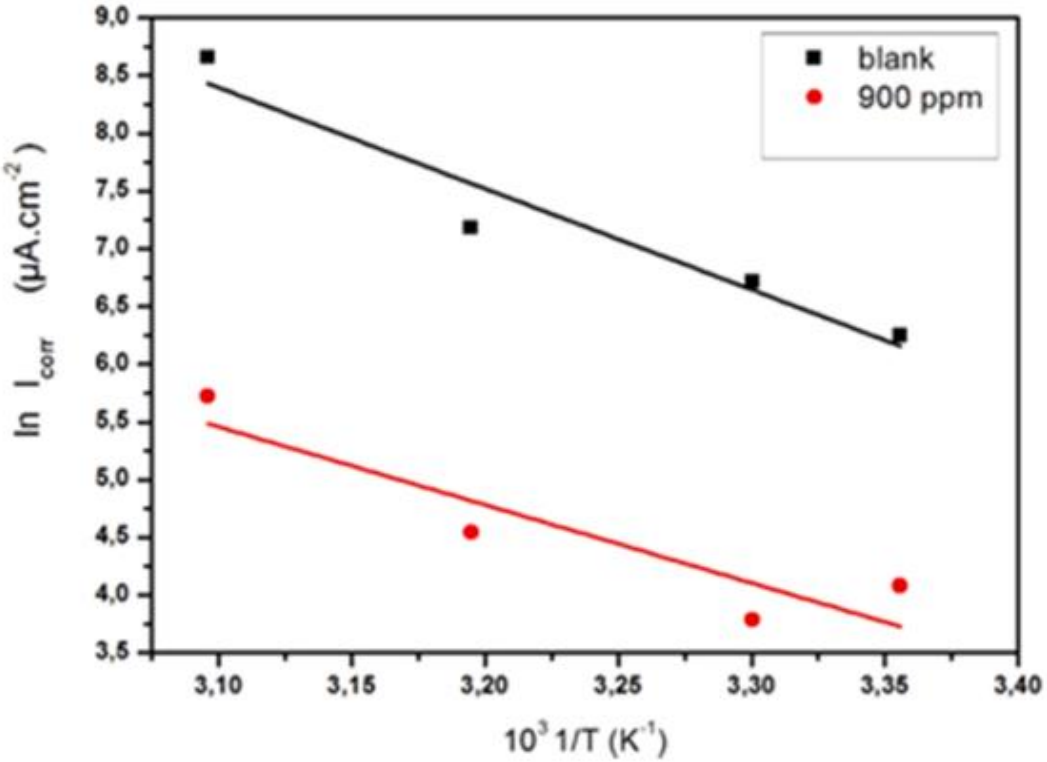

Figure III.7: ***A***rrhenius graphs for mild steel in **1** ***M HCl*** without (black line) and with (red line) **900** ***ppm*** of ***Artemisia***'s extract.

In **Figure III. 8** the logarithm $\ln(i_{corr}/T)$ is depicted as a function of the inverse of the absolute temperature $(1/T)$. This variation is a linear representation for both solutions with or without an inhibitor where the slope corresponds to $(-\Delta H_a^0/R)$, and the intercept is $\ln(\mathrm{R/Nh} + \Delta S_a^0/R)$.

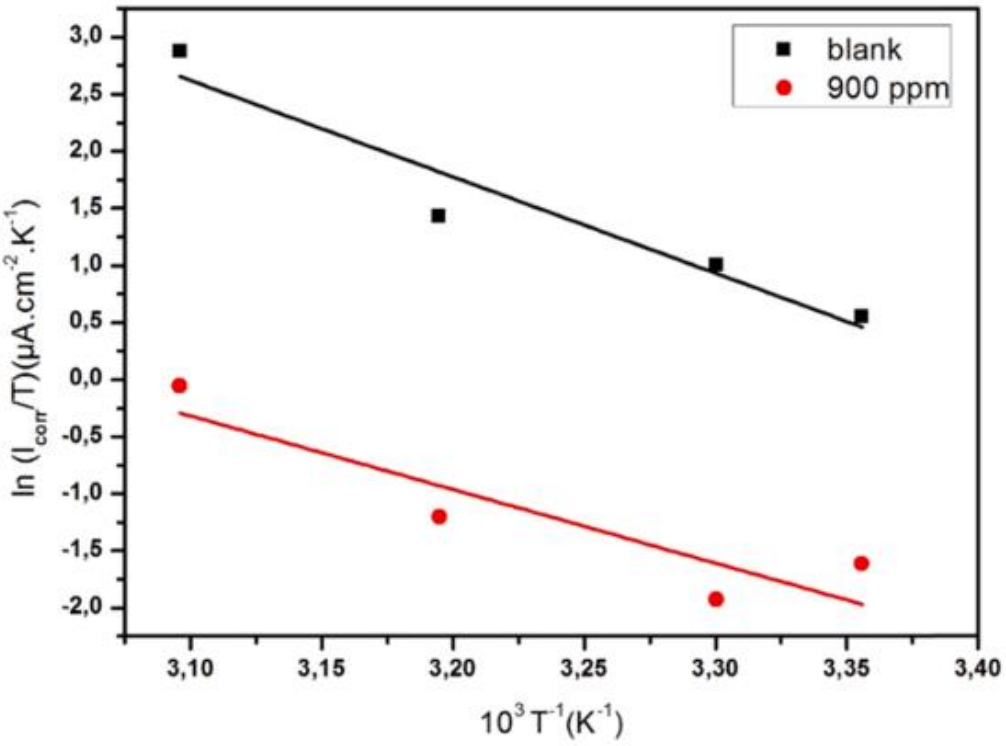

Figure III.8: the variation of $\boldsymbol{ln}$ $(\boldsymbol{I_{corr}/T})$ as a function of $\mathbf{1}/\boldsymbol{T}$ in $\boldsymbol{HCl}$ medium without (black line) and with (red line) $\mathbf{900}$ $\boldsymbol{ppm}$ of $\boldsymbol{Artemisia}$'s extract

$E_a,\ \Delta H_a^0, \Delta S_a^0$ are the activated parameters provided in **Table III.7**.

Table III.7: Thermodynamic parameters calculated for M.steel in **1 M HCl** without and with **900 ppm** of Artemisia's polyphenols.

	$E_a(kJ\ mol^{-1})$	$\Delta H_a^0(kJ\ mol^{-1})$	$\Delta S_a^0(kJ\ mol^{-1})$
Blank	72.80	70.27	41.96
AHA polyphenols	56.22	53.68	−33.90

The adsorption activation energy is reduced when the *AHA* polyphenols are present in the solution. As a result of the high temperatures that were used in the trials, the inhibitor's delayed adsorption can provide an explanation for this decrease on the metal surface. Another possible explanation for the variation in activation energy is that the surface possesses a heterogeneous energetic composition Given the circumstances, there are a restricted number of active sites that are involved in the corrosion process [115].

Regarding the adsorption nature, the endothermic process of the inhibitor's adsorption is indicated by the positive values of ΔH_a^0. Chemisorption may be linked to an endothermic process, while physisorption is characterized as exothermic [121]. *AHA's* inhibitory mechanism involves chemisorption, resulting in a drop in ΔH_a^0 value due to the chemical absorption of the inhibitor's molecules on the steel surfaces. Adsorbed molecules have higher formation energy than reactants.

The rate-determining step in the presence of the inhibitor causes the entropy value (ΔS_a^0) to be negative, which involves the formation of an activated complex through an association rather than a dissociation mechanism. This indicates that the transition from reactants to adsorbed species is linked to a reduction in the system's degree of disorder [122]. Moreover, the adsorption of inhibitor molecules could occur in a more organized manner due to the low entropy value, leading to a more stable layer and enhanced corrosion protection [123].

III.1.5. Morphological studies

III.1.5.1. Atomic Force Microscopy

Figure III.9 (a) presents the $2D$ and $3D$ images of the metal specimen prior to immersion, displaying a mean surface roughness (R_a) of $9.73\ nm$. Upon immersing of the specimen in the acidic environment without the inhibitor, the value increases to $115.94\ nm$, resulting in a rougher surface, as depicted in **Figure III.9 (b)**.

Conversely, the R_a decreases to $62.87\ nm$ 62.87 nm in the presence of the inhibitor within the acidic solution. As demonstrated in **Figure III.9 (c)**, such a decrease results in a smoother surface. Moreover, the deposition of inhibitor molecules on the metal surface has resulted in the formation of a protective layer, which guarantees strong corrosion inhibition performance at the optimal concentration of $900\ ppm$. The outcomes of both the electrochemical and the gravimetric experiments support these findings.

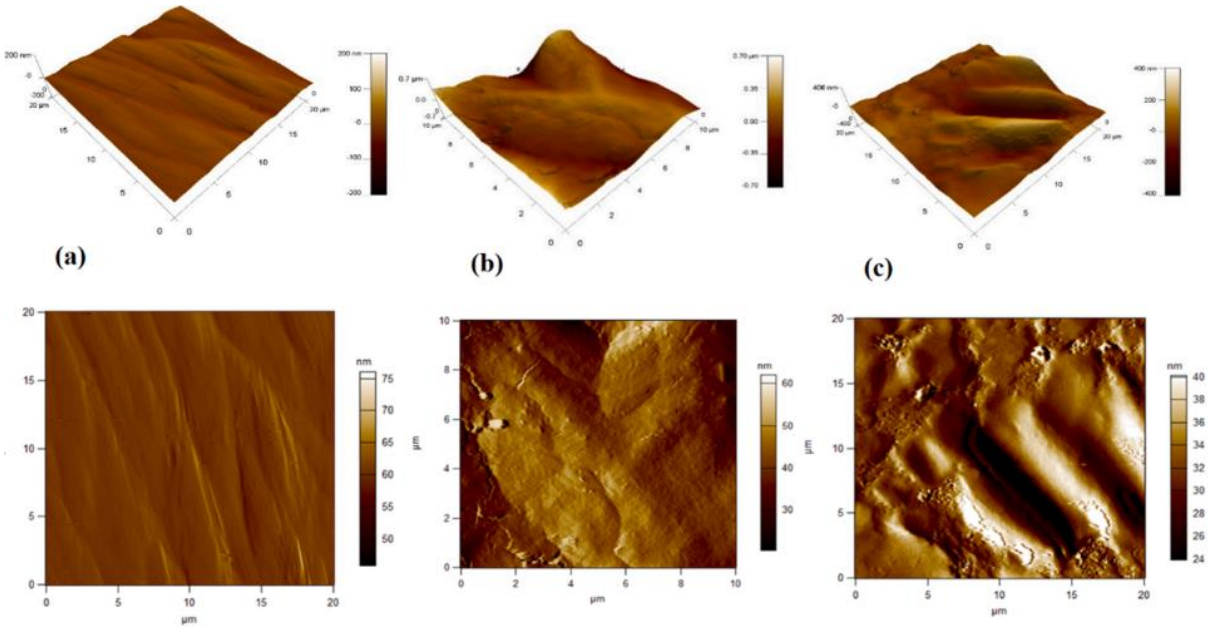

Figure III.9: $\boldsymbol{AFM\ 2D}$ and $\boldsymbol{3D}$ pictures of M. steel: (a) polished, (b) in $\boldsymbol{1\ M\ HCl}$ and (c) in $\boldsymbol{1\ M\ HCl}$ containing $\boldsymbol{900\ ppm}$ of $\boldsymbol{AHA}$ extract

III.1.5.2. *S*canning *E*lectron *M*icroscopy

Figure III. 10 illustrates the surface of the specimen prior to and post to immersion in the acidic liquid. Upon comparing **Figure III.10 (a)** and **(b)**, it is evident that immersion in the acidic environment without an inhibitor results in noticeable corrosion on the surface.

Figure III.10 (c) shows the properties of a metal surface submerged in an acidic mixture containing 900 ppm of *Artemisia* extract. The specimen exhibits a less damaged surface, suggesting that inhibitor molecules have formed layers to help protect the steel from corrosion. Moreover, this reveals that the prevention of corrosion by *Artemisia* extract when it is adsorbed on the surface of steel. This finding corroborates the conclusions drawn from the electrochemical characterization.

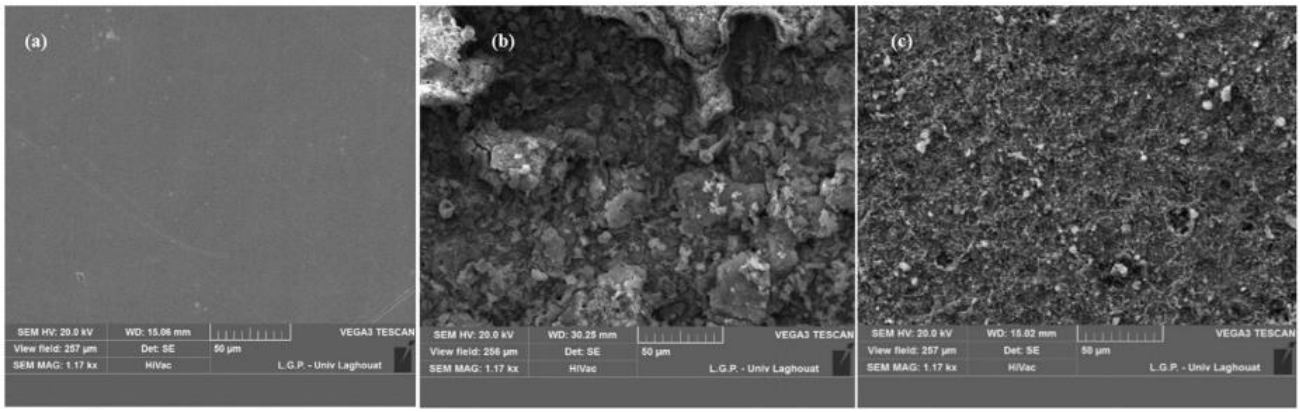

Figure III.10: $\boldsymbol{SEM}$ pictures for metal sample: (a) polished, (b) after immersion in inhibitor free $\mathbf{1}\ \boldsymbol{M\ HCl}$ solution and (c) immersed in acidic mixture containing $\mathbf{900}\ \boldsymbol{ppm}$ of *Artemisia* extract

III.1.5.3. $\boldsymbol{X-R}$ay $\boldsymbol{D}$iffraction analysis

Employing $X-R$ay $d$iffraction, the study examined the protective layer that was formed on the surface of metal after being submerged in the acidic mixture in the presence and the absence of the studied inhibitor. The spectrum of newly polished metal, as shown in **Figure III.11 (a)** reveals two peaks at 2θ of 44.76° and 50.80°, which correspond to the crystalline arrangement of metallic iron.

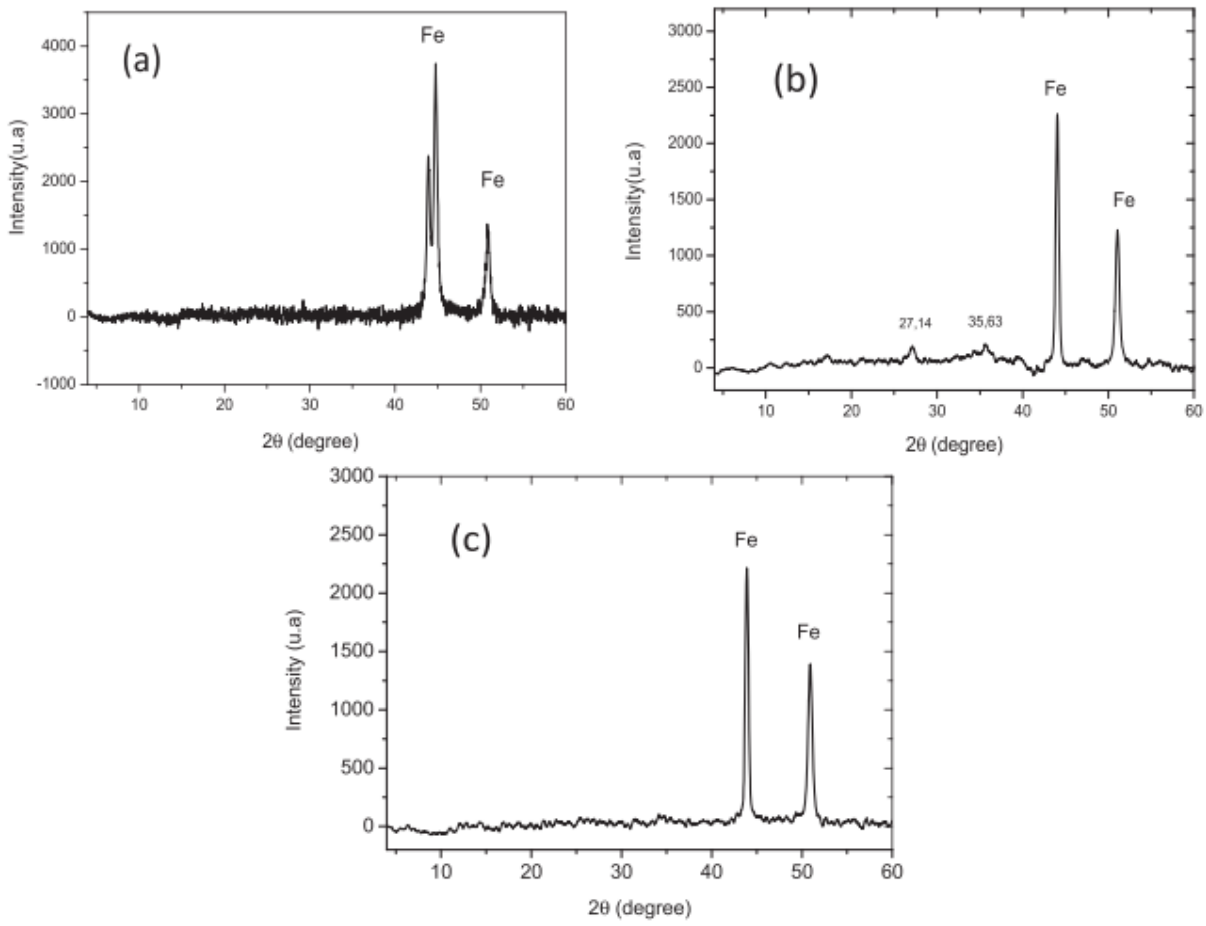

Figure III.11: ***XRD*** diffractograms of M. steel (a) blank (b) **24 *h*** submerged in **1 *M HCl*** (c) **24 *h*** submerged in **1 *M HCl*** mixture in the presence of **900 *ppm*** *AHA* polyphenols

The diffractogram acquired for the metal surface following 24 $hours$ of immersion in a 1 $M\ HCl$ solution is displayed in **Figure III.11 (b)**. Iron oxides, such as Fe_3O_4 and $FeOOH$, developed at $2\theta = 27.14°$ and 35.63°, respectively, as a result of mild steel specimen corrosion in the acidic solution [124, 125]. Whereas the XRD spectrum of mild steel submerged in a 1 $M\ HCl$ solution containing 900 ppm of *AHA* polyphenols (**Figure III.11 (c)**) reveals characteristic iron peaks at $2\theta = 43{,}89°$ and 50,90° [126]. By adsorbing substances from the *AHA* crude extract onto the surface of the mild steel, which ultimately results in the formation of a protective coating, the lack of iron oxide peaks can be explained. [127, 128].

III.1.5.4. X-Ray Photoelectron spectroscopy analysis

The layer that was adsorbed on the surface of the mild steel after being immersed in a 1$M\ HCl$ solution containing *AHA* polyphenols for 24 $hours$ was studied using XPS to

determine its chemical composition. **Figure III. 12 (a–e)** illustrates the high-resolution spectra that were acquired.

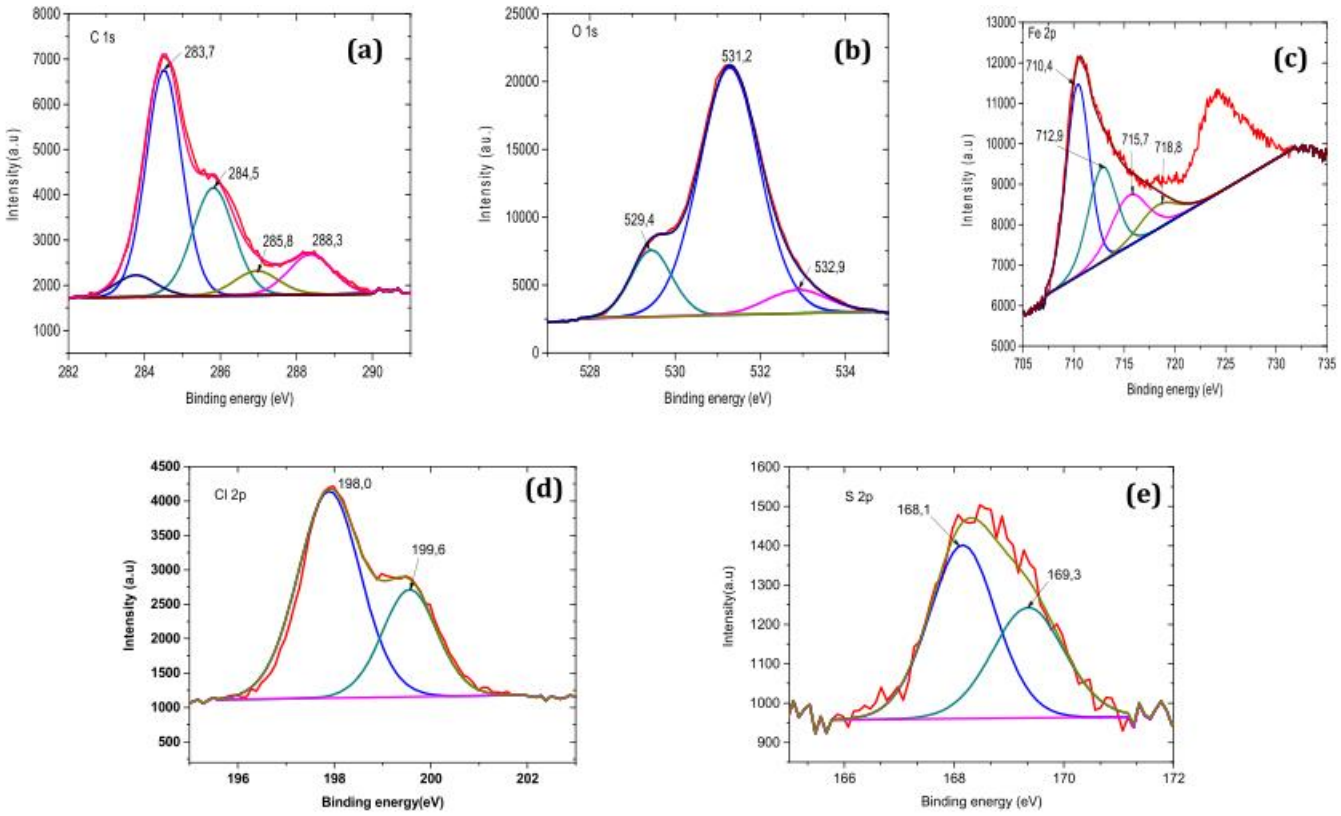

Figure III.12: ***XPS*** spectra of M. steel after **24 *h*** in **1 *M HCl*** mixture containing *Artemisia Herba Alba* extract.

The C 1s spectrum of the coated mild steel, measured with high-resolution, may be fitted into 4 separate peaks with different intensities (**Figure III.12 (a)**). $C-Fe$ and $C-C/C=C/C-H$ bonds are the first peaks at 283.7 and 284.5 eV, respectively [129, 130]. This demonstrates that the $C-C$ bonds are linked to the molecules of the *Artemisia Herba Alba* extract adsorbed on the surface of metal rather than the non-oxidized carbon-rich zones of the sample. The presence of $C-O/C=O$ bonds is associated to 285.9 eV peak [131], potentially corresponding to $C=O$ bonds in compounds derived from *Artemisia* extract. The last peak with a greater binding energy at around 288.3 eV might also be caused by $C=O$ [132].

(**Figure III.12 (b)**) shows the deconvolution of $O\ 1s$ spectrum including three compounds. The preceding values pertain to metallic iron [133], $\frac{Fe_2O_3}{Fe_3O_4}$ $FeOOH$ attributed to Fe^{3+}

ions, and $Fe\ \frac{2p1}{2}$ [134], respectively. (**Figure III.12 (d)**) illustrates the chlorine $(Cl\ 2p)$ spectra where two peaks can be observed. At $198\ eV$, the first peak is attributed to Cl, while at $199.6\ eV$ is the second peak which can be attributed to $FeCl_3$ [135]. The observations indicate that Cl ions are also adsorbed onto the steel surface. XPS analysis identifies the sulfur element $(S\ 2p)$ even at low energy levels. Deconvoluting the associated spectra (**Figure III.12 (e)**) revealed two components located, the first peak at $168.1\ eV$ may be ascribed to the $S-Fe$ bonds and/or S atoms in an environment that is more positive [136]. Whereas the second peak at $169.3\ eV$is attributed to $C-S$ bonds [137]. The obtained XPS spectra indicate that the inhibitory coating on the mild steel surface comprises a combination of molecules containing carbon, oxygen, and nitrogen atoms. It can be confirmed from this findings that the plant extract is present in the produced corrosion inhibitory layer.

Part Two: Inhibition Effect Of *Ammophila Arenaria* Extract

III.1.1. Characterization of the polysaccaride

The $FTIR$ analysis was used to characterize the organic groups contained in polysaccharide molecules. **Figure III.13** , illustrates various peaks, notably a significant and sa strong peak located at around $3297\ cm^{-1}$, indicative of the stretching vibration of hydroxyl $(-OH)$ groups, that is considered distinctive of $glycosidic$ structures seen in sugar residues [91]. Furthermore, a band at $2930\ cm^{-1}$ is ascribed to the stretching vibration of $C-H$ bonds. At $1639\ cm^{-1}$, The observed band matches with the asymmetric stretching vibration of $C=O$ present in $galacturonic$ acid, and the two bands, with medium size, at $1365\ and\ 1413\ cm^{-1}$ are ascribed to $(O-C=O)$ stretching [138].

Moreover, each individual polysaccharide displays a unique band in the region from $1200\ cm^{-1}\ to\ 1000\ cm^{-1}$, where coincide the ring stretch vibrations with the $glycosidic$ band vibration of $(C-OH)$ and $(C-O-C)$ [92]. Taking into Consideration preceding research papers indicating that cellulose, hemicellulose, and lignin are the major compounds of $Ammophila\ Arenaria$. Our study focuses on these three main compounds, cellulose, hemicellulose, and lignin, analyzing their potential as effective corrosion inhibitors for mild steel.

Figure III.13 illustrates the structure of the molecules of these specific compounds revealed in the $Ammophila\ Arenaria$ extract. The identification and characterization of these polysaccharide compounds present new opportunities for investigating their corrosion inhibition capabilities and their potential as environmentally friendly and effective inhibitors for preserving mild steel against corrosion.

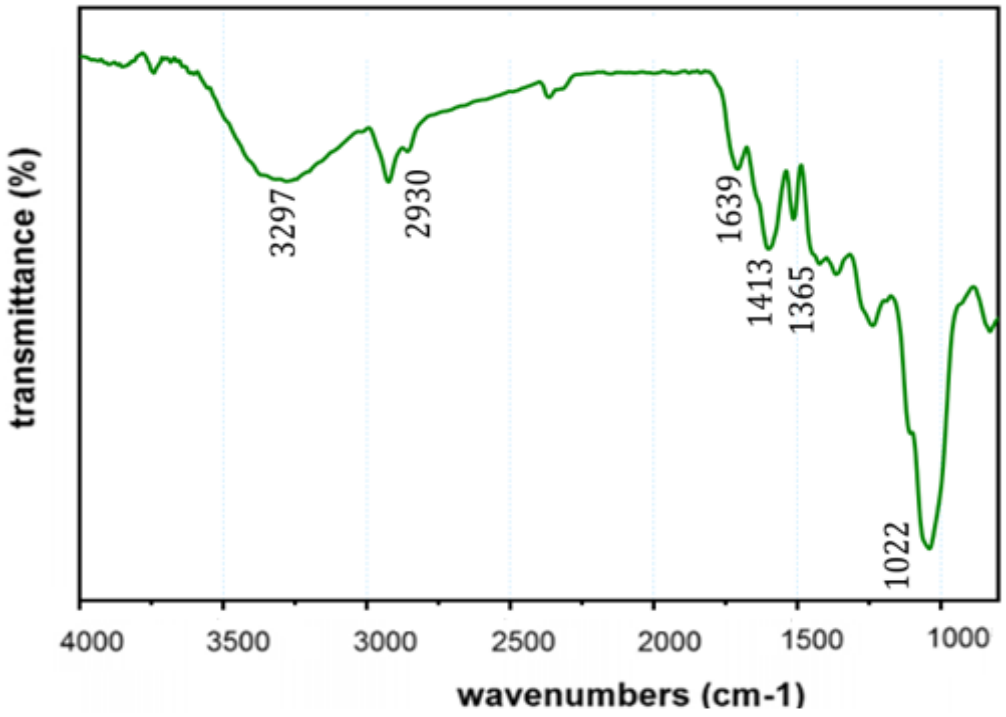

Figure III.13: FTIR spectra of the aqueous extract of **Ammophila *Arenaria*.**

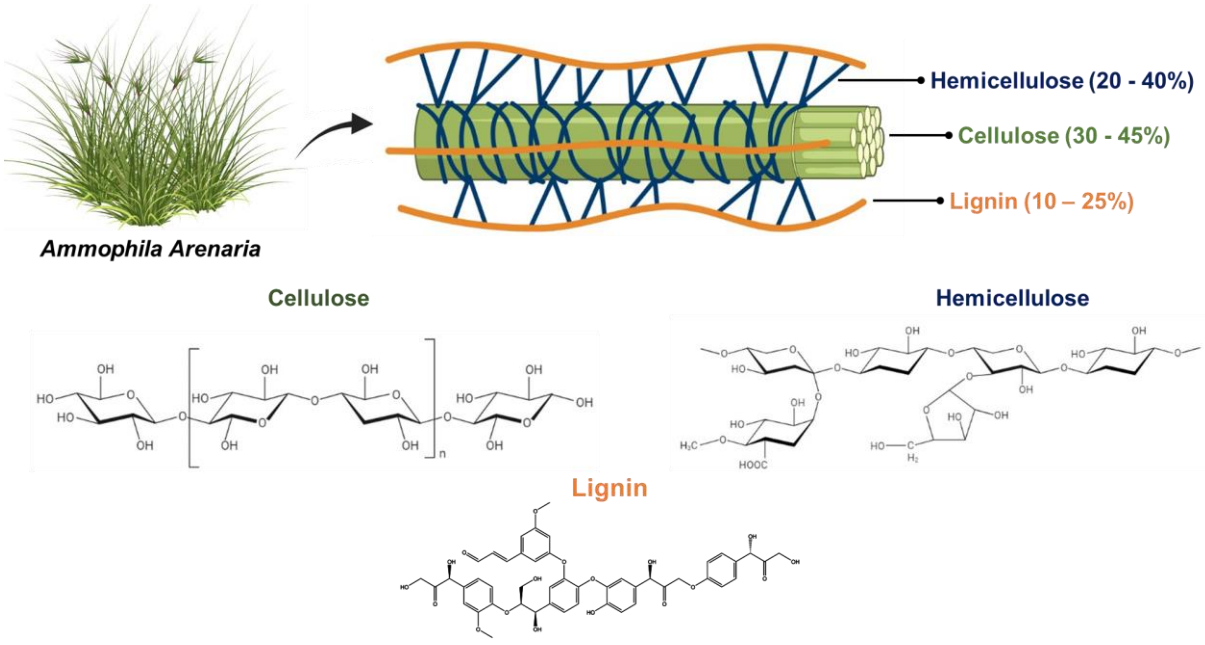

Figure III.14: The chemical structures Representation of the ***Ammophila Arenaria***'s major compounds: ***cellulose, hemicellulose, and lignin***.

III.1.2. Electrochemical characterization

III.1.2.1. Polarization Curves

Potentiodynamic polarization studies were conducted to assess the kinetics of the cathodic and the anodic reactions. The potentiodynamic polarization curves for mild steel in inhibitor-free and inhibitor-containing solutions with different amount are presented in **Figure III.15** . The extract functions as mixed-type inhibitor since both hydrogen release ,the cathodic reaction, and mild steel dissolution, the anodic reaction, were effectively inhibited as revealed in the obtained curves. **Table III.8** lists the electrochemical kinetic parameters, including the corrosion potential E_{corr}, I_{corr}, cathodic and anodic Tafel slope (βc), (βa), respectively, determined from "Tafel extrapolation" of the curves of polarization. Clearly, the increase in the inhibitor concentrations causes a notable decrease in the I_{corr} values, demonstrating that when the inhibitor is present in the medium, the corrosion reaction is reduced significantly. Furthermore, the increased negative values of E_{corr} while the inhibitor is present suggest that it operates predominantly as a cathodic inhibitor. The mixed style of inhibition is suggested by the fact that the β_a and β_c values do not follow a regular trend. However, the studied inhibitor shows a stronger cathodic inhibition than anodic inhibition. [8, 139-142].

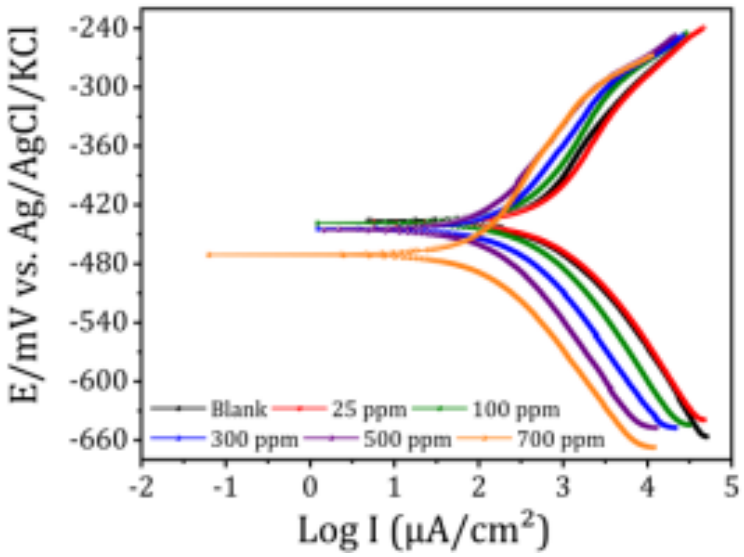

Figure III.15: Tafel curve variation for mild steel in $\mathbf{1}\ \boldsymbol{M\ HCl}$ solutions with different ***Ammophila Arenaria*** aqueous extract concentrations at $\mathbf{298}\ \boldsymbol{K}$.

Table III.8: Electrochemical parameters of ***Ammophila Arenaria*** aqueous extract inhibiting corrosion.

$C\ (ppm)$	$E_{corr}\ (mV\ vs\ SCE)$	$I_{corr}(\mu A/cm^2)$	$\beta_a\ (mV/dec)$	$\beta_c\ (mV/dec)$	$IE_{PDP}\ (\%)$
Blank	-435.980	309.393	136.0	111.8	-
25	-438.237	342.017	132.9	108.4	-
100	-438.422	200.026	130.4	110.1	35.34
300	-444.374	107.800	116.2	101.8	65.15
500	-445.322	50.523	97.1	94.0	83.67
700	-470.754	56.685	134.7	102.9	81.67

III.1.2.2. Electrochemical impedance spectroscopy

Within the scope of this investigation, EIS was utilized to evaluate the efficacy of the protective layer that was produced by *Ammophila arenaria* extract on mild steel in a solution of 1 $M\ hydrochloric\ acid$. The Nyquist curves of mild steel are depicted in **Figure III.16**. These curves were obtained through experimentation after the metal was submerged in the acidic solution for one hour, both with and without various quantities of the extract. Upon the comparison of the obtained curves, it is notable that a single capacitive loop appears with a slight deformed center. That deformation in the curve shape might be caused by a number of identified phenomena that has an impact on the plot's shape such as the presence of impurities, the non-homogeneity causing frequency dispersion, and roughness on the metal surface, which causes deviations from the ideal shape of typical semicircle known for solid electrodes. The observed capacitive loop has bigger diameters compared to those obtained from the blank solution in the presence of the inhibitor. This indicates that the metal impedance increases as a result of inclusion of the inhibitor into the corrosive environment. It is observed that the semicircles diameter become lager with the increase of the inhibitor's concentration in the corrosive environment, which suggests that the *Ammophila arenaria* improves charge transfer resistance through a processes that is reliant on the concentration of the inhibitor [146]. As the size of semicircles grows, they demonstrate a more efficient inhibition of corrosion, which ultimately results in an increase in the metal resistance against

corrosion. Because the metal-electrolyte interface is defined by a double electric layer. The introduction of a strange additive, like an inhibitor, might result in structural or compositional modifications that impact the reactivity of system. The adsorption of inhibitor molecules may be monitored by assessing the double-layer capacitance prior and following the inclusion of anti-corrosive compounds.

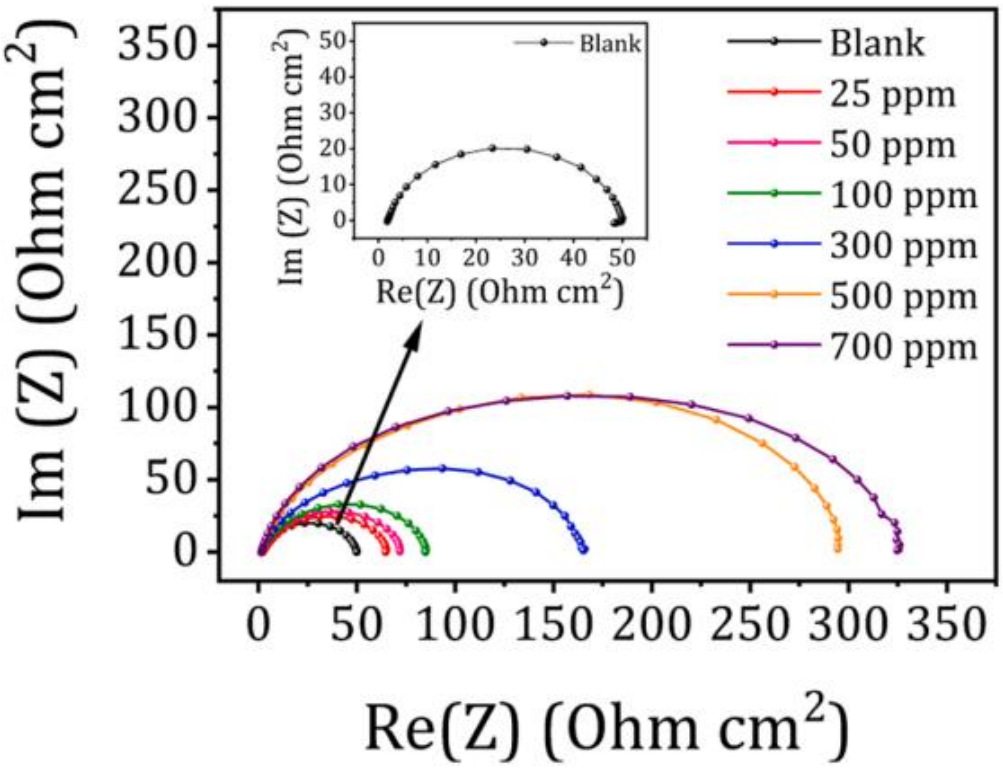

Figure III.16: Nyquist plots for mild steel at 1 M HCl solution contains the aqueous extract of *Ammophila Arenaria* with various quantities.

As depicted in **Figure III.17**, the EIS data were fitted to a proper equivalent circuit using "EC-Lab software" to further quantify these observations. The Nyquist curve of the unprotected system can simulated by a "simple Randles circuit" replacing Capacity by Q_{dl}, representing a one-time constant system. On the other hand, the protected system necessitated a more complicated model that includes more electric components as the "film resistance" (R_f) and the "constant phase element" of the film (C_{dl}), proving that a protective layer is formed on the metal surface. A summary of the retrieved parameters, like R_{ct} and C_{dl} values among the investigated rage of concentration is presented in **Table III.9**. Following the addition of $Ammophila\ arenaria$ aqueous extract, there is a notable decrease in the values of CPE, which suggests that there is a major modification in the characteristics of the double layer as a result of the inhibitor's adsorption on the surface.

Table III.9: $\boldsymbol{EIS}$ parameters for mild steel in **1** $\boldsymbol{M\ HCl}$ in the absence and the presence of various quantities of $\boldsymbol{Ammophila\ Arenaria}$ extract.

$C\ (ppm)$	$R_{ct}\ (\Omega.cm^2)$	$C_{dl}\ (\mu F.cm^{-2})$	$EI_{EIS}(\%)$
Blank	95.26	439.6	-
25	123.36	499.4	22.77
100	165.36	25.34	42.39
300	324	129.8	70.59
500	581.8	105.88	83.62
700	652.8	64.16	85.40

It is observed that the C_{dl} values are decreasing while the R_{ct} values are increasing with the increase of inhibitor concentration. This observation can be explained by the gradual adsorption of the inhibitor molecules on the metal surface.

As a result of this adsorption, the coverage of the surface is enhanced, which means that the inhibitor layer has become thicker. This is demonstrated by the decreased double-layer capacitance [147, 148]. Additional confirmation from the SEM and AFM tests showed that this behavior is in agreement with the creation of a layer that blocks ion exchange and slows down corrosion. The EIS findings, when combined with the surface morphology investigations, provide strong evidence that $Ammophila\ arenaria$ inhibits corrosion. The extract demonstrates its effectiveness as an enduring and environmentally practicable corrosion inhibitor by reaching an inhibitory efficacy up to $85.40\%\ at\ 700\ ppm$, as confirmed by both $PDP\ and\ EIS$ evaluations. This makes the extract appropriate for use in industry in acidic environments.

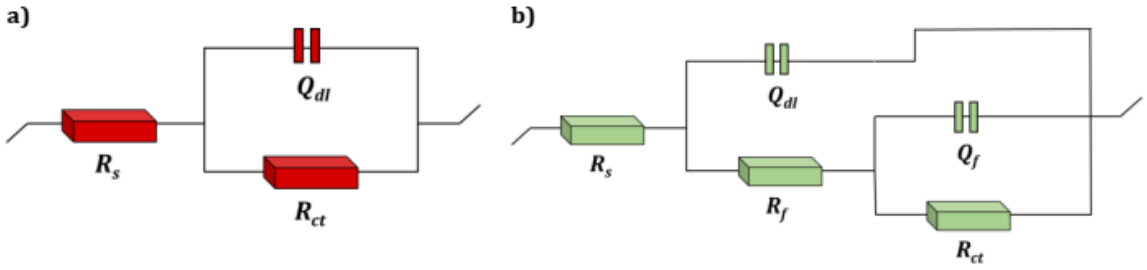

Figure III.17: Fitted equivalent circuit for a) Blank and b) *Ammophila Arenaria* extract inhibitor.

III.1.2.3. Adsorption isotherm study

The mechanism by which the $Ammophila\ Arenaria$ extract inhibits corrosion inhibits can be deciphered by examining its adsorption characteristics onto the surface of steell by several isotherm models. In our case we have employed three models "Langmuir, Frumkin, and Temkin" to the data obtained from the experiment in order to identify which one of them best describes the adsorption process.

Figure III.18 shows the fitting of the three isotherm plots to the data obtained from experiments. The "Langmuir isotherm" model, presented in **Figure III.18 (a)**, proposes that adsorption occurs in a monolayer on a surface characterized by a limited number of similar sites. Two isotherms are depicted in **Figure III.18**: (a) the "Frumkin isotherm", which takes into consideration interactions between adsorbed molecules, and (b) the "Temkin isotherm", which takes into consideration interactions between adsorbates as well as variations in energy of adsorption within the coverage range. The comparative analysis indicates that the "Langmuir isotherm" gave the most precise correlation with the experimental data in our study, demonstrated by the coefficient of correlation ($R^2 = 0.99$). The findings indicate that the adsorption of the inhibitor on the surface of M. steel aligns most closely with the "Langmuir model", which implies a uniform adsorption process devoid of interactions among the adsorbed species. The Langmuir adsorption isotherm can be expressed through the following equations:

$$\frac{C}{\theta} = \frac{1}{K_{ads}} + C$$

$$\Delta G^{\circ}_{ads} = -RTln(55.5 \times K_{ads})$$

With C: the inhibitor concentration ($mol\ l^{-1}$), K_{ads} : the adsorption equilibrium constant, ΔG°_{ads}: the Gibbs free energy of adsorption, 55.5: water concentration in solution ($mol\ l^{-1}$), T: is the thermodynamic temperature (K) and R: the universal gas constant in (J $mol\ l^{-1}\ K^{-1}$).

ΔG°_{ads} offers a detailed understanding of the spontaneity and characteristics of the adsorption process. When ΔG°_{ads} Values are more negative than $-40\ kJ\ mol^{-1}$ generally signify chemisorption, whereas values near $-20\ kJ\ mol^{-1}$ or less negative imply physisorption resulting from electrostatic interactions [149]. The "Langmuir model", yields a ΔG°_{ads} value of $-17.252\ kJ\ mol^{-1}$ (**Table III.10**), pointing that the primary mechanism is physisorption. This observation suggests that the molecules of inhibitor adhere to the metal surface primarily through physical interactions instead of forming chemical bond. The negative ΔG°_{ads} indicates the adsorption process occurs spontaneously and that it is thermodynamically favorable [150].

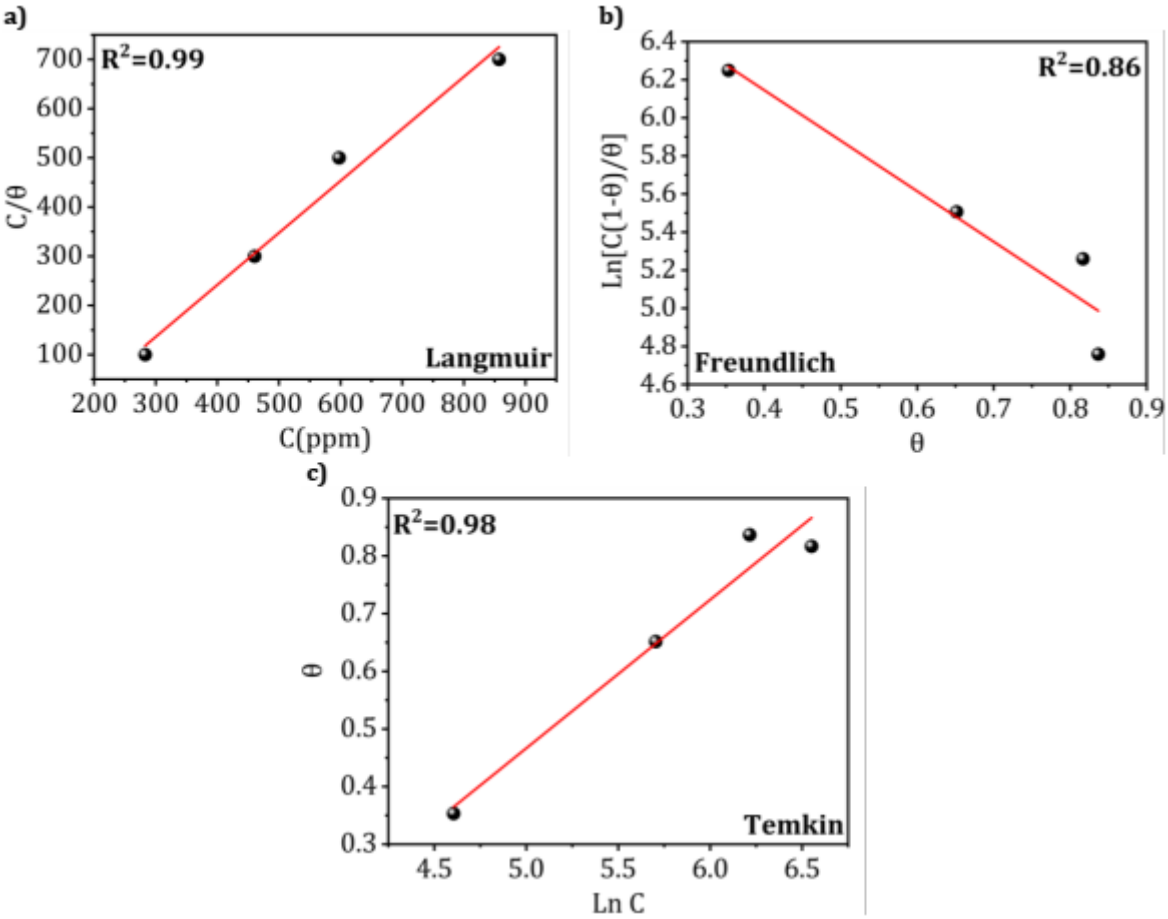

Figure III.18: Adsorption isotherm plots for M. steel in **1** ***M HCl*** containing ***Ammophila Arenaria*** extract: (a) "Langmuir isotherm", (b) "Frumkin isotherm", and (c) "Temkin isotherm".

Thus, the comprehensive Langmuir isotherm analysis, particularly, with its elevated K_{ads} value, indicates a solid interaction between the inhibitor molecules and the metallic surface, resulting in a strong defense towards metal. This aligns with the findings observed in electrochemical studies. The applicability of the "Langmuir isotherm" indicates that the extract of *Ammophila Arenaria* creates a monolayer on the metal, effectively safeguarding it against the corrosive attack.

Table III.10: adsorption of ***Ammophila Arenaria*** extract inhibitor: Thermodynamic parameters.

Method	*Slope*	R^2	K_{ads}	$\Delta G^{\circ}_{ads}\ KJ\ mol^{-1}$
Langmuir	1.057	0.99	945.939	-17.252

III.1.3. Morphological studies

III.1.3.1. Atomic Force Microscopy

AFM is considered as a highly effective technique method for investigating the corrosion morphological development of metal surfaces on both micrometer and nanoscales [151]. This method was utilized, in the present study, to examine the morphology of mild steel surface and derive quantitative data regarding its topographic characteristics. The aim was to examine the effects of the $Ammophila\ Arenaria$ extract on the surface of mild steel under different conditions, specifically soaking in a $1\ M\ HCl$ solution with $700\ ppm$ of the extract, alongside a blank HCl medium at $298\ K$, as illustrated in **Figure III.19**. The utilization of images from AFM offers a distinct chance for a detailed inspection of surface features, permitting a thorough examination of topographical distinctions. Inspecting the roughness parameters of surface, allows a quantitative measurement of the degree of topographic variations present on the surface. After gathering the images from AFM study, a detailed analysis of the surface morphology and its reaction to various experimental conditions became easy to perform. The morphology of the mild steel surface after being immerged for $24\ H$ in a $1M\ HCl$ solution is depicted in **Figure III. 19 (a)**. **Table III.11**gives "the average roughness" R_a which represents the average deviation of every single point in the roughness profile from a mean line over the evaluation length alongside "Root Mean Square roughness" R_q defined as the average of the measurements from the mean line. Without the presence of inhibitors, the mild steel surface experiences significant deterioration because it's directly exposed to the corrosive $1M\ HCl$ solution (**Figure IIIIII.19 (b)**), showing "an average roughness" (R_a) of $157.67\ nm$. Given such circumstances, the impact of aggressive ions on the metal surface is clearly observable, resulting in significant dissolution of the surface. As a result, a topography that is both irregular and rough, characterized by serious harm, was the outcome of several corrosion pits. With the inclusion of the $Ammophila\ Arenaria$ extract (**Figure IIIIII.19 (c)**), a significant enhancement in the surface morphology is noted, suggesting the development of a layer of protection on the surface of the metal. The adsorbed film serves as an inhibitory barrier, significantly restricting the contact between the corrosive agents and the metallic surface and diminishing the number of available reaction locations. Consequently, it offers effective protection against the metal corrosion. The efficacy of the corrosion inhibitory data obtained from the electrochemical measurements is supported by the $R_a$value which is equal to $101.08\ nm$.

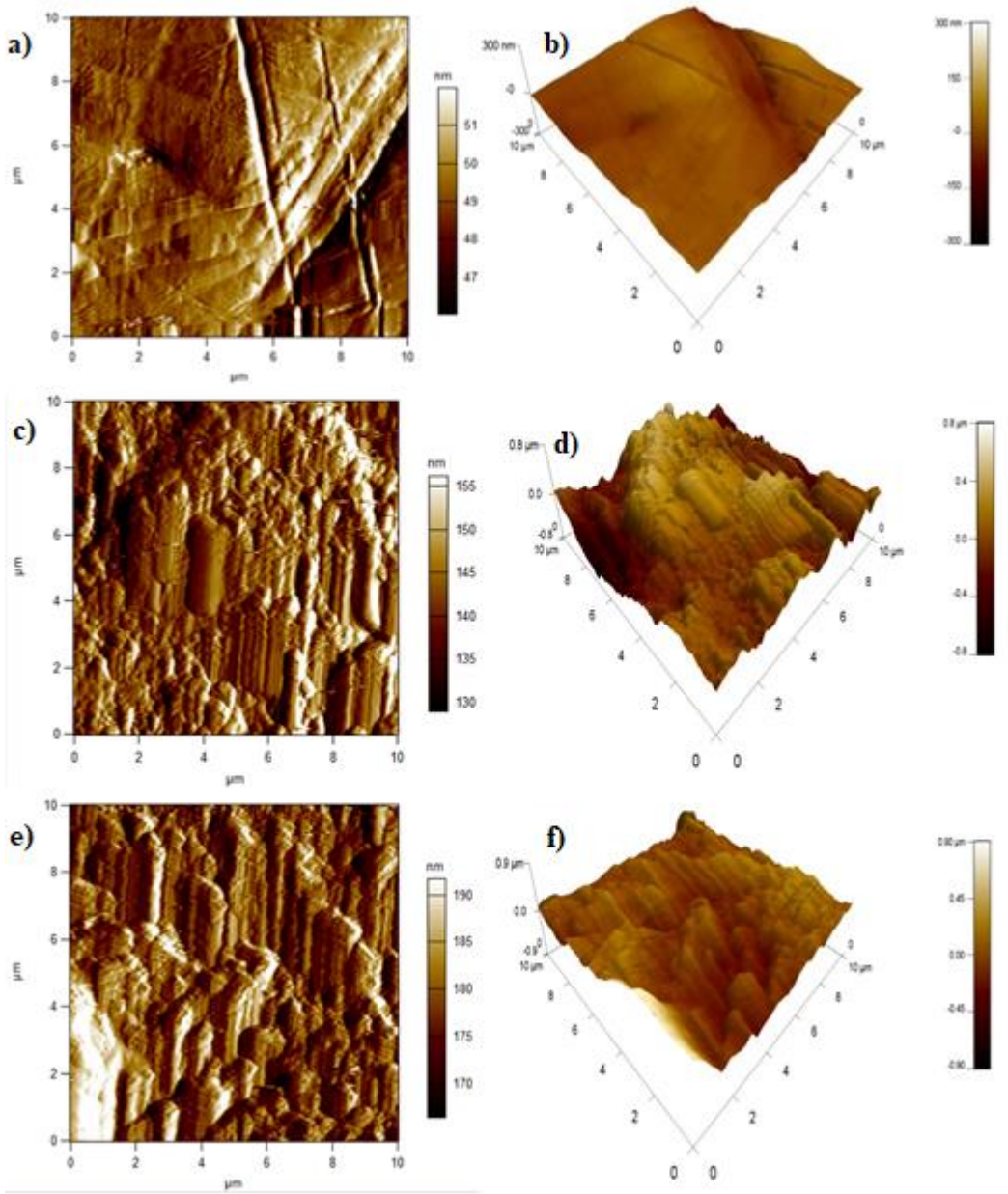

Figure III.19: ***AFM*** images "2D and 3D" for: polished mild steel in (a and b), immerged in blank $\mathbf{1}\boldsymbol{M\ HCl}$ in (c and d) and emerged in $\mathbf{1}\boldsymbol{M\ HCl}$ with $\mathbf{700}\ \boldsymbol{ppm}$ of ***Ammophila Arenaria*** extract in (e and f)

Table III.11: $\boldsymbol{AFM}$ parameters of mild steel in blank $\mathbf{1}\ \boldsymbol{M\ HCl}$ and $\mathbf{1}\ \boldsymbol{M\ HCl}$ with $\mathbf{700}\ \boldsymbol{ppm}$ of ***Ammophila Arenaria*** extract.

Sample	*Average Roughness* ($R_a\ nm$)	*RMS Roughness* ($R_q\ nm$)
Polished metal	22.52	27.86
Uninhibited metal	157.665	195.855
Inhibited metal/Ammophila Arenaria extract	101.081	138.437

The results obtained from the AFM are consistent with the results from the SEM, providing robust evidence for the inhibitory function of the *Ammophila aerenaria* extract. This strongly demonstrates its capacity for minimizing corrosion by creating a barrier of defense on the metallic surface. The decrease in pits of corrosion and the enhancement of surface topography provide additional evidence for the beneficial impact of the *Ammophila Arenaria* extract as an inhibitor. *Ammophila arenaria* extract has the ability to be a powerful inhibitor of mild steel corrosion, and these findings about surface morphology provide strong proof of the inhibitory procedure.

III.1.3.2. Scanning Electron Microscopy

In this study, SEM was employed to analyze the variations in mild steel surface properties in the presence and absence of the *Ammophila Arenaria* extract as a corrosion inhibitor. **Figure III. 20** depicts the SEM images acquired throughout the experiment.

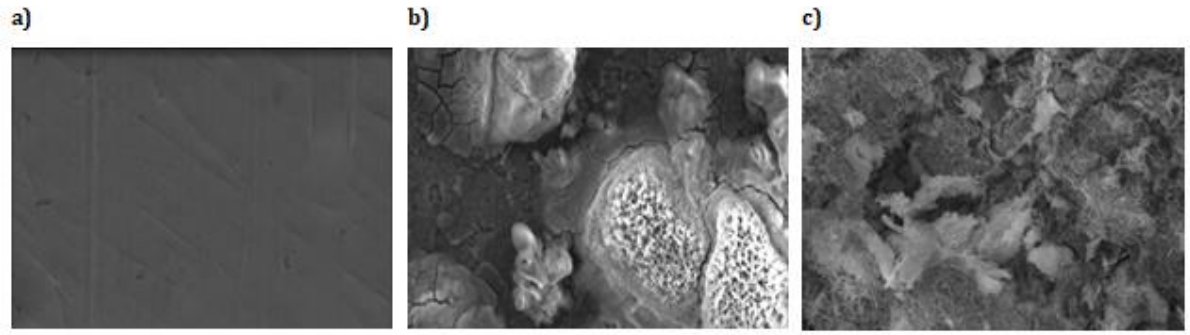

Figure III.20: $\boldsymbol{SEM}$ images for mild steel surface at a scale of $\mathbf{10}\ \boldsymbol{\mu m}$ for: (a) polished mild steel, (b) emerged in blank $\mathbf{1}\ \boldsymbol{M\ HCl}$ and (c) emerged in $\mathbf{1}\ \boldsymbol{M\ HCl}$ with *Ammophila Arenaria*.

Figure III.20 (a) presents the SEM image that illustrates the polished surface of the steel, characterized by its clean and smooth appearance. The obtained image provides a baseline for assessing the initial condition of the surface. **Figure III.20 (b)** illustrates the SEM image of a metal specimen that was submerged in $1M\ HCl$ in the absence of the $Ammophila\ Arenaria$ extract. The corrosive effects of the acidic environment have clearly led to surface deterioration, resulting in the formation of pits. The image shows how the corrosive medium ruined the metal's surface notably. Conversely, **Figure III.20 (c)** illustrates the SEM image of mild steel sample submerged in a mixture of $1\ M\ HCl$ solution containing $700\ ppm$ of $Ammophila\ Arenaria$ extract. The surface destruction shows a notable decrease when compared with **Figure III.20 (b)**. The increase in metal resistance towards corrosion can be attributed to the adsorption of the $Ammophila\ Arenaria$ extract inhibitor, which results in the formation of a protective layer on its surface. The formed layer functions as a layer of defense, significantly decreasing the corrosion impact and limiting surface deterioration. The SEM study provides important proof illustrating the advantageous impacts of the $Ammophila\ Arenaria$ corrosion inhibitor on the surface of steel sample. It demonstrates how the inhibitor protects the material from harmful conditions and reduces corrosion.

III.1.3.3. ATR/FTIR analysis

The immersion of steel specimen in a $1M\ HCl$ mixture with $700\ ppm$ of $Ammophila\ Arenaria$ extract led to the formation of a surface protective coating on the electrode, which was subsequently analyzed using “ATR-FTIR spectroscopy”. In **Figure III.21**, we can see the ATR spectra of the metal surface protective coating and the untreated $Ammophila\ Arenaria$ extract.

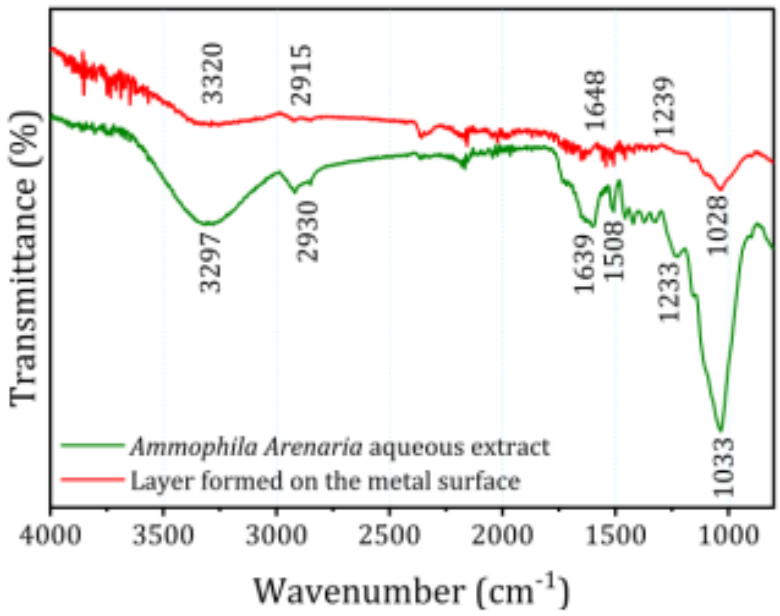

Figure III.21: ***ATR*** spectra of the steel sample surface following immersion in $\mathbf{1}\boldsymbol{M\ HCl}$ mixture with $\mathbf{700}\ \boldsymbol{ppm}$ of ***Ammophila Arenaria*** extract inhibitor.

The comparison of the ATR spectra showed significant distinctions, emphasizing the interactions between the inhibitor's molecules and the metallic surface. It was noticed that specific absorption bands found in the spectrum of the extracted material were shifted in the coated metal surface spectrum. The observed shifts in absorption bands, including the $O-H$ stretch at approximately $3290\ cm^{-1}$, the $C=O$ stretch close to $1630\ cm^{-1}$, and the $C-O$ stretch at around $1230\ cm^{-1}$, suggest a creation of a compound involving the extract components and the surface of steel. The large band seen at$3290\ cm^{-1}$ in the extract, which is attributed to the $O-H$ stretching, gets more precise and switches to $3320\ cm^{-1}$ in the processed specimen. This indicates a potential contribution from hydrogen bonding in the adsorption procedure. In a similar manner, the peak observed at $1630\ cm^{-1}$, which corresponds to the $C=O$ stretching, suggests the presence of compounds that contains carbonyl. This peak shifts slightly in the spectrum of the processed metal, indicating a potential contribution from the carbonyl site. The reported spectral shifts support the hypothesis regarding molecules interacting and align with the "physisorption mechanism" proposed by the studies of thermodynamic [152, 153]. The ATR outcomes, along with the changes noted in the $FTIR$ spectra, indicate a significant interaction between the $Ammophila\ Arenaria$ molecules and the surface components [154, 155]. The interactions in question appear to play a significant role in the development of a strong protective layer,

which is associated with the corrosion inhibition stated. The comparative $ATR - FTIR$ outcomes enhance our comprehension of the surface chemistry related to corrosion inhibition by $Ammophila\ Arenaria$. These findings indicate that the dynamics of molecules interacts in a complex manner at the interface and that the inhibitor forms a stable complex with the mild steel surface that has a powerful role in controlling corrosion.

Part Three: Comparative study between the inhibition effect of *Artemisia Herba Alba* and *Ammophila Arenaria*

Table III.12 Presents a meticulous side-by-side comparison of the results obtained in our study discussing the two plant extracts.

Table III.12: Compared efficacy of corrosion inhibition of ***Artemisia Herba Alba*** with ***Ammophila Arenaria***.

Plant name	***Concentratio***	***Metal and elctrol***	***Technique use***	***Inhibition effica***
Artemisia Herb ***Alba***	900 ppm	$Mild\ steel, 1M\ HCl$	$Weight\ loss, PL$ $and\ EIS$	92.92%
Ammophila ***Arenaria***	700 ppm	$Mild\ steel, 1M\ HCl$	OCP, PDP $and\ EIS$	85.40%

The main conclusions drawn from this part of our study for the two plants are summarized in the following points:

- ***ARTEMISIA HERBA ALBA (AHA):***

The corrosion inhibition effectiveness was found more than 94% once the amount of extract attained 900 ppm in a 1 $M\ HCl$ solution.

The electrochemical data indicates that the inhibitor under investigation can be categorized as a mixed-type inhibitor.

The inhibiting efficiencies assessed through gravimetric measurement and electrochemical analysis show a notable degree of comparability. The inhibitory effectiveness of $Artemisia$ H.A extract remains mostly unaltered throughout varying temperatures. The "Langmuir isotherm" governs the adsorption process of inhibitor molecules onto the surface of mild steel.

Morphological studies conducted by means of SEM and AFM approaches reveal that the inhibitor molecules adhere to steel in a parallel arrangement, forming a protective barrier that effectively prevents steel corrosion.

❖ ***AMMOPHILA ARENARIA (AA):***

The optimal value of the inhibition efficiency was found at $700\,ppm$ of $Ammophila\ Arenaria$ extract, reaching more than 84%.

The Langmuir isotherm controls the adsorption of $Ammophila\ Arenaria$ on mild steel and found to be spontaneous and predominanted by physisorption.

The application of methods for surface characterization such as SEM and AFM, combined with $ATR-IR$ spectroscopy, has demonstrated the presence of a thick and consistent film on the mild steel surface. This film is abundant in organic constituents containing polar functional groups, which play a crucial role in the inhibition procedure.

The results indicate that the $Artemisia\ Herba\ Alba$ extract demonstrates superior corrosion inhibition performance, exceeding that of the $Ammophila\ Arenaria$ extract under similar conditions. The inhibitory efficacy points out the potential of both extracts to be sustainable and economical inhibitors for mild steel corrosion in acidic environments, attributed to their strong protective properties towards corrosive substances.

Chapter IV

Modeling and simulation

CHAPTER IV. Modeling and simulation

Part One: Quantum Chemistry Calculations Of Polyphenols Extracted From *AHA*

IV.1.1. Quantum chemical study

The results of the quantum chemical calculations are presented in **Table IV.1**, using parameters like $electronegativity$, $hardness$, E_{HOMO}, E_{LUMO}, and others that were examined for the six isomer molecules. [156, 157].

Table IV.1: Global reactivity parameters.

$Isomer$	$E_{HOMO}\ (eV)$	$E_{LUMO}\ (eV)$	$E_{Gap}\ (eV)$	χ	η	ω	ΔN
$13DA$	-5.274	-3.015	2.259	4.144	1.129	7.605	0.299
$Prot\_13DA$	-4.479	-3.464	1.015	3.972	0.507	15.540	0.836
$14DA$	-5.502	-2.914	2.588	4.208	1.294	6.843	0.236
$Prot\_14DA$	-4.006	-3.004	1.001	3.505	0.501	12.267	1.313
$15DA$	-5.328	-2.928	2.400	4.128	1.200	7.100	0.288
$Prot\_15DA$	-3.889	-3.352	0.536	3.620	0.268	24.452	2.238
$34DA$	-5.565	-2.988	2.577	4.276	1.288	7.096	0.211
$Prot\_34DA$	-4.166	-3.132	1.034	3.649	0.517	12.877	1.132
$35DA$	-5.459	-2.920	2.539	4.189	1.269	6.912	0.248
$Prot\_35DA$	-4.016	-2.980	1.037	3.498	0.518	11.802	1.275
$45DA$	-5.524	-2.912	2.612	4.218	1.306	6.810	0.231
$Prot\_45DA$	-5.132	-4.044	1.088	4.588	0.544	19.338	0.213

With regard to the neutral isomer's shape, the figures in **Table IV.2** demonstrate that the $HOMO$ orbitals are centered around the $\pi - double\ bonds$, whilst the $LUMO$ orbitals are focused around the $C = C\ double\ bond$. For protonated molecules, where the protonation occurs at the $C = C\ double\ bond$, the $HOMO$ and $LUMO$ exhibit a concentration around the $phenyl\ \pi - double\ bonds$. This localization leads to increased activity in comparison to the

neutral form. The centralized electronic concentrations within the heteroatomic groups of $oxygen$ and $\pi - bonds$ exhibit a tendency to establish chemical and physical bonds with electrophilic molecules, such as the atoms of iron. The isomer molecules display larger $HOMO$ and $LUMO$ orbitals, indicating the existence of both donor and receptor electron sites. These sites have the potential to facilitate electron exchange with metal ion $D - orbitals$, thereby forming a back-donating bond.

The values estimated for the dissolved inhibitor molecules (both neutral and charged structures) presented in **Table IV.1**T indicate that the charged structure of each isomer exhibits higher E_{HOMO} and lower E_{LUMO} values compared to the corresponding neutral structure. This observation implies that the charged structure has a greater tendency for adsorption on the metallic surface than the neutral structure [158, 159]. This indicates that the inhibition occurs via the charged molecules of each inhibitor in an acidic environment. The protonated form exhibits lower $gap\ energy$ and $hardness$, along with higher ΔN values compared to the neutral molecules, indicating a greater level of activity. This indicates that the charged molecules exhibit superior performance in comparison to the neutral molecules. The homolytic fission of the $C = C\ \pi - bond$ in the acidic solution is a potential mechanism associated with this phenomenon. This mechanism enables the reaction with the H^+ ions present in the solution and the Fe^{2+} ions present on the surface of the metallic material.

Table IV.1 indicates that the charged structure ($Prot - 15DA$) of the $1{,}5DA$ appears to exhibit the highest activity in inhibiting iron site corrosion.

Table IV.2: Frontiers molecular orbitals.

Isomer		HOMO	LUMO
1,3 DA	Neutral	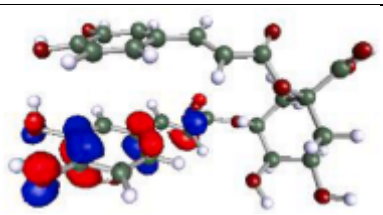	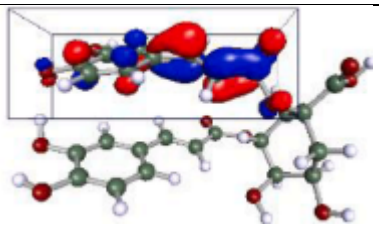
	Protonated	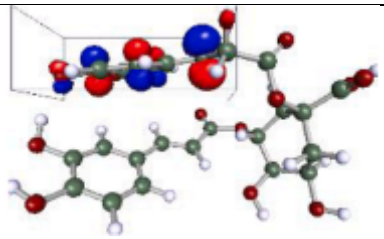	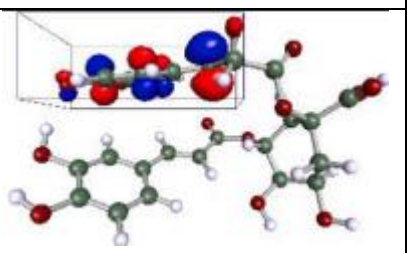
1,4 DA	Neutral	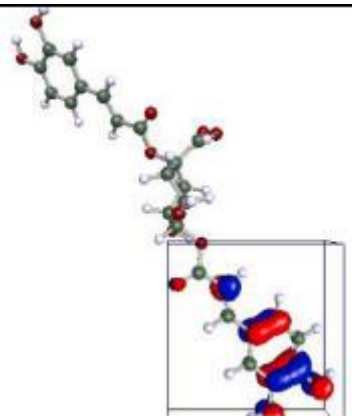	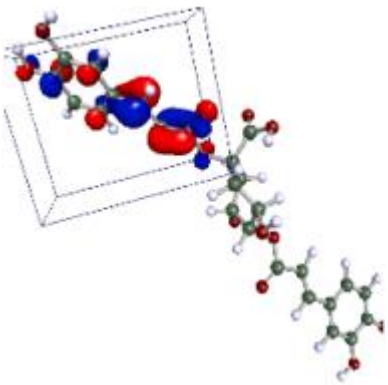
	Protonated	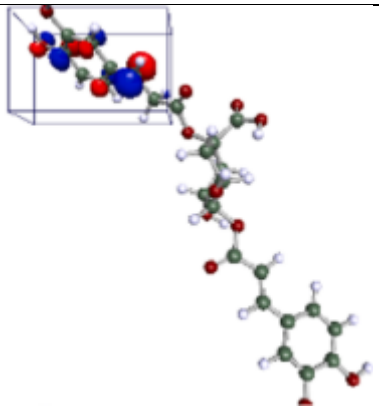	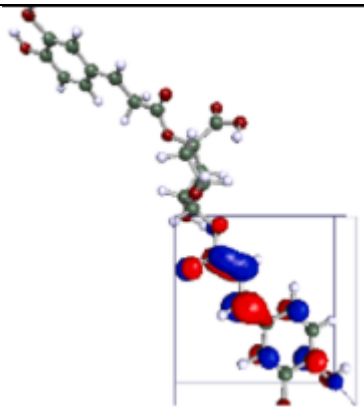

1,5 DA	Neutral	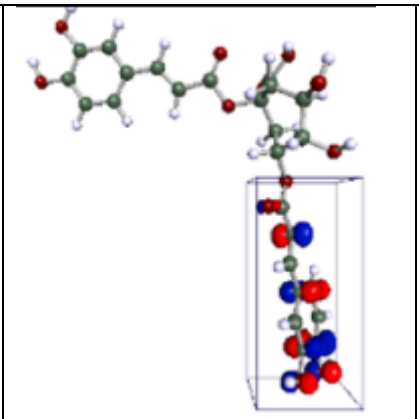	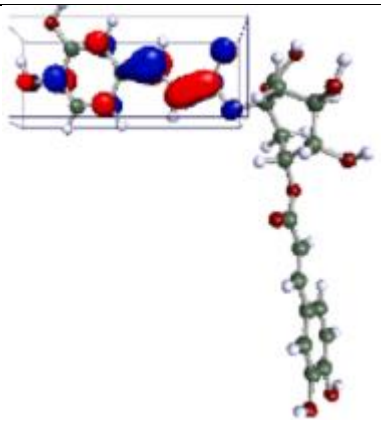
	Protonated	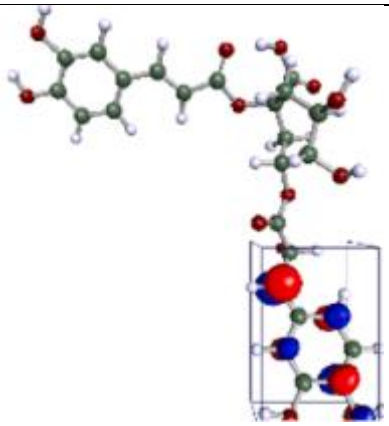	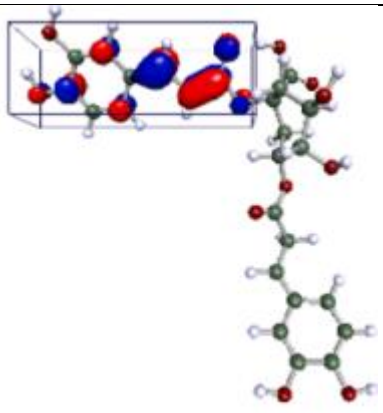
3,4 DA	Neutral	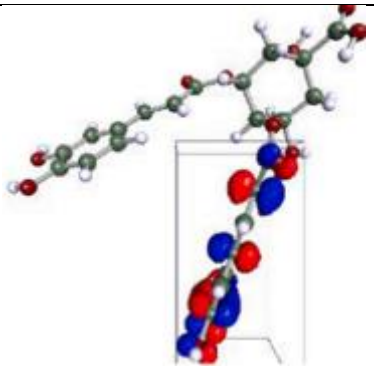	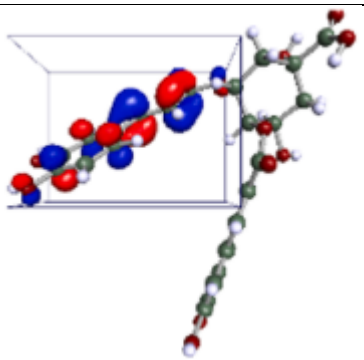
	Protonated	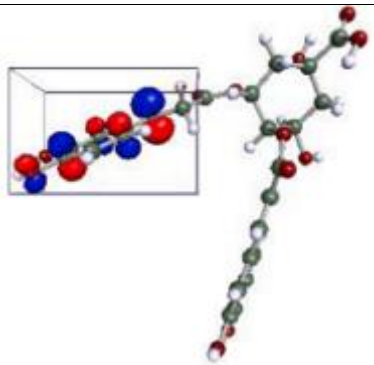	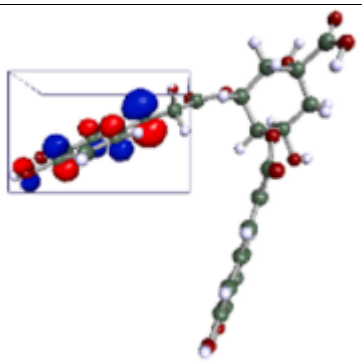

3,5 DA	Neutral	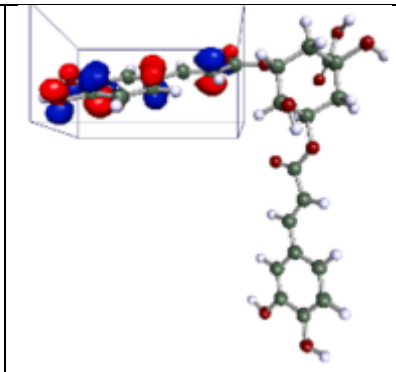	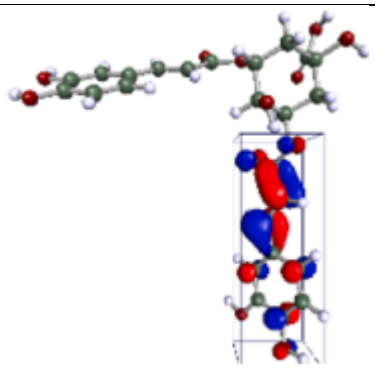
	Protonated	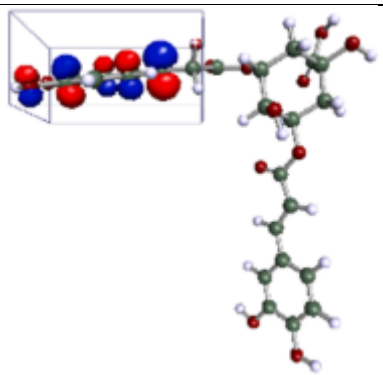	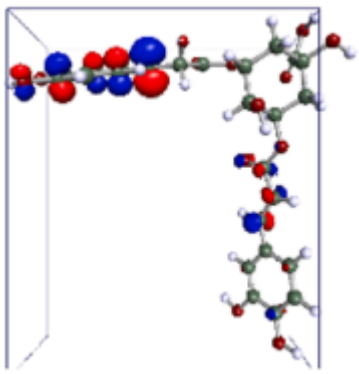
4,5 DA	Neutral	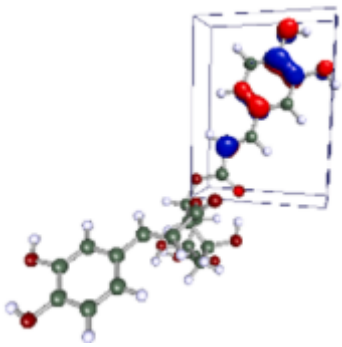	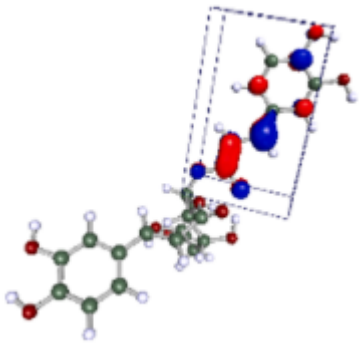
	Protonated	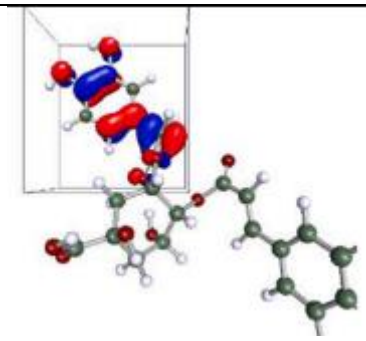	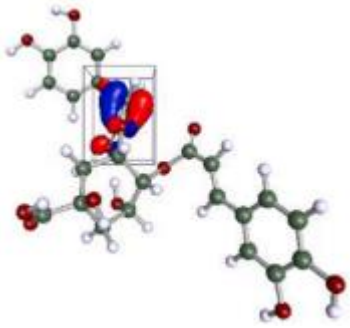

Figure IV.1.illustrates the probability distributions of the six inhibitors evaluated alongside their corresponding $\sigma - potentials$. $P(\sigma)$ represents the total amount of molecular surface segments that possess a particular screening density of charges σ [160, 161]. When $\sigma > 0$, it indicates surfaces of negative polarity, while $\sigma < 0$ corresponds to positive polarity surfaces [162, 163]. The area characterized by $\sigma \approx 0$ is identified as non-polar and

hydrophobic. Consequently, the profile curves can be categorized into three distinct sections: “the hydrogen bond donor (HBD) region”, defined by the range $-0.025 < \sigma < -0.010$; “the non-polar region”, which covers $-0.010 < \sigma < +0.010$; and “the hydrogen bond acceptor (HBA) zone”, characterized by $+0.010 < \sigma < +0.025$.

In **Figure IV.1**, the classification of the molecules as either "HBA" or "HBD" is not straightforward. The complexity of the inhibitors arises from the fact that many of the molecules can be classified as both hydrogen bond acceptors and hydrogen bond donors. Additionally, an examination of the $\sigma - potentials$ of the six isomers reveals that they exhibit a favorable interaction with $HBDs$ ($\sigma < 0$), an intense interaction with HBA ($\sigma > 0$), and a minimal interaction with non-polar surfaces or particles.

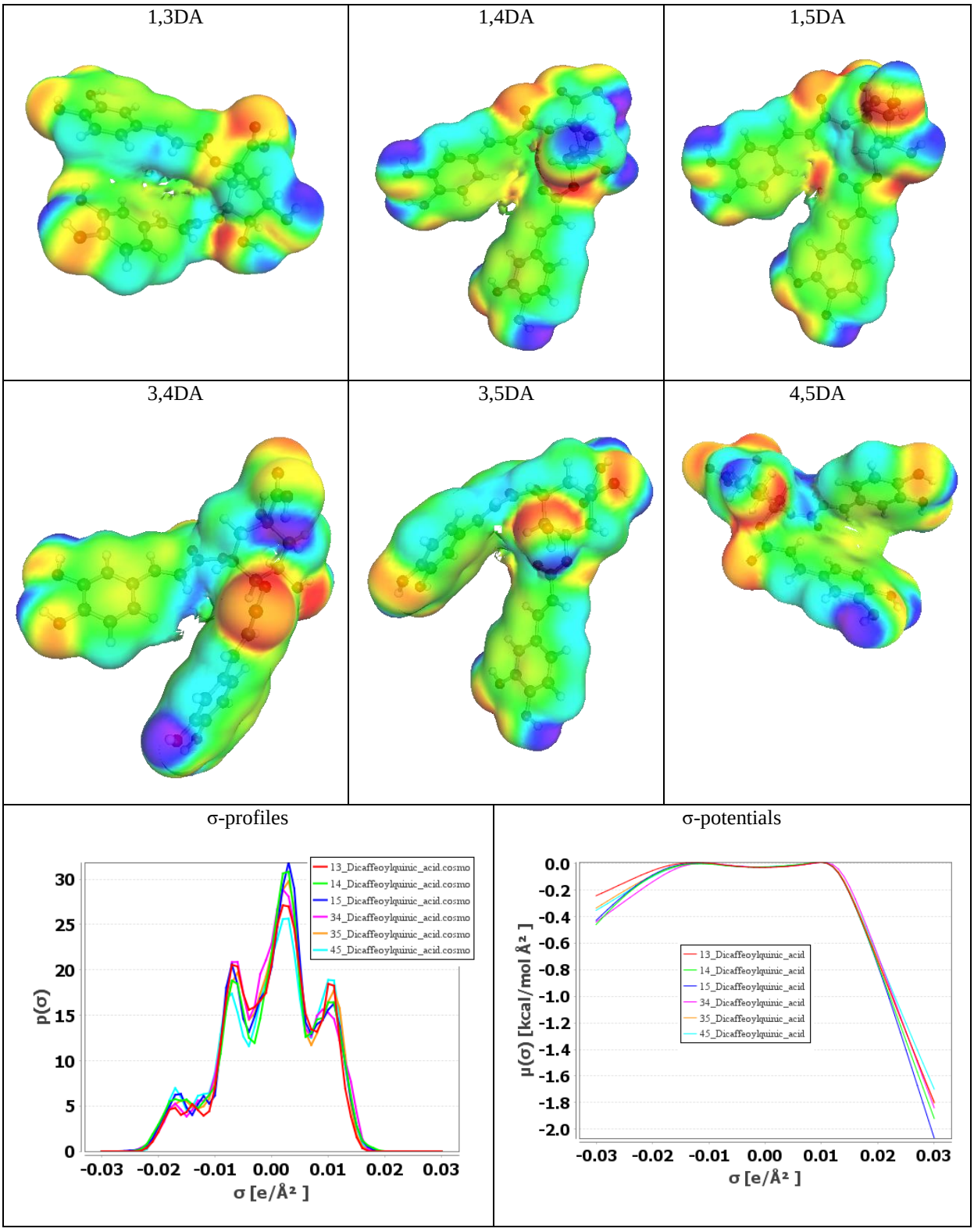

Figure IV.1: $COSMO - RS$ study: "surfaces, polarities, and potentials".

IV.1.2. $\boldsymbol{M}$onte−$\boldsymbol{C}$arlo $\boldsymbol{S}$imulations ($\boldsymbol{MCS}$)

Figure IV.2 illustrates the optimal adsorption configuration of the inhibitor on the surface of $Fe(110)$. As can be seen in the illustration, all three inhibitors are adsorbed on the surface of $Fe(110)$) in an almost exactly flat configuration. The interaction between the molecule of the inhibitor and the metallic surface can be characterized as a donor-acceptor relationship, leading to "the parallel adsorption" of various inhibiting substances. It is the p-electrons that are present in the inhibitor isomer molecules that are responsible for supplying a significant number of electrons to the vacant orbitals of iron. Conversely, the vacant antibonding orbitals of the phenyl rings have the capacity to receive an electron from the $4s$ or $3d$ orbitals of iron, resulting in the formation of feedback bonds. A variety of massive amount of organic corrosion inhibitors, as outlined in References. [164, 165] , exhibit this similar parallel configuration on the surface of steel, where $p-d\ hybridization$ is a significant factor. On the other hand, inhibitors with tiny compounds like benzimidazole have the ability to chemisorb perpendicular to the surface of iron by utilizing unsaturated heteroatoms through s molecular orbitals [166]. **Table IV.3** presents the values for both "adsorption-desorption" and "deformation energy". The findings indicate that the $45DA$ isomer exhibits a strong adsorption on the surface of iron within an acidic aqueous mixture. The strength of the adsorption correlates directly with the level of the solution acidity. The fact that all of the adsorption energies were negative suggests that the adsorption is exothermic and occurs spontaneously.

Table IV.3: Adsorption energies (kcal mol-1) determined by the MCS.

	Total	***Adsorptio***	***Rigid adso***	***Deformatio***	Inhibitor: ***dEad/dNi***	H_2O: ***dEad/dNi***	Cl^-: ***dEad/dNi***	H_30+: ***dEad/dNi***
Steel/D13/100H2O/5HCl	84.315	-3173.792	-3.037	-3170.755	-1873.68	-9.062	-0.86	−17.525
Steel/D13/100H2O /10HCl	79.567	-3277.137	-7.349	-3269.788	-1883.57	-9.124	-0.910	-18.186
Steel/D14/100H2O/5HCl	76.088	-1958.677	-3.948	-1954.730	-662.661	-9.014	-1.087	-17.926
Steel/D14/100H2O /10HCl	73.973	-1998.365	-7.389	-1990.975	-653.892	-8.925	-0.060	-18.169
Steel/D15/100H2O/5HCl	83.368	-2017.388	-0.974	-2016.415	-720.648	-9.368	-0.426	-18.092
Steel/D15/100H2O /10HCl	86.212	-2052.117	-0.800	-2051.317	-714.195	-8.717	-0.992	-17.850
Steel/D34/100H2O/5HCl	69.539	-19554.65	-3.158	-1952.306	-651.574	-10.106	-1.584	-18.561
Steel/D34/100H2O /10HCl	59.486	-2003.091	-12.628	-1990.462	-649.861	-9.597	-1.043	-17.008
Steel/D35/100H2O/5HCl	68.129	-2288.853	-4.762	-2284.091	-992.964	-9.704	-1.002	-17.319
Steel/D35/100H2O/ 10HCl	66.202	-2328.353	-7.080	-2321.273	-980.564	-9.745	-0.646	-17.607
Steel/D45/100H2O/5HCl	76.151	-3743.141	-3.659	-3739.482	-2443.445	-9.877	-0.496	-17.799
Steel/D45/100H2O /10HCl	69.199	-3787.665	-12.340	-3775.325	-2448.414	-9.492	-0.364	-17.656

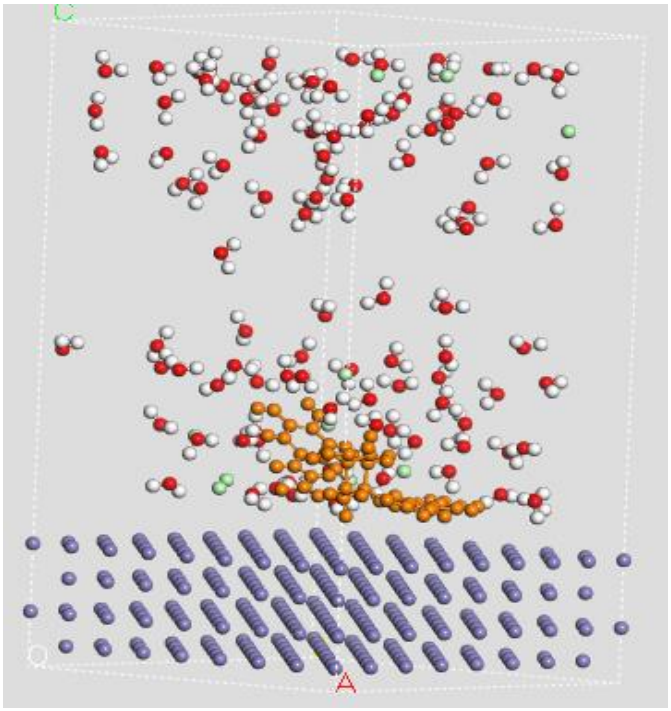

Figure IV.2: MCS study data: a) $steel$: $blue$; $inhibitor$: $brown$ / H_2O (O: red; H: $white\ and\ Cl^-\ green$).

Moreover, the stability of the adsorption system may be verified by measuring the magnitude of E_{ads}. It has been found that higher absolute values of E_{ads} are related with more powerful interactions between the inhibitor and $Fe(110)$ as well as a greater level of corrosion inhibition efficiency. **Table IV.3** indicates that the $D45@Fe(110$ and $D13@Fe(110)$ adsorption structures exhibit the highest stability within the group, as well as the greatest inhibitory efficiency, effectively decreasing the corrosion rate of mild steel.

Part Two: Quantum Chemistry Calculations Of Polysaccharide Compounds From *AA*

IV.1.1. Computational modeling results

IV.1.1.1. Optimization and *F*rontier *M*olecular *O*rbital (FMO) results

The "Frontier Molecular Orbital" (FMO) study provided a thorough analysis of the $electrical\ characteristics$, $optical\ potential$, and $reactivity$ of the components $Cellulose$, $Hemicellulose$, and $Lignin$. The FMO energies of these polysaccharide molecules were calculated utilizing the $def2-TZVP$ basis set alongside the $B3LYP-DFT$ method [167-171] within the "Turbomole 7.4 software" [171-173]. The visualization of $HOMO$ and $LUMO$ electron concentrations, along with their Eg [93], was conducted using $Multiwfn$ and VMD [94] programs, as illustrated in **Figure IV.3**. The examination indicates that the $HOMO$ electron densities in $Cellulose$, $Hemicellulose$, and $Lignin$ are primarily concentrated in particular areas of the structures of molecules. In contrast, the $LUMO$ electron densities are distributed throughout other areas. In particular, the $HOMO$ electron density in $Hemicellulose$ shows significant distribution across specific regions, suggesting intensified molecular reactivity. The determined bandgap energies for $Cellulose$, $Hemicellulose$, and $Lignin$ are 6.345 eV, 0.399 eV, and 3.431 eV, respectively. $Cellulose$ clearly shows the highest value, whereas $Hemicellulose$ presents the lowest. In addition to providing an explanation for the energy gaps, the distribution of $HOMO$ and $LUMO$ electron densities also is able to provide information on the stability of the compounds. In $Hemicellulose$, the regions exhibiting the greatest dispersion of $HOMO$ electron density may align with functional groups such as hydroxyl ($-OH$) and carbonyl ($-C=O$) groups. As it is known the presence of these functional groups which can contribute to many chemical reactions such as the involvement in nucleophilic processes, makes $Hemicellulose$ may react with specific substances or metal surfaces. In comparison to cellulose and lignin, hemicellulose is more reactive and kinetically less stable due to a reduced energy gap caused by the considerable dispersion of $HOMO$ electron density over particular regions. Additionally, the energy values denoted as E_{HOMO} for $HOMO$ and E_{LUMO} for $LUMO$, offer significant insights regarding the electron-accepting and -donating characteristics of molecules. It is essential to have an overview of these features in order to comprehend the interactions of the compounds with metal surfaces and their capacity to operate as corrosion inhibitors [170, 174, 175]. **Table IV.4**. provides the DFT global reactivity descriptors, with

χ and η values serving crucial functions in assessing the compounds' capacity to donate or accept electrons, which in turn affects their chemical reactivity [176]. Increased electronegativity values imply a greater capacity to attract electrons, whereas higher values of hardness suggest a greater resistance to activities that involve the transfer of electrons. However, σ measures the molecular polarizability and indicates the facilitation of charge transfer processes [147, 148, 177, 178]. Incorporating these reactivity descriptors along with the $HOMO$ and $LUMO$ energy values enhances our comprehension of the electronic properties of polysaccharide compounds, establishing a basis for improving their effectiveness as corrosion inhibitors.

Table IV.4: DFT global reactivity parameters.

	$E_{HOMO}(eV)$	$E_{LUMO}(eV)$	$E_g(eV)$	X	H	σ	ω
Cellulose	-6.658412	-0.313156	6.345257	3.4858	3.1726	0.1576	0.9575
Humicellulose	-5.266619	-4.866976	0.399643	5.0668	0.1998	2.5022	32.1192
Lignin	-6.062229	-2.631253	3.430976	4.3467	1.7155	0.2915	2.7535

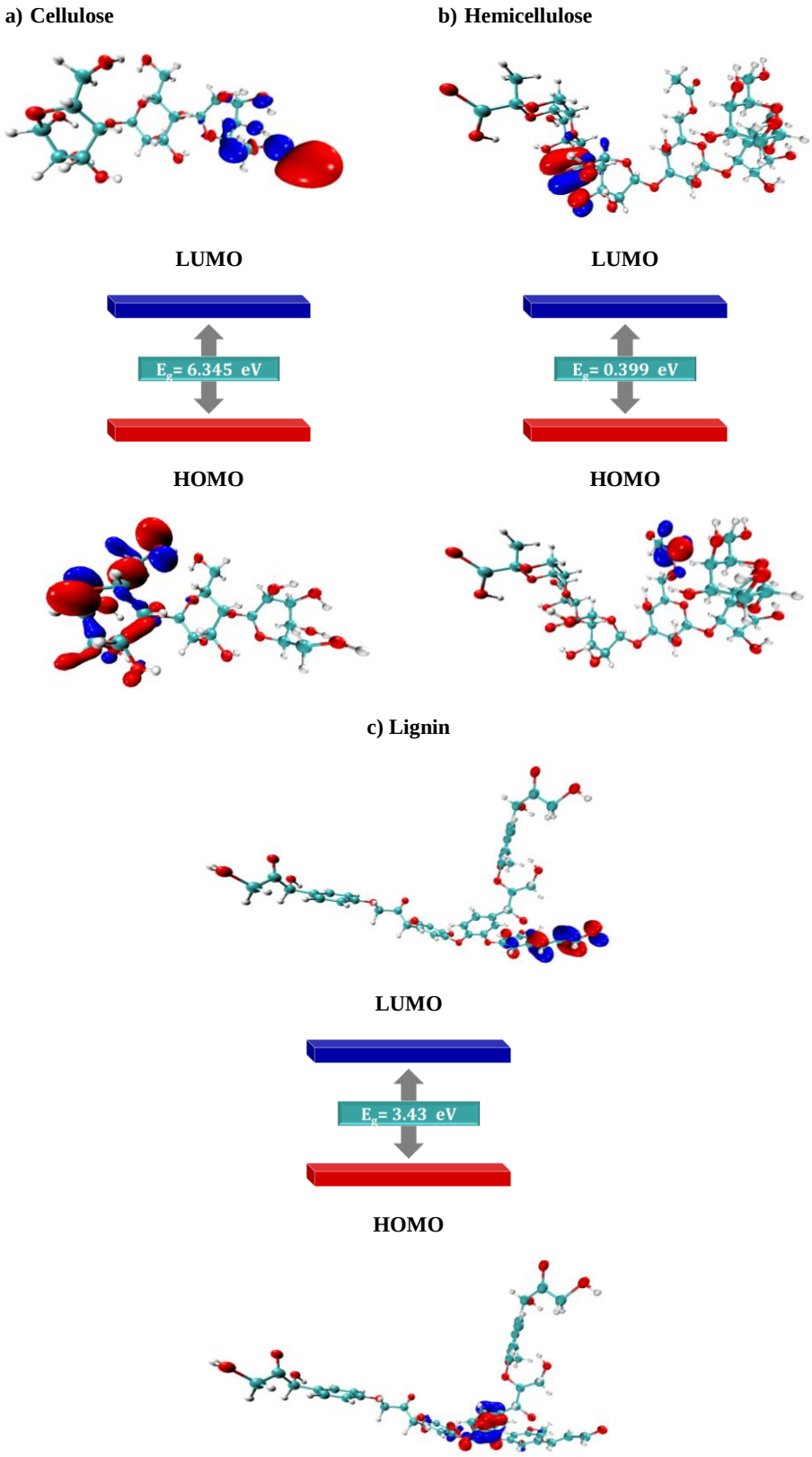

Figure IV.3: FMO surface plots for the molecules of polysaccharide with their corresponding energy gaps Eg (eV).

IV.1.1.2. *M*olecular *e*lectrostatic *p*otential (*MEP*) results

The "Molecular Electrostatic Potential" (*MEP*) serves as an effective instrument for examining surface charge and investigating the chemical and physical characteristics of a chemical system [179, 180]. The *MEP* surfaces of *cellulose*, *hemicellulose*, and *lignin*, the polysaccharide molecules under study, are shown in **Table IV.4**. The analysis of *MEP*, which is strongly linked to electron density, provides useful information into the nucleophilic or electrophilic sites within a structure. This approach provides a visual representation of the manner in which charges are distributed among chemical compounds. Additionally, it illustrates features that are associated with charges, such as reactivity and binding properties [148] [181-183]. Also, *MEP* maps provide a clear representation of the dimensions and configurations of molecules, aiding in the evaluation of possible interactions within the binding sites of target receptors. Understanding the structure-activity relationship is crucial for many reasons, but it is especially important for assessing the corrosion inhibitory capability of polysaccharide compounds.

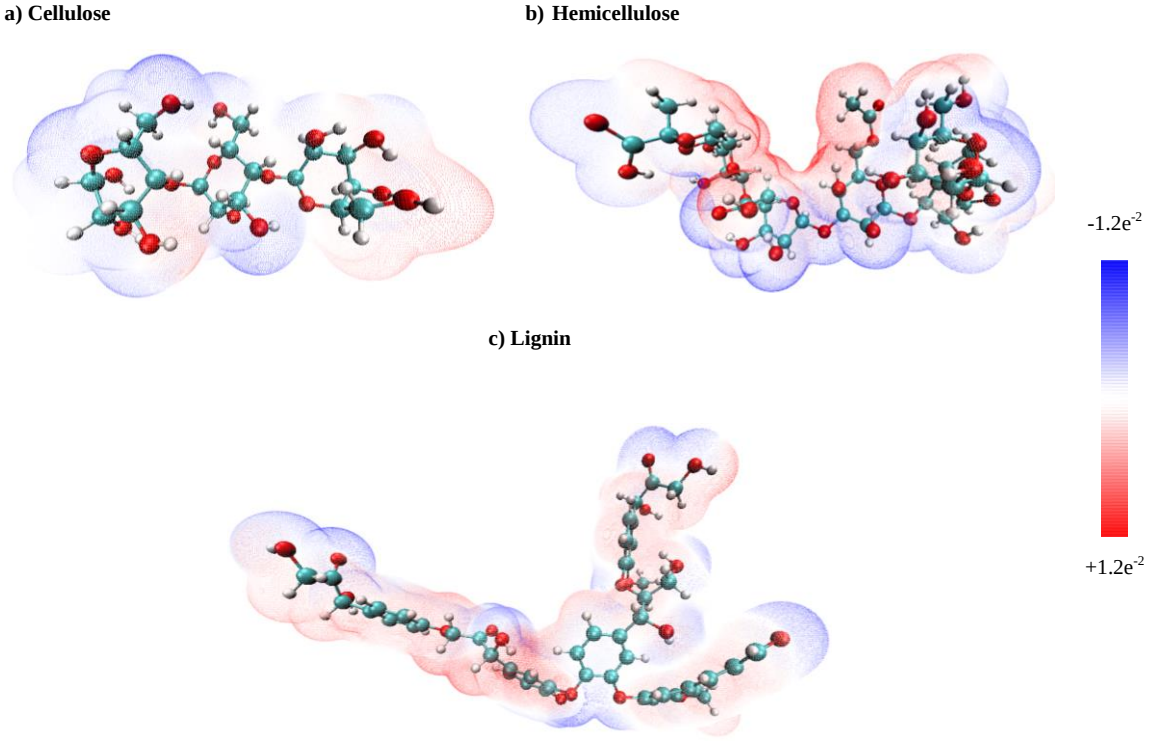

Figure IV.4: "Molecular electrostatic potential (*MEP*)" surface plots of polysaccharide compounds: a) *Cellulose*, b) *Hemicellulose*, and c) *Lignin*.

Upon examination of **Figure IV.4**, the MEP surfaces of the studied polysaccharides display significant red color spots in particular areas. The red color spots signify regions of elevated electron density, typically linked to locations exhibiting considerable nucleophilic potential. A good example of this is the fact that cellulose possesses a large nucleophilic potential due to the presence of $-OH$ groups in the glucose units. In chemical processes, these $-OH$ groups play an active role as nucleophilic centers, drawing electrophiles to them. Furthermore, blue spots on the MEP surfaces denote areas that are low in electrons, which could be electrophilic locations. The aromatic rings and $C = O$ groups exhibiting electrophilic properties are responsible on the presence of electrophilic centers in $cellulose$. $Hemicellulose$ has also $-OH$ groups, just like $cellulose$, which enhance its nucleophilic properties. The presence of functional groups including $-OH$ groups and $-C = O$ groups in $hemicellulose$, boosts the nucleophilic sites in its structure. Additionally, areas that are low in electrons in the MEP surfaces may be indicative of the existence of electrophilic sites. Functional groups in $hemicellulose$, such as carbonyls and aromatic rings, have the potential to give rise to electrophilic centers. At the same time, $lignin$ contains phenolic groups and methoxy groups ($-OCH_3$) that are essential for offering possible nucleophilic centers. The presence of these functional groups in $Lignin$ enhances its nucleophilic reactivity. In a similar manner, the blue regions observed in the MEP surfaces signify areas that are low in electrons, which imply the existence of potential electrophilic centers within lignin. Furthermore, the electrophilic sites identified in lignin may correlate might be linked with -C=O groups and the aromatic structures present in its chemical composition. As a result, the MEP analysis is crucial for enhancing our comprehension of the reactivity and binding properties of these polysaccharide compounds, thereby facilitating the development of effective and environmentally sustainable corrosion inhibitors.

IV.1.1.3. *N*on−*c*ovalent interaction*s* analysi*s*

IV.1.1.3.1. *R*educed *d*ensity *g*radient (*RDG*)

The NCI theory represents a sophisticated theoretical framework widely utilized for clarifying intermolecular interactions and defining weak forces in molecular structures. This advanced theory employs representation signs that are supported by density and relevant parameters, which are systematically color-coded according to a strength scale established by the RDG values at lower densities. The NCI method entails a computation of the electron density (ρ) and its multiplication by the sign of the second-highest eigenvalue (λ_2) derived

from the $Hessian\ matrix$ of the electron density at every point on the isosurface. This multiplication, denoted as $(\lambda_2) \times \rho$, acts as a significant measure to evaluate the nature of intermolecular forces, determining if they are attractive or repulsive interactions. If the multiplication $(\lambda_2) \times \rho$ has a negative value, that indicates basically attractive interactions, typically linked to the formation of hydrogen bonds, which are essential in molecular connections. But when$(\lambda_2) \times \rho$ has a positive value, it means that steric repulsion or interactions without bonds are happening and they are crucial to comprehend how molecules are preserving their whole structure while they interact with each other [184, 185].

Figure IV.5 presents the $NCI - RDG$ plots derived from the density examination of the examined polysaccharide molecules. The obtained plots reveal a variety of interactions between molecules among the polysaccharide compounds, including $cellulose, hemicellulose,$ and $lignin$. In this case, the colors blue, green, and red represent hydrogen bonding, Van $d$er Waals forces, and $s$teric repulsive interactions, respectively. The RDG is quantified within a range of $-0.035\ to\ 0.020\ a.u.$, and the sign of $(\lambda_2) \times \rho$ offers important clues towards the strength and characteristics of these interactions. Remarkably, the electron clouds in these areas exhibit a notable stability when interacting with suitable acceptors. Particularly The scatter graph shown in red clearly demonstrates the effectiveness of polysaccharide inhibitors in reducing steric-repellent interactions with the targeted metal surfaces. The presence of O atoms that are rich of electrons, along with phenolic or aromatic rings in the molecules of these corrosion inhibitory compounds, facilitates this accomplishment. The $NCI - RDG$ plots provide insightful visualizations that clarify the complex interactions between molecules present with the polysaccharide structure. This more profound comprehension of the inhibition mechanism improves our insight into how these chemicals properly safeguard metal surfaces against deterioation.

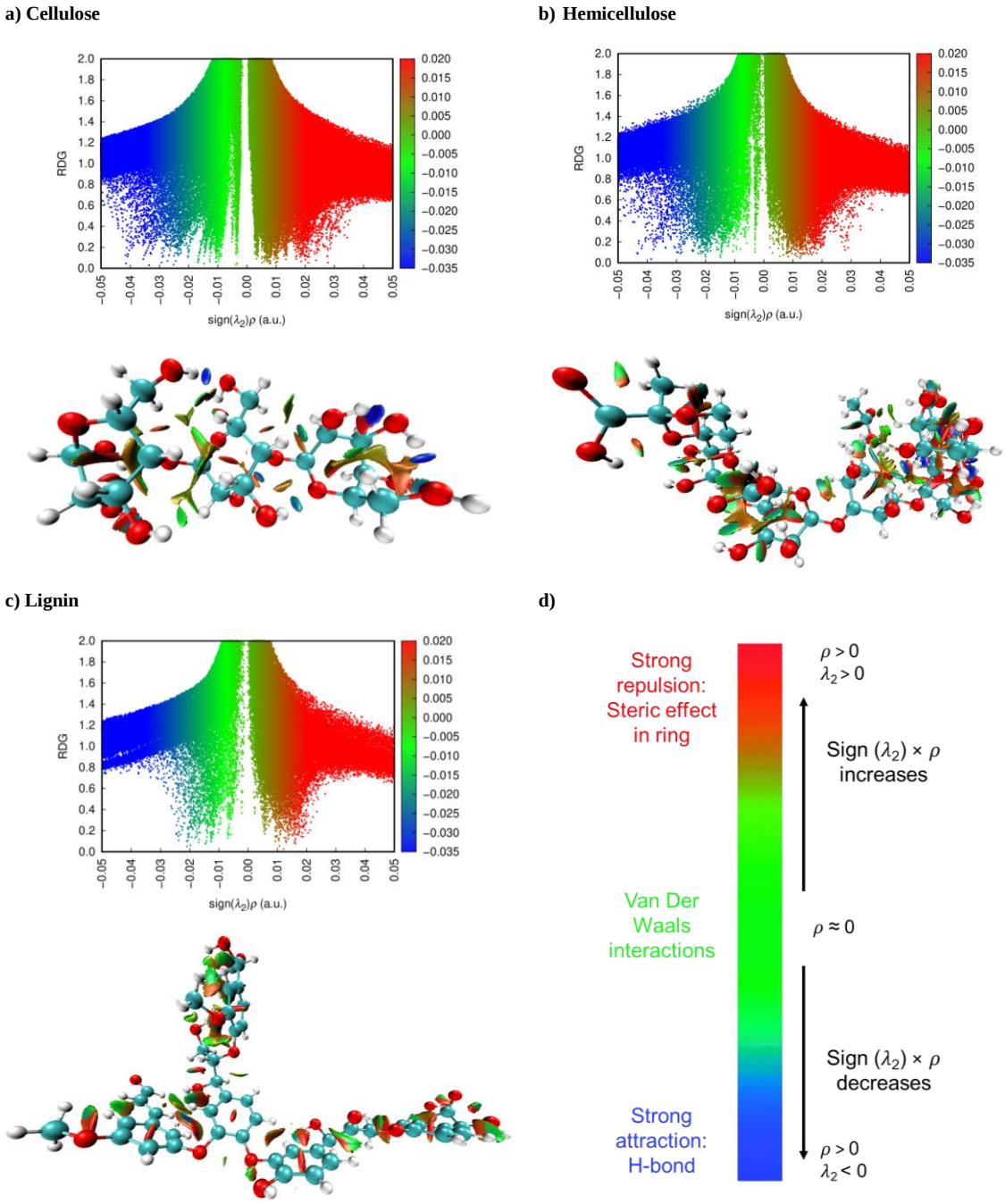

Figure IV.5: The RDG *s*catter *p*lots (upper) and NCI *p*lots (bottom) isosurface ($s = 0.5\ a.u.$) of polysaccharide components: a) $Cellulose$, b) $Humicellulose$, and c) $Lignin$, and d) color map and chemical explanation.

Additionally, thorough examination was carried out to analyze the interactions between the polysaccharide inhibitors ($cellulose$, $hemicellulose$, and $lignin$) and the Fe_{60} cluster surface. The optimized interfaces of $cellulose@Fe_{60}$, $hemicellulose@Fe_{60}$, and $lignin@Fe_{60}$ were analyzed to better understand the physical nature of bonding and associated interactions. This examination utilized "Turbomole 7.4 software" and included

NCI analysis with "Multiwfn software" [93]. **Figure IV.6** presents the RDG versus sign $(\lambda_2) \times \rho$ plots for these complexes, effectively distinguishing between attractive and repulsive interactions at the interfaces between the metal surface and the inhibitors. The presence of the green zone at the compound and the metal surface interfaces highlights the important role of weak Van Der Waals interactions. The interactions between them significantly contribute to the reduction of steric-repellent forces at the interfaces of $cellulose$, $hemicellulose$, and $lignin$ with the studied mild steel surfaces. The existence of particular functional groups, including $phenolic\ groups$, $carboxy$ or $methoxy\ groups$, characterized by a high density of electrons in the chemical structure of corrosion inhibitory compounds, particularly $oxygen\ atoms$, enhances the generated interaction between them. Van Der Waals interactions play a crucial role in the corrosion control process, as indicated by the presence of green zones that are influenced by the amount of coverage and protonation levels of $cellulose$, $hemicellulose$, and $lignin$. The cooperation of these elements significantly improves the efficacy of corrosion control [186]. A variety of intramolecular and intermolecular interactions, including attractive and repulsive forces, can be visualized through the use of coloration schemes. The NCI analyses offered important knowledge regarding the important interactions between the Fe_{60} surface and the adsorbed inhibitors within the corrosion control mechanism, as evidenced by the zones in green depicted in **Figure IV.6**. In group of polysaccharides examined, $hemicellulose$ exhibits notable electron donor and acceptor properties, which promote the development of a robust adsorption barrier and improve interactions with the mild steel surface [182, 187, 188]. The conclusions are consistent with previous findings regarding FMO and Molecular MEP analyses, which emphasized the reactivity and bonding properties of $hemicellulose$. The advantageous characteristics of $hemicellulose$ lead to its higher efficiency in corrosion inhibition when compared to $cellulose$ or $lignin$. This points out the important role of $hemicellulose$ and demonstrates the necessity for additional investigation and study on $A.Arenaria$ to effectively extract and utilize the benefits of $hemicellulose$.

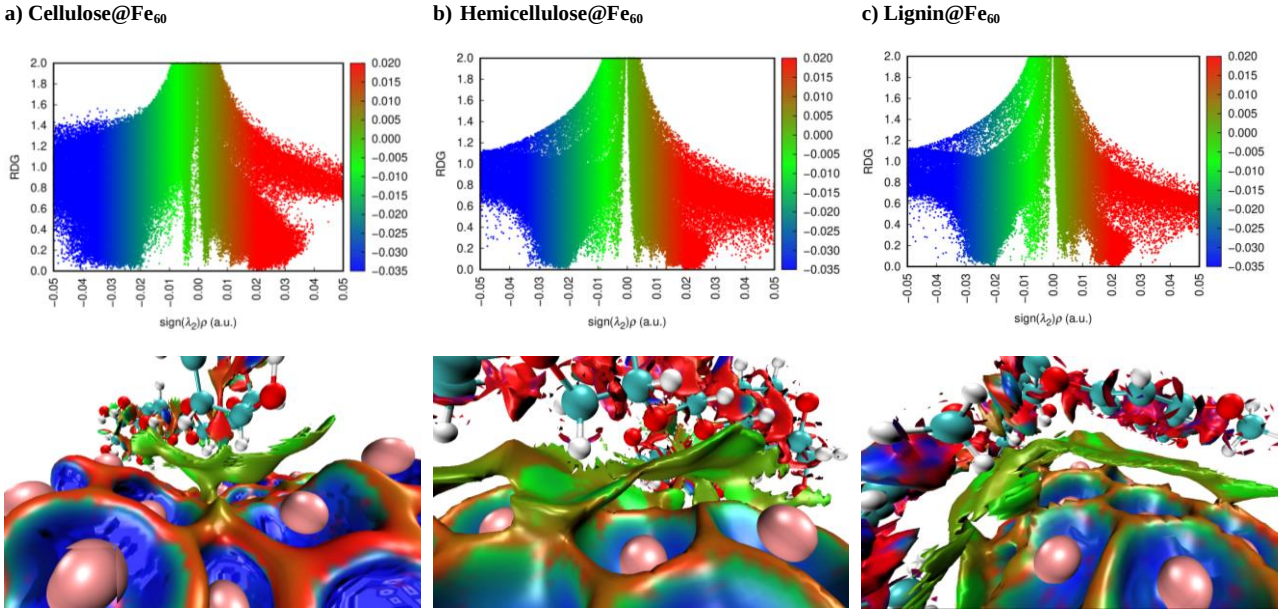

Figure IV.6: The RDG scatter plots (upper) and NCI plots (bottom) isosurface (s = 0.5 a.u.) of a) Cellulose@Fe60, b) Humicellulose@Fe60, and c) Lignin@Fe60 isosurfaces (IGM = 0.01 a.u.). The color of the isosurface depends on the sign values (λ2) ρ, from − 0.05 to 0.05 a.u.

IV.1.1.3.2. *Q*uantum *T*heory of *A*tom In molecule−*I*ndependent *G*radient *M*odel *F*unction (*IGM*) analysis

The $QTAIM$ theory, introduced by "Bader", has been extensively utilized to clarify various interactions in molecular systems and to examine bonding interactions through real space functions, including "electron density" at Bond Britical Points ($BCPs$) [189, 190]. $QTAIM$ serves as an essential method for assessing the strength of interactions between electron-acceptor and electron-donor molecules, thereby providing significant utility for experimental scientists. This study employs the $QTAIM$ approach to examine intermolecular and intramolecular interactions, with a particular emphasis on the donor-acceptor sites within the molecular frameworks. Particularly, Our objective was to measure and define the interactions of hydrogen bonds through topological parameters derived from specific $BCPs$, as illustrated in **Figure IV.7**. The parameters consist of electron density ($\rho(r)$), the Laplacian of electron density ($\nabla^2\rho(r)$), and the ratio $|V(r)|/G(r)$ (with $G(r)$ indicating "kinetic energy density" and $V(r)$ signifying "potential energy density"), in addition to "the interaction energy density $H(r)$".

Table IV.5. displays the computed topographic features, offering a detailed examination of the nature and how strong the hydrogen bonding interactions are between the studied polysaccharides and the targeted surface. Furthermore, to provide a visual representation of noncovalent interactions in real space, IGM have been integrated, as shown in **Figure IV.8**. This innovative representative technique accurately illustrates the interactions that occur between the studied polysaccharides and the mild steel surface, specifically focusing on hydrogen bonding and Van Der Waals forces. The δg values in the IGM analysis clearly define the areas of interaction.

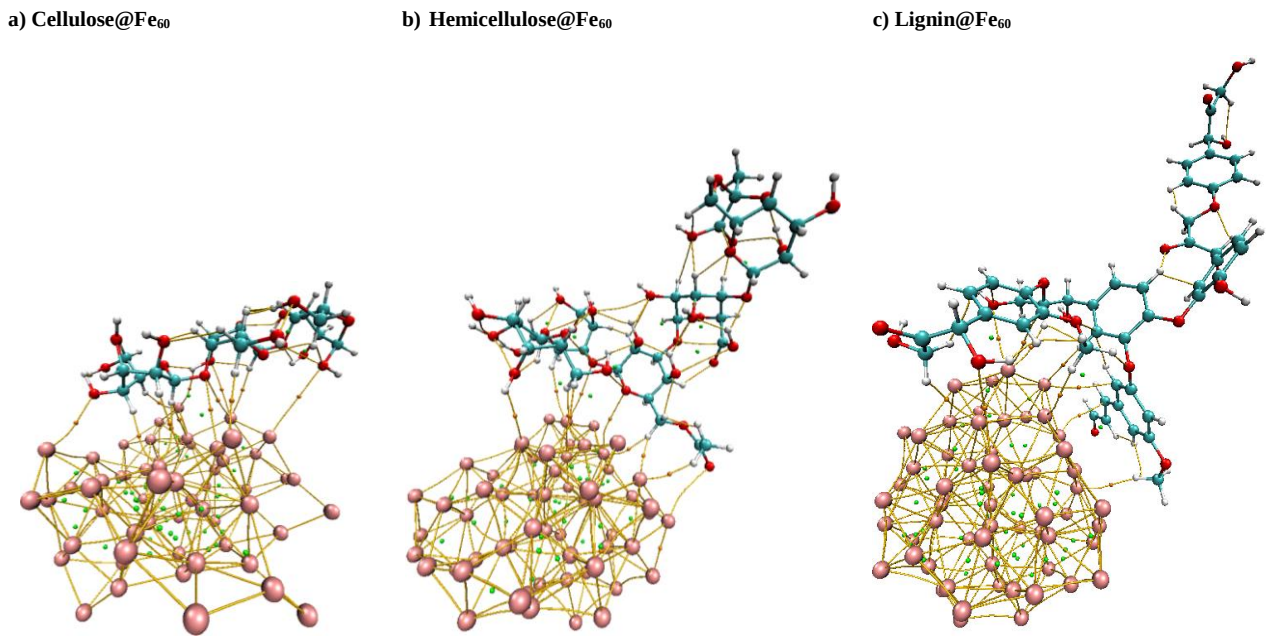

Figure IV.7: $QTAIM$ molecular graphs of a) $Cellulose@Fe_{60}$, b) $Humicellulose@Fe_{60}$, and c) $Lignin@Fe_{60}$ complexes.

Based on the measured parameters it was found that all $Cellulose@Fe_{60}$, $Humicellulose@Fe_{60}$, and $Lignin@Fe_{60}$ complexes exhibited positive $\rho(r)$ values. Additionally, the positive values of $\Delta^2\rho(r)$ suggest the presence of hydrogen bond interactions involving $O-Fe$ and $H-Fe$ pairs, respectively. For instance, At the $BCPs$ of $347, 427,$ and 609 in $Lignin@Fe_{60}$, positive $\Delta^2\rho(r)$ and negative $H(r)$ values were observed, indicating that the majority of atomic interactions within the substances display a partially covalent character. The above statement is proven by the notion that the capacity to combine electrons, $V(r)$, is less than their tendency to diffuse, $G(r)$, as demonstrated by $|V(r)|/G(r) < 1$.

Furthermore, $E\,HB < 0$ indicates weak hydrogen bonding [39] for the bonds $97(O) \ldots 26(Fe)$ and $114(H) \ldots 26(Fe)$ in $cellulose$ and $hemicellulose$, respectively, suggesting that the majority of atomic interactions within the substances display a non-covalent character (physical interaction) [191]. Consequently, these results indicate that the interactions within $Cellulose@Fe_{60}$, $Humicellulose@Fe_{60}$, and $Lignin@Fe_{60}$ complexes are characterized by hydrogen bonding, with certain interactions displaying a partial covalent nature. This comprehension offers significant perspectives on the characteristics of bonding interactions within these systems and clarifies their potential effectiveness as corrosion inhibitors for Fe_{60} surfaces.

Table IV.5: Topological characteristics of the interaction sites (in $a.u.$) at selected $BCPs$ in $Cellulose@Fe_{60}$, $Humicellulose@Fe_{60}$, and $Lignin@Fe_{60}$ complexes.

BCP	$X-Y$	$\rho(r)$	$\nabla^2\rho(r)$	$V(r)$	$G(r)$	$\lvert V(r)\rvert / G(r)$	$H(r)$
Cellulose@Fe$_{60}$							
170	103(O) − 53(Fe)	0.00467	0.01324	-0.00223	0.00277	-0.80505	0.00054
194	107(H) − 38(Fe)	0.00526	0.01104	-0.00158	0.00217	-0.72811	0.00059
199	117(H) − 38(Fe)	0.00240	0.00540	-0.00056	0.00095	-0.58947	0.00040
235	97(O) − 26(Fe)	0.00413	0.01248	0.00266	0.00266	**1.00000**	0.00046
238	108(H) − 35(Fe)	0.00465	0.00862	-0.00133	0.00174	-0.76437	0.00041
250	111(H) − 59(Fe)	0.00414	0.00821	-0.00129	0.00167	-0.77246	0.00038
252	110(H) − 35(Fe)	0.00358	0.00672	-0.00083	0.00125	-0.66400	0.00043
255	90(O) − 26(Fe)	0.00195	0.01114	-0.00181	0.00230	-0.78696	0.00049
261	111(H) − 35(Fe)	0.00364	0.00636	-0.00098	0.00129	-0.75969	0.00030
265	114(H) − 26(Fe)	0.00494	0.01201	-0.00203	0.00252	-0.80556	0.00048
275	90(O) − 39(Fe)	0.00286	0.00754	-0.00119	0.00154	-0.77273	0.00035
361	69(O) − 11(Fe)	0.00035	0.00114	-0.00008	0.00018	-0.44444	0.00010
280	119(H) − 41(Fe)	0.00492	0.01062	-0.00140	0.00203	-0.68966	0.00063
Humicellulose@Fe$_{60}$							
235	97(O) − 26(Fe)	0.00413	0.01248	-0.00220	0.00266	-0.82707	0.00046
238	108(H) − 35(Fe)	0.00465	0.00862	-0.00133	0.00174	-0.76437	0.00041

250	111(H) − 59(Fe)	0.00414	0.00821	-0.00129	0.00167	-0.77246	0.00038
252	110(H) − 35(Fe)	0.00358	0.00672	-0.00083	0.00125	-0.66400	0.00043
255	90(O) − 26(Fe)	0.00390	0.01114	-0.00181	0.00230	-0.78696	0.00049
261	111(H) − 35(Fe)	0.00364	0.00636	-0.00098	0.00129	-0.75969	0.00030
265	114(H) − 26(Fe)	0.00494	0.01201	0.00252	0.00252	**1.00000**	0.00048
275	90(O) − 39(Fe)	0.00286	0.00754	-0.00119	0.00154	-0.77273	0.00035
280	119(H) − 41(Fe)	0.00492	0.01062	-0.00140	0.00203	-0.68966	0.00063
361	69(O) − 11(Fe)	0.00035	0.00114	-0.00008	0.00018	-0.44444	0.00010
$\boldsymbol{Lignin@Fe_{60}}$							
184	125(O) − 6(Fe)	0.00141	0.00321	-0.00033	0.00057	-0.57895	0.00023
211	168(H) − 45(Fe)	0.00482	0.00808	-0.00160	0.00181	-0.88398	0.00021
246	164(H) − 54(Fe)	0.00345	0.00639	-0.00107	0.00133	-0.80451	0.00026
255	113(C) − 16(Fe)	0.00326	0.00472	-0.00110	0.00114	-0.96491	0.00004
332	16(Fe) − 110(O)	0.00317	0.00729	-0.00125	0.00153	-0.81699	0.00029
347	16(Fe) − 157(H)	0.00603	0.00882	-0.00226	0.00223	-1.01345	-0.00003
427	143(H) − 32(Fe)	0.00554	0.00747	-0.00197	0.00192	-1.02604	-0.00005
490	32(Fe) − 99(C)	0.00392	0.00519	-0.00106	0.00118	-0.89831	0.00012
602	40(Fe) − 149(H)	0.00397	0.00663	-0.00125	0.00145	-0.86207	0.00020
609	36(Fe) − 102(C)	0.00475	0.00508	-0.00154	0.00140	-1.10000	-0.00013

a) Cellulose@Fe_{60} **b) Humicellulose@Fe_{60}**

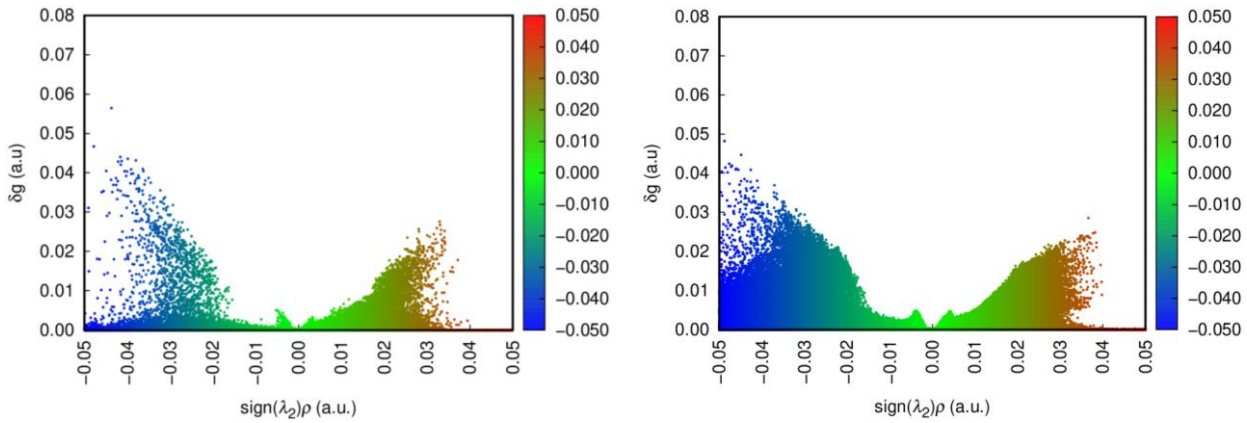

c) Lignin@Fe_{60}

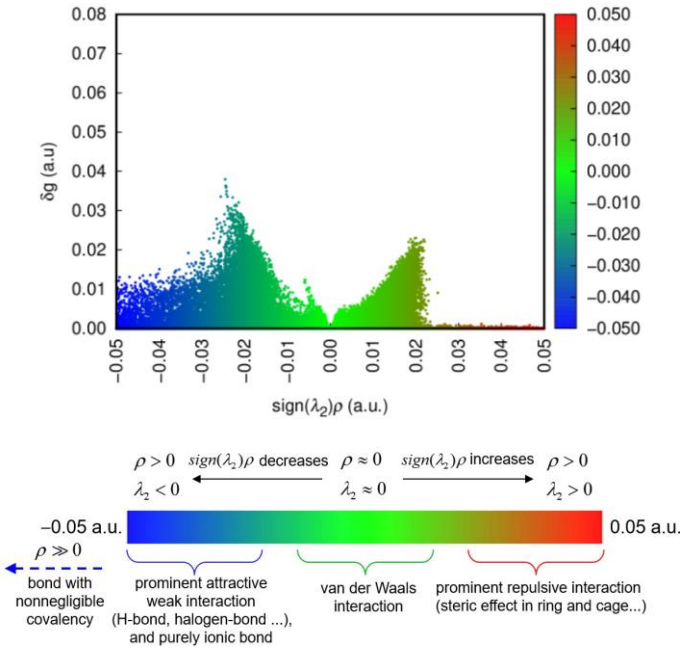

Figure IV.8: The IGM scatter plots of of a) $Cellulose@Fe_{60}$, b) $Humicellulose@Fe_{60}$, and c) $Lignin@Fe_{60}$ complexes. The green zone for Van Der Waals phenomenon, the blue region for Hydrogen bonds.

IV.1.2. Suggested mechanism for the corrosion inhibitor's work

The mechanism of *Ammophila Arenaria* extract as a corrosion inhibitor, including its primary compounds; *cellulose*, *hemicellulose* and *lignin* on mild steel in a $1M\ HCl$ medium was rigorously assessed through an integration of both experimental and theoretical studies. The theoretical calculations, which include interaction energies, RDG, IGM, and AIM analysis, were supported and confirmed by the experimental data regarding inhibiting corrosion of mild steel by the inclusion of the named compounds in the acidic environment.

Figure IV.9 presents an overview that highlights the corresponding mechanism, utilizing electrochemical studies and morphological analysis to enhance comprehension of the process. In the anodic part of the electrochemical process occurring at the mild steel surface, oxidation of iron atoms takes place, resulting in the formation of iron ions and the buildup of positive charges on the metallic surface, which catches the negative free chloride ions (Cl^-) that exist in the solution of hydrochloric acid [170, 192, 193]. The adsorption ptocess is significantly affected by the characteristics of the metal, the charges present on the surface, and the chemical structure of the inhibitors [87, 194, 195]. The major components of $Ammophila\ Arenaria$ extract, namely $cellulose, hemicellulose,$ and $lignin$ [78], are crucial in determining its corrosion inhibition characteristics. The existence of electron-rich aromatic components and heteroatoms within these polysaccharides facilitates chemisorption, thereby creating a more robust interaction between the studied inhibitors and the metallic surface. Coordination bonds arise from the interaction between the $\pi - electrons$ and lone pairs of electrons in these areas and the vacant $d\ orbitals$ of iron atoms present on the surface of metal. In order to ensure that the corrosion inhibition benefits are enduring, the process of chemisorption improves the durability and adhesion of the protective layer. The processes of physisorption and chemisorption involving the $Ammophila\ Arenaria$ extract operate together to form a hydrophobic adsorption film, which effectively shields reactive sites and restricts the contact with the destructive substances [196, 197]. The existence of rhamnose sugar moiety significantly improves the dissolution and long-term stability of polysaccharides in aqueous fluids, which plays a crucial role in enhancing corrosion inhibition when electrolytic solutions are present. The $Ammophila\ Arenaria$ extract employs multiple adsorption processes that involve polar groups and atoms in its structure, successfully displacing water molecules in contact with the surface of mild steel. The generation of a hydrophobic adsorption layers occurs, which effectively blocks reactive sites, isolates H_2O molecules and Cl^- ions, and limits the development of H precipitation processes and the dissolution of the steel. As a result, our thorough examination reveals the significant corrosion inhibition properties of $Ammophila\ Arenaria$ extract, primarily due to the presence of its $polysaccharide$ components. The presence of $-OH$ groups, $O - CH_3$, and aromatic rings is crucial in the processes of adsorption and chemisorption, whereas the $C = O$ moiety contributes to the enduring and dissolution of the extract in aqueous mediums. The findings indicate the potential of $Ammophila\ Arenaria$ extract as a sustainable and effective inhibitor for mild steel corrosion.

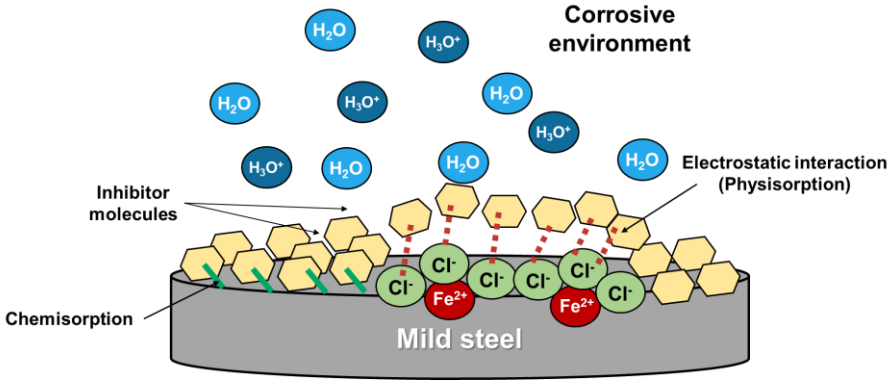

Figure IV.9: Suggested schematic diagram of the mechanism of the studied polysaccharide inhibitors towards steel corrosion inhibition.

General Conclusion

General Conclusion

The study highlighted the protective effect of $Artemisia\ Herba\ Alba$ (AHA) and $Ammophila\ Arenaria$ (AA) on mild steel corrosion in acidic $1M\ HCl$ as an ecofriendly corrosion inhibitor.

Traditional extraction methods were used according to the targeted compounds for each plant. Fourier-transform infrared spectroscopy $(FTIR)$ was applied to investigate structural properties of the plant extracts.

The investigations were made experimentally through the gravimetric measurements, Potentiodynamic $p$olarization (PDP) and Electrochemical Impedance Spectroscopy (EIS) methods.

In order to analyze the metal surface we performed several analyses such as Scanning Electron Microscopy (SEM) with $X-ray$ Photoelectron Spectroscopy (XPS) and $X-ray$ Diffraction (XRD) were performed. Finally, quantum chemistry simulations show that the tested plant extracts are effective corrosion inhibitors.

AHA and AA were selected on the basis of chemical and ecological criteria, after detailed study in previous studies. The aim was to provide a contribution to the valorization of the local natural resources and also a useful addition to the literature.

It has been clearly demonstrated that the inhibition efficiency increased with the increasing of the inhibitors concentrations according to the electrochemical study, reaching an optimal value at $700\ ppm$ (AA) and $900\ ppm$ (AHA). Both inhibitors may be classified as a mixed-type inhibitor.

The Langmuir isotherm controls the adsorption of AHA an AA molecules on the mild steel surface.

Surface analysis done using SEM and AFM methods confirm the protective properties of the two inhibitor molecules attach to steel forming a protective barrier that inhibits steel corrosion in $1M\ HCl$.

The quantum chemistry calculations indicated that the Dicaffeoylquinic acids in AHA extract and $cellulose, hemicellulose,$ and $lignin$ in AA extract are excellent corrosion

inhibitors for mild steel in $1M\ HCl$ and this finding is in a good correlation with the experimental results.

Future Work:

As an outcome of this work, other future studies became evident and are cited below.

- Green extraction methods need to be developed to obtain plant extracts such as Accelerated Solvent Extraction (ASE) and microwave assisted-extraction (MAE).

- The extracts must be characterized and separated to determine if the compounds are acting alone, synergistically, or additively to impact (negatively and positively) corrosion inhibitory effects.

- The demonstrated results on the inhibition efficiency of the extracts are interesting, exceptional and encouraging for testing on other challenging metals such as copper, and in other aggressive environments.

References

References

1. Sastri, V.S., *Challenges in corrosion: costs, causes, consequences, and control*. 2015: John Wiley & Sons.
2. Harsimran, S., K. Santosh, and K. Rakesh, *Overview of corrosion and its control: A critical review.* Proc. Eng. Sci, 2021. **3**(1): p. 13-24.
3. Verink, E., *Economics of corrosion.* Uhlig's Corrosion Handbook, 2011. **51**: p. 21.
4. Sánchez, M., et al., *Iron chemistry at the service of life.* IUBMB life, 2017. **69**(6): p. 382-388.
5. Wei, H., et al., *Green inhibitors for steel corrosion in acidic environment: state of art.* Materials Today Sustainability, 2020. **10**: p. 100044.
6. Abdallah, M., et al., *Some natural aqueous extracts of plants as green inhibitor for carbon steel corrosion in 0.5 M sulfuric acid.* Green Chemistry Letters and Reviews, 2018. **11**(3): p. 189-196.
7. Elabbasy, H. and A. Fouda, *Olive leaf as green corrosion inhibitor for C-steel in Sulfamic acid solution.* green chemistry letters and reviews, 2019. **12**(3): p. 332-342.
8. Belakhdar, A., et al., *Computational and experimental studies on the efficiency of Rosmarinus officinalis polyphenols as green corrosion inhibitors for XC48 steel in acidic medium.* Colloids and Surfaces A: Physicochemical and Engineering Aspects, 2020. **606**: p. 125458.
9. Pourbaix, M., *Applications of electrochemistry in corrosion science and in practice.* Corrosion Science, 1974. **14**(1): p. 25-82.
10. Esmailzadeh, S., M. Aliofkhazraei, and H. Sarlak, *Interpretation of cyclic potentiodynamic polarization test results for study of corrosion behavior of metals: a review.* Protection of metals and physical chemistry of surfaces, 2018. **54**: p. 976-989.
11. Hernández, H.H., et al., *Electrochemical impedance spectroscopy (EIS): A review study of basic aspects of the corrosion mechanism applied to steels.* Electrochemical impedance spectroscopy, 2020: p. 137-144.
12. Feliu Jr, S., *Electrochemical impedance spectroscopy for the measurement of the corrosion rate of magnesium alloys: Brief review and challenges.* Metals, 2020. **10**(6): p. 775.
13. Verma, D.K., et al., *Computational modeling: theoretical predictive tools for designing of potential organic corrosion inhibitors.* Journal of Molecular Structure, 2021. **1236**: p. 130294.
14. Roberge, P.R., *Corrosion engineering: principles and practice.* (No Title), 2008.
15. Ahamed, M.I., M. Luqman, and T. Altalhi. *Sustainable Corrosion Inhibitors*. 2021. Materials Research Forum LLC.
16. Landolt, D., *Corrosion and surface chemistry of metals*. 2007: EPFL press.
17. G193-12d, N.A., *Standard terminology and acronyms relating to corrosion.* 2012.
18. Fontana, M., et al., *All about corrosion science and engineering Header Right By Mariano Iannuzzi.*
19. Heusler, K., D. Landolt, and S. Trasatti, *Electrochemical corrosion nomenclature.* Journal of Electroanalytical Chemistry and Interfacial Electrochemistry, 1989. **274**(1-2): p. 345-348.
20. McCafferty, E., *Introduction to corrosion science*. 2010: Springer Science & Business Media.
21. Bensaada, S., *Phenomenon of corrosion and the industrial safety.* LARHYSS Journal P-ISSN 1112-3680/E-ISSN 2521-9782, 2013(15).

22. Levy, A., *Erosion and erosion-corrosion of metals.* Corrosion, 1995. **51**(11): p. 872-883.
23. Davis, J.R., *Corrosion: Understanding the basics*. 2000: Asm International.
24. Sieradzki, K. and R. Newman, *Stress-corrosion cracking.* Journal of physics and chemistry of solids, 1987. **48**(11): p. 1101-1113.
25. Crolet, J.-L., *Mechanisms of Uniform Corrosion Under a Corrosion Deposit.* Metaux-Corros.-Ind., 1988. **63**(757): p. 279-302.
26. Bénard, J., et al., *Métallurgie Générale, Masson et Cie.* Editeurs, Paris VI, 1969: p. 49-52.
27. Fiaud, C., *Inhibiteur de corrosion, Université Pierre & Marie curie, ENSC, Paris.* Techniques de l‟ ingénieur, Traité corrosion–Vieillissement, Vol. Cor, 2006. **1005**.
28. Koch, G.H., et al., *Corrosion cost and preventive strategies in the United States*. 2002, United States. Federal Highway Administration.
29. Sastri, V.S., *Green corrosion inhibitors: theory and practice*. 2012: John Wiley & Sons.
30. Shehata, O.S., L.A. Korshed, and A. Attia, *Green corrosion inhibitors, past, present, and future.* Corrosion inhibitors, principles and recent applications, 2018. **121**.
31. Emran, K.M., S.M. Ali, and H.A. Al Lehaibi, *Green methods for corrosion control.* Corrosion inhibitors, principles and recent applications, 2018: p. 61-78.
32. Sharma, S.K., A. Mudhoo, and E. Khamis, *Adsorption studies, modeling, and use of green inhibitors in corrosion inhibition: an overview of recent research.* Green corrosion chemistry and engineering, 2012.
33. Brasher, D.M. and A. Mercer, *Comparative study of factors influencing the action of corrosion inhibitors for mild steel in neutral solution: I. Sodium benzoate.* British Corrosion Journal, 1968. **3**(3): p. 120-129.
34. Xu, C. and W. Gao, *Pilling-Bedworth ratio for oxidation of alloys.* Material Research Innovations, 2000. **3**: p. 231-235.
35. West, J.M., *Basic corrosion and oxidation.* 1986.
36. Acemioğlu, B., *Removal of Fe (II) ions from aqueous solution by Calabrian pine bark wastes.* Bioresource Technology, 2004. **93**(1): p. 99-102.
37. Acemioglu, B. and M.H. Alma, *Equilibrium Studies on Adsorption of Cu(II) from Aqueous Solution onto Cellulose.* Journal of Colloid and Interface Science, 2001. **243**(1): p. 81-84.
38. Akinbulumo, O.A., O.J. Odejobi, and E.L. Odekanle, *Thermodynamics and adsorption study of the corrosion inhibition of mild steel by Euphorbia heterophylla L. extract in 1.5 M HCl.* Results in Materials, 2020. **5**: p. 100074.
39. Donohue, M.D. and G.L. Aranovich, *Classification of Gibbs adsorption isotherms.* Advances in colloid and interface science, 1998. **76**: p. 137-152.
40. Block, J., *JM Thomas and WJ Thomas: Introduction to the Principles of Heterogeneous Catalysis. Academic Press London, New York 1967. 544 Seiten, 166 Abbildungen. Preis: 120 s*. 1968, Wiley Online Library.
41. Mu, G., X. Li, and G. Liu, *Synergistic inhibition between tween 60 and NaCl on the corrosion of cold rolled steel in 0.5 M sulfuric acid.* Corrosion Science, 2005. **47**(8): p. 1932-1952.
42. Khaled, K., *Studies of iron corrosion inhibition using chemical, electrochemical and computer simulation techniques.* Electrochimica Acta, 2010. **55**(22): p. 6523-6532.
43. McCafferty, E. and E. McCafferty, *Thermodynamics of corrosion: Pourbaix diagrams.* Introduction to corrosion science, 2010: p. 95-117.
44. Buchanan, R. and E. Stansbury, *Electrochemical corrosion*, in *Handbook of environmental degradation of materials*. 2005, Elsevier. p. 81-103.

45. Martínez, M.J.A., et al., *The Artemisia L. genus: a review of bioactive sesquiterpene lactones.* Studies in natural products chemistry, 2012. **37**: p. 43-65.
46. Bouyanzer, A. and B. Hammouti, *A study of anti-corrosive effects of Artemisia oil on steel.* Pigment & resin technology, 2004. **33**(5): p. 287-292.
47. Ouachikh, O., et al., *Application of essential oil of Artemisia herba alba as green corrosion inhibitor for steel in 0.5 MH 2 SO 4.* Surface Review and Letters, 2009. **16**(01): p. 49-54.
48. Boumhara, K., et al., *Artemisia Mesatlantica essential oil as green inhibitor for carbon steel corrosion in 1 M HCl solution: Electrochemical and XPS investigations.* Journal of Industrial and Engineering Chemistry, 2015. **29**: p. 146-155.
49. Echihi, S., et al., *Performance of methanolic extract of artemisia herba alba as a potential green inhibitor on corrosion behavior of mild steel in hydrochloric acid solution.* Biointerface Res. Appl. Chem, 2021. **11**(6): p. 14751-14763.
50. Ben Salem, F., et al. *Variation of Biomass Production and Essential Oil Yield of Artemisia herba-alba Asso. in Relation to Planting Density in Southern Tunisia*. in *International Symposium on Medicinal and Aromatic Plants-SIPAM2009 853*. 2009.
51. Nigam, M., et al., *Bioactive compounds and health benefits of Artemisia species.* Natural product communications, 2019. **14**(7): p. 1934578X19850354.
52. Gacem, M.A., et al., *Phytochemistry, Toxicity and Pharmacology of Pistacia lentiscus, Artemisia herba-alba and Citrullus colocynthis.* Sustainable Agriculture Reviews 39, 2020: p. 57-93.
53. BOUDJELAL, A., *Extraction, identification et détermination des activités biologiques de quelques extraits actifs de plantes spontanées (Ajuga iva, Artemisia herba alba et Marrubium vulgare) de la région de M'Sila, Algérie*. 2013, Université de Annaba-Badji Mokhtar.
54. BENMAMMAR Razika, L.N., *Contribution à l'étude physico-chimique, phytochimique et évaluation des propriétés antioxydantes d'Artemisia Herba alba*. 2021.
55. SEDIRA, F. and L. RAMDANI, *Activité répulsive et larvicide de l'huile essentielle d'Artemisia herba alba sur Plodia interpunctella et Ephestia kuehniella, deux espèces ravageurs des denrées stockées*. 2018, Universite laarbi tebessi tebessa.
56. Liu, Y., et al., *Effect of ginger extract as green inhibitor on chloride-induced corrosion of carbon steel in simulated concrete pore solutions.* Journal of cleaner production, 2019. **214**: p. 298-307.
57. Mohammadi, Z. and M. Rahsepar, *The use of green Bistorta Officinalis extract for effective inhibition of corrosion and scale formation problems in cooling water system.* Journal of Alloys and Compounds, 2019. **770**: p. 669-678.
58. Popova, A., et al., *AC and DC study of the temperature effect on mild steel corrosion in acid media in the presence of benzimidazole derivatives.* Corrosion science, 2003. **45**(1): p. 33-58.
59. de Souza, F.S. and A. Spinelli, *Caffeic acid as a green corrosion inhibitor for mild steel.* Corrosion science, 2009. **51**(3): p. 642-649.
60. Singh, P., V. Srivastava, and M. Quraishi, *Novel quinoline derivatives as green corrosion inhibitors for mild steel in acidic medium: electrochemical, SEM, AFM, and XPS studies.* Journal of Molecular Liquids, 2016. **216**: p. 164-173.
61. Basiuk, V.A. and L.V. Henao-Holguín, *Effects of orbital cutoff in DMol3 DFT calculations: a case study of meso-tetraphenylporphine–C60 complex.* Journal of Computational and Theoretical Nanoscience, 2013. **10**(5): p. 1266-1272.

62. Kresse, G. and J. Hafner, *Norm-conserving and ultrasoft pseudopotentials for first-row and transition elements.* Journal of Physics: Condensed Matter, 1994. **6**(40): p. 8245.
63. Luo, Y., et al., *Effects of global orbital cutoff value and numerical basis set size on accuracies of theoretical atomization energies.* Theoretical Chemistry Accounts, 2014. **133**: p. 1-11.
64. Pearson, R.G., *The electronic chemical potential and chemical hardness.* Journal of Molecular Structure: THEOCHEM, 1992. **255**: p. 261-270.
65. Klamt, A. and G. Schüürmann, *COSMO: a new approach to dielectric screening in solvents with explicit expressions for the screening energy and its gradient.* Journal of the Chemical Society, Perkin Transactions 2, 1993(5): p. 799-805.
66. Frenkel, D. and B. Smit, *Understanding molecular simulation: from algorithms to applications*. 2023: Elsevier.
67. Nakhli, A., et al., *Molecular insights through computational modeling of methylene blue adsorption onto low-cost adsorbents derived from natural materials: A multi-model's approach.* Computers & Chemical Engineering, 2020. **140**: p. 106965.
68. Sun, H., *COMPASS: an ab initio force-field optimized for condensed-phase applications overview with details on alkane and benzene compounds.* The Journal of Physical Chemistry B, 1998. **102**(38): p. 7338-7364.
69. Mayo, S.L., B.D. Olafson, and W.A. Goddard, *DREIDING: a generic force field for molecular simulations.* Journal of Physical chemistry, 1990. **94**(26): p. 8897-8909.
70. Kamel-Eddine, B., *Vegetation and landscape dynamics of the Guerbes-Benazouz dune cordon in Skikda, Algeria.* Ukrainian Journal of Ecology, 2022. **12**(3): p. 36-45.
71. Jebali, Z., et al., *Cationic cellulose nanofibrils as a green support of palladium nanoparticles: catalyst evaluation in Suzuki reactions.* Cellulose, 2018. **25**: p. 6963-6975.
72. Coste, H., *Flore descriptive et illustrée de la France, de la Corse, et des contrées limitrophes*. Vol. 3. 1906: P. Klincksieck.
73. Fournier, P., *Les quatre flores de la France, Corse comprise:(generale, alpine, mediterraneenne, littorale)-v. 1: Texte.-v. 2: Atlas-2*. 1977.
74. Pavlik, B.M., *Nutrient and productivity relations of the dune grasses Ammophila arenaria and Elymus mollis: I. Blade photosynthesis and nitrogen use efficiency in the laboratory and field.* Oecologia, 1983. **57**: p. 227-232.
75. Battandier, J. and L. Trabut, *Analytical and synoptic flora of Algeria and Tunisia.* Alger: Vve Giralt, 1902. **152**.
76. Calderón-Ayala, J., *SAN JUAN, PUERTO RICO*. 2012.
77. Huiskes, A., *Ammophila arenaria (L.) Link (Psamma arenaria (L.) Roem. et Schult.; Calamgrostis arenaria (L.) Roth).* Journal of Ecology, 1979. **67**(1): p. 363-382.
78. Jebali, Z., et al., *Cellulose nanofibrils (CNFs) from Ammophila arenaria, a natural and a fast growing grass plant.* International journal of biological macromolecules, 2018. **107**: p. 530-536.
79. Chaouch, M.A., et al., *Effect of pH during extraction on the antioxidant and antiglycated activities of polysaccharides from Opuntia ficus indica.* Journal of Food Biochemistry, 2016. **40**(3): p. 316-325.
80. Obot, I., D. Macdonald, and Z. Gasem, *Density functional theory (DFT) as a powerful tool for designing new organic corrosion inhibitors. Part 1: an overview.* Corrosion Science, 2015. **99**: p. 1-30.
81. Rouibah, K., et al., *Biosorption of zinc (II) from synthetic wastewater by using Inula Viscosa leaves as a low-cost biosorbent: Experimental and molecular modeling studies.* Journal of Environmental Management, 2023. **326**: p. 116742.

82. Uka, D., et al., *An innovative and environmentally friendly approach for resveratrol solubilization and bioaccessibility enhancement by using natural deep eutectic solvents.* Journal of Molecular Liquids, 2023. **391**: p. 123411.
83. Bousba, D., et al., *Efficient biodiesel production from recycled cooking oil using a NaOH/CoFe2O4 magnetic nano-catalyst: synthesis, characterization, and process enhancement for sustainability.* Energy Conversion and Management, 2024. **300**: p. 118021.
84. Ferkous, H., et al., *A comparative study of novel synthesized sulfamide compounds: Electrochemical, morphological, XPS, and theoretical investigations on copper corrosion inhibition in 1.0 M HCl.* Journal of Molecular Liquids, 2024. **394**: p. 123781.
85. Boublia, A., et al., *Enhancing precision in PANI/Gr nanocomposite design: robust machine learning models, outlier resilience, and molecular input insights for superior electrical conductivity and gas sensing performance.* Journal of Materials Chemistry A, 2024. **12**(4): p. 2209-2236.
86. Elboughdiri, N., et al., *Comprehensive investigation of Cu2+ adsorption from wastewater using olive-waste-derived adsorbents: experimental and molecular insights.* International Journal of Molecular Sciences, 2024. **25**(2): p. 1028.
87. Madaci, A., et al., *Experimental and theoretical study of polysaccharides extracted from prickly pear nopales Pulp (PPUN) of Opuntia ficus-indica as corrosion inhibitors.* Journal of Molecular Liquids, 2023. **384**: p. 122272.
88. Boukerche, S., et al., *Anti-corrosion performance of dehydroacetic acid thiosemicarbazone on XC38 carbon steel in an acidic medium.* Arabian Journal of Chemistry, 2023. **16**(9): p. 105061.
89. Mouffok, A., et al., *Synergy of garlic extract and deep eutectic solvents as promising natural antibiotics: experimental and COSMO-RS.* Journal of Molecular Liquids, 2023. **375**: p. 121321.
90. Saha, S.K., et al., *Benzothiazolylhydrazine azomethine derivatives for efficient corrosion inhibition of mild steel in acidic environment: Integrated experimental and density functional theory cum molecular dynamics simulation approach.* Journal of Molecular Liquids, 2022. **364**: p. 120033.
91. Johnson, E.R., et al., *Revealing noncovalent interactions.* Journal of the American Chemical Society, 2010. **132**(18): p. 6498-6506.
92. Boutouil, A., et al., *Towards a deeper understanding of the inhibition mechanism of a new 1, 2, 3-triazole derivative for mild steel corrosion in the hydrochloric acid solution using coupled experimental and theoretical methods.* Materials Chemistry and Physics, 2020. **241**: p. 122420.
93. Lu, T. and F. Chen, *Multiwfn: A multifunctional wavefunction analyzer.* Journal of computational chemistry, 2012. **33**(5): p. 580-592.
94. Humphrey, W., A. Dalke, and K. Schulten, *VMD: visual molecular dynamics.* Journal of molecular graphics, 1996. **14**(1): p. 33-38.
95. Williams, T., et al., *Gnuplot 4.5: an interactive plotting program. 2011.* URL http://www. gnuplot. info, 2017. **56**.
96. Li, X.-H., S.-D. Deng, and H. Fu, *Inhibition by Jasminum nudiflorum Lindl. leaves extract of the corrosion of cold rolled steel in hydrochloric acid solution.* Journal of Applied Electrochemistry, 2010. **40**: p. 1641-1649.
97. Abdel-Gaber, A., et al., *Inhibitive action of some plant extracts on the corrosion of steel in acidic media.* Corrosion science, 2006. **48**(9): p. 2765-2779.

98. Souhila, T., B. Fatma Zohra, and H.S. Tahar, *Identification and quantification of phenolic compounds of Artemisia herba-alba at three harvest time by HPLC–ESI–Q-TOF–MS.* International Journal of Food Properties, 2019. **22**(1): p. 843-852.
99. Trendafilova, A., et al., *Phenolic profile of Artemisia alba Turra.* Chemistry & biodiversity, 2018. **15**(7): p. e1800109.
100. Deng, S., X. Li, and H. Fu, *Nitrotetrazolium blue chloride as a novel corrosion inhibitor of steel in sulfuric acid solution.* Corrosion Science, 2010. **52**(11): p. 3840-3846.
101. Nasibi, M., et al., *Corrosion inhibition of mild steel by Nettle (Urtica dioica L.) extract: polarization, EIS, AFM, SEM and EDS studies.* Journal of adhesion science and technology, 2013. **27**(17): p. 1873-1885.
102. Zhang, J., et al., *The inhibition mechanism of imidazoline phosphate inhibitor for Q235 steel in hydrochloric acid medium.* Corrosion science, 2011. **53**(10): p. 3324-3330.
103. Bammou, L., et al., *Inhibition effect of natural Artemisia oils towards tinplate corrosion in HCL solution: chemical characterization and electrochemical study.* International Journal of Electrochemical Science, 2011. **6**(5): p. 1454-1467.
104. Morad, M., *An electrochemical study on the inhibiting action of some organic phosphonium compounds on the corrosion of mild steel in aerated acid solutions.* Corrosion Science, 2000. **42**(8): p. 1307-1326.
105. Amin, M.A., et al., *The inhibition of low carbon steel corrosion in hydrochloric acid solutions by succinic acid: Part I. Weight loss, polarization, EIS, PZC, EDX and SEM studies.* Electrochimica Acta, 2007. **52**(11): p. 3588-3600.
106. Lenderink, H., M. Linden, and J. De Wit, *Corrosion of aluminium in acidic and neutral solutions.* Electrochimica acta, 1993. **38**(14): p. 1989-1992.
107. Sherif, E. and S.-M. Park, *Effects of 1, 4-naphthoquinone on aluminum corrosion in 0.50 M sodium chloride solutions.* Electrochimica acta, 2006. **51**(7): p. 1313-1321.
108. Kelly, E.J., *The active iron electrode: I. Iron dissolution and hydrogen evolution reactions in acidic sulfate solutions.* Journal of the Electrochemical Society, 1965. **112**(2): p. 124.
109. Rahmouni, K., et al., *Corrosion and protection of high leaded tin bronze covered with patina in NaHCO3+ Na2SO4 solution simulating acid rain in urban environment.* Bulgarian Chem Com, 2005. **1**: p. 26-34.
110. Ahamad, I., R. Prasad, and M. Quraishi, *Thermodynamic, electrochemical and quantum chemical investigation of some Schiff bases as corrosion inhibitors for mild steel in hydrochloric acid solutions.* Corrosion Science, 2010. **52**(3): p. 933-942.
111. Bentiss, F., et al., *Electrochemical study of substituted triazoles adsorption on mild steel.* Industrial & engineering chemistry research, 2000. **39**(10): p. 3732-3736.
112. Schweitzer, P., *Fundamentals of corrosion: mechanisms, causes, and preventative methods*. 2010: CRC press.
113. Jyothi, S. and J. Ravichandran, *Corrosion inhibition of mildsteel in sulphuric acid by methanol extract of Luffa aegyptiaca leaves–electrochemical and statistical view.* Journal of adhesion science and Technology, 2017. **31**(21): p. 2285-2299.
114. Yaro, A.S., A.A. Khadom, and R.K. Wael, *Apricot juice as green corrosion inhibitor of mild steel in phosphoric acid.* Alexandria Engineering Journal, 2013. **52**(1): p. 129-135.
115. Vračar, L.M. and D.M. Dražić, *Adsorption and corrosion inhibitive properties of some organic molecules on iron electrode in sulfuric acid.* Corrosion Science, 2002. **44**(8): p. 1669-1680.

116. Tang, Y., et al., *Experimental and molecular dynamics studies on corrosion inhibition of mild steel by 2-amino-5-phenyl-1, 3, 4-thiadiazole.* Corrosion Science, 2010. **52**(1): p. 242-249.
117. Geler, E. and D. Azambuja, *Corrosion inhibition of copper in chloride solutions by pyrazole.* Corrosion Science, 2000. **42**(4): p. 631-643.
118. Bouklah, M., et al., *Thermodynamic characterisation of steel corrosion and inhibitor adsorption of pyridazine compounds in 0.5 M H2SO4.* Materials Letters, 2006. **60**(15): p. 1901-1905.
119. Yan, Y., et al., *Electrochemical and quantum chemical study of purines as corrosion inhibitors for mild steel in 1 M HCl solution.* Electrochimica acta, 2008. **53**(20): p. 5953-5960.
120. Deyab, M. and S. Abd El-Rehim, *Effect of succinic acid on carbon steel corrosion in produced water of crude oil.* Journal of the Taiwan Institute of Chemical Engineers, 2014. **45**(3): p. 1065-1072.
121. Durnie, W., et al., *A study of the adsorption properties of commercial carbon dioxide corrosion inhibitor formulations.* Journal of Applied Electrochemistry, 2001. **31**: p. 1221-1226.
122. Martinez, S. and I. Stern, *Thermodynamic characterization of metal dissolution and inhibitor adsorption processes in the low carbon steel/mimosa tannin/sulfuric acid system.* Applied surface science, 2002. **199**(1-4): p. 83-89.
123. Kosari, A., et al., *Theoretical and electrochemical assessment of inhibitive behavior of some thiophenol derivatives on mild steel in HCl.* Corrosion Science, 2011. **53**(10): p. 3058-3067.
124. Verma, D.K. and F. Khan, *Corrosion inhibition of mild steel in hydrochloric acid using extract of glycine max leaves.* Research on Chemical Intermediates, 2016. **42**: p. 3489-3506.
125. Gopi, D., et al., *Corrosion and corrosion inhibition of mild steel in groundwater at different temperatures by newly synthesized benzotriazole and phosphono derivatives.* Industrial & Engineering Chemistry Research, 2014. **53**(11): p. 4286-4294.
126. Karthik, R., et al., *Anti-corrosion inhibition of mild steel in 1M hydrochloric acid solution by using Tiliacora accuminata leaves extract.* International Journal of Electrochemical Science, 2015. **10**(5): p. 3707-3725.
127. Muthukrishnan, P., B. Jeyaprabha, and P. Prakash, *Adsorption and corrosion inhibiting behavior of Lannea coromandelica leaf extract on mild steel corrosion.* Arabian Journal of Chemistry, 2017. **10**: p. S2343-S2354.
128. Pitchaipillai, M., et al., *Benevolent behavior of Kleinia grandiflora leaf extract as a green corrosion inhibitor for mild steel in sulfuric acid solution.* International Journal of Minerals, Metallurgy, and Materials, 2014. **21**: p. 1083-1095.
129. Fang, D., et al., *Calibration of binding energy positions with C1s for XPS results.* Journal of Wuhan University of Technology-Mater. Sci. Ed., 2020. **35**: p. 711-718.
130. Nadi, I., et al., *Sargassum muticum extract based on alginate biopolymer as a new efficient biological corrosion inhibitor for carbon steel in hydrochloric acid pickling environment: Gravimetric, electrochemical and surface studies.* International Journal of Biological Macromolecules, 2019. **141**: p. 137-149.
131. Berrissoul, A., et al., *Anticorrosion effect of a green sustainable inhibitor on mild steel in hydrochloric acid.* Journal of Colloid and Interface Science, 2020. **580**: p. 740-752.
132. El Hamdani, N., et al., *Alkaloids extract of Retama monosperma (L.) Boiss. seeds used as novel eco-friendly inhibitor for carbon steel corrosion in 1 M HCl solution: Electrochemical and surface studies.* Applied Surface Science, 2015. **357**: p. 1294-1305.

133. Garai, S., et al., *A comprehensive study on crude methanolic extract of Artemisia pallens (Asteraceae) and its active component as effective corrosion inhibitors of mild steel in acid solution.* Corrosion Science, 2012. **60**: p. 193-204.
134. Berrissoul, A., et al., *Evaluation of Lavandula mairei extract as green inhibitor for mild steel corrosion in 1 M HCl solution. Experimental and theoretical approach.* Journal of Molecular Liquids, 2020. **313**: p. 113493.
135. Cao, S., et al., *Task-specific ionic liquids as corrosion inhibitors on carbon steel in 0.5 M HCl solution: An experimental and theoretical study.* Corrosion Science, 2019. **153**: p. 301-313.
136. Lebrini, M., et al., *Electrochemical and quantum chemical studies of new thiadiazole derivatives adsorption on mild steel in normal hydrochloric acid medium.* Corrosion Science, 2005. **47**(2): p. 485-505.
137. Benabid, S., et al., *Molecular modeling of anionic and cationic dyes adsorption on sludge derived activated carbon.* Journal of molecular liquids, 2019. **289**: p. 111119.
138. Mandal, S., S. Bej, and P. Banerjee, *Insights into the uses of two azine decorated d10-MOFs for corrosion inhibition application on mild steel surface in saline medium: Experimental as well as theoretical investigation.* Journal of Molecular Liquids, 2023. **381**: p. 121789.
139. Kumar, K.V., M.S.N. Pillai, and G.R. Thusnavis, *Seed extract of Psidium guajava as ecofriendly corrosion inhibitor for carbon steel in hydrochloric acid medium.* Journal of Materials Science & Technology, 2011. **27**(12): p. 1143-1149.
140. Ferkous, H., et al. *2-(2-Methoxybenzylidene) Hydrazine-1-Carbothioamide as Efficient Organic Inhibitor for Mild Steel in Hydrochloric Acid Solution*. in *Recent Advances in Environmental Science from the Euro-Mediterranean and Surrounding Regions (2nd Edition) Proceedings of 2nd Euro-Mediterranean Conference for Environmental Integration (EMCEI-2), Tunisia 2019*. 2021. Springer.
141. Pareek, S., et al., *A new insight into corrosion inhibition mechanism of copper in aerated 3.5 wt.% NaCl solution by eco-friendly Imidazopyrimidine Dye: experimental and theoretical approach.* Chemical Engineering Journal, 2019. **358**: p. 725-742.
142. Fekri, M.H., et al., *Turnip peel extract as green corrosion bio-inhibitor for copper in 3.5% NaCl solution.* Materials Chemistry and Physics, 2022. **286**: p. 126150.
143. Tsuru, T., S. Haruyama, and B. Gijutsu, *Corrosion inhibition of iron by amphoteric surfactants in 2M HCl.* J Jpn Soc Corros Eng, 1978. **27**: p. 573-581.
144. Sedik, A., et al., *Synergistic effect of L-methionine and KI on copper corrosion inhibition in HNO3 (1M).* Sensors & Transducers, 2014. **27**(Special Issue).
145. Sedik, A., et al., *Experimental and theoretical insights into copper corrosion inhibition by protonated amino-acids.* RSC advances, 2022. **12**(36): p. 23718-23735.
146. Khaled, K., *The inhibition of benzimidazole derivatives on corrosion of iron in 1 M HCl solutions.* Electrochimica Acta, 2003. **48**(17): p. 2493-2503.
147. Belakhdar, A., et al. *Thermodynamic and electrochemical studies of corrosion inhibition of carbon steel by Rosmarinus officinalis extract in acid medium*. in *Recent Advances in Environmental Science from the Euro-Mediterranean and Surrounding Regions (2nd Edition) Proceedings of 2nd Euro-Mediterranean Conference for Environmental Integration (EMCEI-2), Tunisia 2019*. 2021. Springer.
148. Moumeni, O., et al., *Experimental and detailed DFT/MD simulation of α-aminophosphonates as promising corrosion inhibitor for XC48 carbon steel in HCl environment.* Journal of the Taiwan Institute of Chemical Engineers, 2023. **147**: p. 104918.

149. Prabakaran, M., et al., *Evaluation of polyphenol composition and anti-corrosion properties of Cryptostegia grandiflora plant extract on mild steel in acidic medium.* Journal of Industrial and Engineering Chemistry, 2016. **37**: p. 47-56.
150. Salleh, S.Z., et al., *Plant extracts as green corrosion inhibitor for ferrous metal alloys: A review.* Journal of Cleaner Production, 2021. **304**: p. 127030.
151. Singh, A., et al., *Comprehensive investigation of steel corrosion inhibition at macro/micro level by ecofriendly green corrosion inhibitor in 15% HCl medium.* Journal of colloid and interface science, 2020. **560**: p. 225-236.
152. Meriem, Z., et al., *Experimental and theoretical evaluation of the adsorption process of some polyphenols and their corrosion inhibitory properties on mild steel in acidic media.* Journal of Environmental Chemical Engineering, 2021. **9**(6): p. 106482.
153. Kahlouche, A., et al., *Molecular insights through the experimental and theoretical study of the anticorrosion power of a new eco-friendly Cytisus multiflorus flowers extract in a 1 M sulfuric acid.* Journal of Molecular Liquids, 2022. **347**: p. 118397.
154. Acidi, A., et al., *Examination of the main chemical components of essential oil of Syzygium aromaticum as a corrosion inhibitor on the mild steel in 0.5 M HCl medium.* Journal of Molecular Liquids, 2023. **391**: p. 123423.
155. Ferkous, H., et al., *The removal of a textile dye from an aqueous solution using a biocomposite adsorbent.* Polymers, 2022. **14**(12): p. 2396.
156. Bououden, W., et al., *Surface adsorption of Crizotinib on carbon and boron nitride nanotubes as Anti-Cancer drug Carriers: COSMO-RS and DFT molecular insights.* Journal of Molecular Liquids, 2021. **338**: p. 116666.
157. Benabid, S., et al., *Theoretical study of physicochemical properties of selected ammonium salt-based deep eutectic solvents.* Journal of Molecular Liquids, 2019. **285**: p. 38-46.
158. Gao, L., et al., *A combination of experiment and theoretical methods to study the novel and low-cost corrosion inhibitor 1-hydroxy-7-azabenzotriazole for mild steel in 1 M sulfuric acid.* RSC advances, 2018. **8**(67): p. 38506-38516.
159. Nnaji, N., et al., *Inhibition of aluminium corrosion using benzothiazole and its phthalocyanine derivative.* Electrocatalysis, 2019. **10**: p. 445-458.
160. Lemaoui, T., et al., *Prediction of electrical conductivity of deep eutectic solvents using COSMO-RS sigma profiles as molecular descriptors: a quantitative structure–property relationship study.* Industrial & Engineering Chemistry Research, 2020. **59**(29): p. 13343-13354.
161. Lemaoui, T., et al., *Predicting the density and viscosity of hydrophobic eutectic solvents: Towards the development of sustainable solvents.* Green Chemistry, 2020. **22**(23): p. 8511-8530.
162. Darwish, A.S., et al., *Multicomponent extraction of aromatics and heteroaromatics from diesel using acidic eutectic solvents: Experimental and COSMO-RS predictions.* Journal of Molecular Liquids, 2021. **336**: p. 116575.
163. Lemaoui, T., et al., *Molecular-based guide to predict the pH of eutectic solvents: promoting an efficient design approach for new green solvents.* ACS Sustainable Chemistry & Engineering, 2021. **9**(17): p. 5783-5808.
164. Ding, N., X. Chen, and C.-M.L. Wu, *Interactions between polybrominated diphenyl ethers and graphene surface: a DFT and MD investigation.* Environmental Science: Nano, 2014. **1**(1): p. 55-63.
165. Dutta, A., et al., *Correlating electronic structure with corrosion inhibition potentiality of some bis-benzimidazole derivatives for mild steel in hydrochloric acid: combined experimental and theoretical studies.* Corrosion Science, 2015. **98**: p. 541-550.

166. Kovačević, N. and A. Kokalj, *Chemistry of the interaction between azole type corrosion inhibitor molecules and metal surfaces.* Materials Chemistry and Physics, 2012. **137**(1): p. 331-339.
167. Lemaoui, T., et al., *Predicting the surface tension of deep eutectic solvents using artificial neural networks.* ACS omega, 2022. **7**(36): p. 32194-32207.
168. Boublia, A., et al., *Molecular-based artificial neural network for predicting the electrical conductivity of deep eutectic solvents.* Journal of Molecular Liquids, 2022. **366**: p. 120225.
169. Lemaoui, T., et al., *Machine learning approach to map the thermal conductivity of over 2,000 neoteric solvents for green energy storage applications.* Energy Storage Materials, 2023. **59**: p. 102795.
170. Ferkous, H., et al. *Electrochemical and Surface Morphological Studies of a Carbon Steel Corrosion by Natural Product in Acidic Solution*. in *Recent Advances in Environmental Science from the Euro-Mediterranean and Surrounding Regions: Proceedings of Euro-Mediterranean Conference for Environmental Integration (EMCEI-1), Tunisia 2017*. 2018. Springer.
171. Ahlrichs, R., et al., *Electronic structure calculations on workstation computers: The program system turbomole.* Chemical Physics Letters, 1989. **162**(3): p. 165-169.
172. AlYammahi, J., et al., *Molecular guide for selecting green deep eutectic solvents with high monosaccharide solubility for food applications.* ACS omega, 2023. **8**(29): p. 26533-26547.
173. Boublia, A., et al., *Multitask neural network for mapping the glass transition and melting temperature space of homo-and co-polyhydroxyalkanoates using σprofiles molecular inputs.* ACS Sustainable Chemistry & Engineering, 2022. **11**(1): p. 208-227.
174. Boudjelida, S., et al., *Physicochemical properties and atomic-scale interactions in polyaniline (Emeraldine Base)/starch bio-based composites: experimental and computational investigations.* Polymers, 2022. **14**(8): p. 1505.
175. Ferkous, H., et al., *Corrosion inhibition of mild steel by 2-(2-methoxybenzylidene) hydrazine-1-carbothioamide in hydrochloric acid solution: Experimental measurements and quantum chemical calculations.* Journal of Molecular Liquids, 2020. **307**: p. 112957.
176. Yasmin, T., et al., *Quince seed mucilage/β-cyclodextrin/Mmt-Na+-co-poly (methacrylate) based pH-sensitive polymeric carriers for controlled delivery of Capecitabine.* International Journal of Biological Macromolecules, 2023. **253**: p. 127032.
177. Zhang, X., et al., *Combined electrochemical/surface and theoretical assessments of Rosa laevigata extract as an eco-friendly corrosion inhibitor for copper in acidic medium.* Journal of the Taiwan Institute of Chemical Engineers, 2022. **136**: p. 104408.
178. Şahin, E.A., *Experimental and theoretical studies of acridine orange as corrosion inhibitor for copper protection in acidic media.* Journal of the Indian Chemical Society, 2022. **99**(3): p. 100358.
179. Zhang, J. and T. Lu, *Efficient evaluation of electrostatic potential with computerized optimized code.* Physical Chemistry Chemical Physics, 2021. **23**(36): p. 20323-20328.
180. Lu, T. and Q. Chen, *van der Waals potential: an important complement to molecular electrostatic potential in studying intermolecular interactions.* Journal of Molecular Modeling, 2020. **26**(11): p. 315.
181. Murray, J.S. and K. Sen, *Molecular electrostatic potentials: concepts and applications.* 1996.

182. Boulechfar, C., et al., *Corrosion inhibition of Schiff base and their metal complexes with [Mn (II), Co (II) and Zn (II)]: Experimental and quantum chemical studies.* Journal of Molecular Liquids, 2023. **378**: p. 121637.
183. Ferkous, H., et al., *Electrochemical and computational approaches of polymer coating on carbon steel X52 in different soil extracts.* Polymers, 2022. **14**(16): p. 3288.
184. Zhang, Q., et al., *Two amino acid derivatives as high efficient green inhibitors for the corrosion of carbon steel in CO2-saturated formation water.* Corrosion Science, 2021. **189**: p. 109596.
185. Murmu, M., et al., *Density functional theory, Monte Carlo simulation and non-covalent interaction study for exploring the adsorption and corrosion inhibiting property of double azomethine functionalised organic molecules.* Journal of Adhesion Science and Technology, 2022. **36**(23-24): p. 2732-2760.
186. Gattinoni, C. and A. Michaelides, *Understanding corrosion inhibition with van der Waals DFT methods: the case of benzotriazole.* Faraday discussions, 2015. **180**: p. 439-458.
187. Boulechfar, C., et al., *Schiff bases and their metal Complexes: A review on the history, synthesis, and applications.* Inorganic Chemistry Communications, 2023. **150**: p. 110451.
188. Behloul, H., et al., *New insights on the adsorption of CI-Reactive Red 141 dye using activated carbon prepared from the ZnCl2-treated waste cotton fibers: Statistical physics, DFT, COSMO-RS, and AIM studies.* Journal of Molecular Liquids, 2022. **364**: p. 119956.
189. Fuster, F. and S.J. Grabowski, *Intramolecular hydrogen bonds: the QTAIM and ELF characteristics.* The Journal of Physical Chemistry A, 2011. **115**(35): p. 10078-10086.
190. Popelier, P.L.A., *The QTAIM perspective of chemical bonding.* The chemical bond: fundamental aspects of chemical bonding, 2014: p. 271-308.
191. Kumar, P.S.V., V. Raghavendra, and V. Subramanian, *Bader's theory of atoms in molecules (AIM) and its applications to chemical bonding.* Journal of Chemical Sciences, 2016. **128**: p. 1527-1536.
192. Hamdy, A. and N.S. El-Gendy, *Thermodynamic, adsorption and electrochemical studies for corrosion inhibition of carbon steel by henna extract in acid medium.* Egyptian Journal of Petroleum, 2013. **22**(1): p. 17-25.
193. Radjai, M., et al. *Methanolic extract of Artemisia Herba Alba as eco-friendly inhibitor of carbon steel corrosion in 1M HCl media*. in *Recent Advances in Environmental Science from the Euro-Mediterranean and Surrounding Regions: Proceedings of Euro-Mediterranean Conference for Environmental Integration (EMCEI-1), Tunisia 2017*. 2018. Springer.
194. Gabsi, M., et al., *The curious case of polyphenols as green corrosion inhibitors: a review on their extraction, design, and applications.* Environmental Science and Pollution Research, 2023. **30**(21): p. 59081-59105.
195. Delimi, A., et al., *Corrosion protection performance of silicon-based coatings on carbon steel in NaCl solution: a theoretical and experimental assessment of the effect of plasma-enhanced chemical vapor deposition pretreatment.* RSC advances, 2022. **12**(24): p. 15601-15612.
196. Qiang, Y., et al., *Evaluation of Ginkgo leaf extract as an eco-friendly corrosion inhibitor of X70 steel in HCl solution.* Corrosion Science, 2018. **133**: p. 6-16.
197. Dehghani, A., G. Bahlakeh, and B. Ramezanzadeh, *Green Eucalyptus leaf extract: A potent source of bio-active corrosion inhibitors for mild steel.* Bioelectrochemistry, 2019. **130**: p. 107339.

Abstract

This study aims to inhibit the corrosion of mild steel in 1M HCl medium by adding two plant extracts: *Artemisia Herba Alba* (AHA) and *Ammophila Arenaria* (AA) at different concentrations. Several techniques were used: Weight loss measurement, Potentiodynamic Polarization, Electrochemical Impedance Spectroscopy to describe the mode of action of each inhibitor experimentally, and quantum chemical parameters were calculated to explain theoretically the adsorption behavior of AHA and AA on the metal surface and the inhibition mechanism

Electrochemical studies proved that both extracts are effective against steel corrosion at 900 ppm with 92.92% and 85.40% at 700 ppm for AHA and AA, respectively. Thermodynamic calculations showed that the adsorption behavior is governed by Langmuir isotherm and the protective layer formed on the metal surface was analyzed by atomic force microscopy (AFM), scanning electron microscopy (SEM), X-ray diffraction (XRD), and X-ray photoelectron spectroscopy (XPS.(
Keywords: Mild Steel, Corrosion, Corrosion Inhibitor, PDP, EIS and DFT.

Résumé

Cette étude vise à inhiber la corrosion de l'acier doux dans un milieu HCl 1M en ajoutant deux extraits de plantes: *Artemisia Herba Alba* (AHA) et *Ammophila Arenaria* (AA) à différentes concentrations. Plusieurs techniques ont été utilisées : La mesure de perte de masse, la polarisation potentiodynamique, la spectroscopie d'impédance électrochimique pour décrire le mode d'action de chaque inhibiteur expérimentalement, et les paramètres chimiques quantiques ont été calculés pour expliquer théoriquement le comportement d'adsorption de l'AHA et de l'AA sur la surface du métal et le mécanisme d'inhibition.

L'étude électrochimique a montré que les deux extraits sont efficaces contre la corrosion de l'acier à 900 ppm avec 92,92 % et 85,40 % à 700 ppm pour l'AHA et l'AA, respectivement. Les calculs thermodynamiques ont montré que le comportement d'adsorption est régi par l'isotherme de Langmuir et la couche protectrice formée sur la surface du métal a été analysé par la microscopie à force atomique (AFM), microscopie électronique à balayage (SEM), diffraction des rayons X (XRD), et spectroscopie photoélectronique à rayons X (XPS).
Mots-clés : Acier doux, corrosion, inhibiteur de corrosion, PDP, EIS et DFT.

ملخص

تهدف هذه الدراسة إلى تثبيط تآكل الفولاذ اللين في وسط حمض الهيدروكلوريك بتركيز 1M وذلك بإضافة مستخلص نبتتين هما: نبات الشيح (AHA) و قصب الرمال(AA) بتراكيز مختلفة. تم الاستعانة بتقنيات مختلفة: قياس مقدار فقدان الوزن، الاستقطاب الديناميكي الفعال، التحليل الطيفي للمعاوقة الكهروكيميائية من أجل وصف طريقة عمل كل مثبط تجريبيا كما تم حساب المعاملات الكيميائية الكمية لتفسير سلوك امتزاز AHA و AA على سطح المعدن و آلية التثبيط نظريا.

ثبت من خلال الدراسات الكهروكيميائية أن كلا المستخلصين فعال لمقاومة لصدأ الفولاذ عند تركيز 900 جزء في المليون بنسبة 92,92% و 85,40% عند التركيز 700 جزء في المليون لمستخلص AHA وAA على التوالي. كما بينت حسابات ديناميكا الحرارية أن سلوك الامتزاز خاضع لمنظم الحرارة لانجموير وتم الكشف عن الطبقة المتكونة علر سطح المعدن بواسطة المسح المجهري للقوة الذرية (AFM)، المسح المجهري الالكتروني (SEM)، حيود الأشعة السينية (XRD)، والتحليل الطيفي الضوئي بالأشعة السينية (XPS).
الكلمات المفتاحية: الفولاذ اللين، تآكل، مثبط التآكل، PDP، EIS و DFT.